Journal of African Earth Sciences 171 (2020) 103946

Contents lists available at ScienceDirect

Journal of African Earth Sciences

journal homepage: www.elsevier.com/locate/jafrearsci

Revised stratigraphic framework for the lower Anti-Atlas supergroup based on U–Pb geochronology of magmatic and detrital zircons (Zenaga and Bou Azzer-El Graara inliers, Anti-Atlas Belt, Morocco)

Abdelhak Ait Lahna [a,*], Nasrrddine Youbi [a,b], Colombo Celso Gaeta Tassinari [c], Miguel Angelo Stipp Basei [d], Richard E. Ernst [e,f], Latifa Chaib [a], Abdelhafed Barzouk [a], João Mata [b], Andreas Gärtner [g], Hassan Admou [a], Moulay Ahmed Boumehdi [a,b], Ulf Söderlund [h,i], Mohamed Khalil Bensalah [a,b], Jean-Louis Bodinier [j,k], Lhou Maacha [l], Andrey Bekker [m,n]

[a] Department of Geology, Faculty of Sciences-Semlalia, Cadi Ayyad University, Prince Moulay Abdellah Boulevard, P.O. Box 2390, Marrakech, Morocco
[b] Instituto Dom Luiz, Faculdade de Ciências, Universidade de Lisboa, 1749-016, Lisboa, Portugal
[c] Centro de Pesquisas Geocronológicas (CPGeo), Instituto de Geociências (IG), Universidade de São Paulo- USP, Caixa Postal 11348, CEP 05422-970, São Paulo, SP, Brazil
[d] Instituto de Geociências (IG), Departamento de Mineralogia e Geotectônica (GMG), Universidade de São Paulo-USP, Rua do Lago, 562 Cidade Universitária, 05508-080, São Paulo, SP, Brazil
[e] Department of Earth Sciences, Carleton University, 1125 Colonel By Drive, Ottawa, Canada, K1S 5B6
[f] Faculty of Geology and Geography, Tomsk State University, 36 Lenin Ave, Tomsk, 634050, Russia
[g] Senckenberg Naturhistorische Sammlungen Dresden, Museum für Mineralogie und Geologie, Sektion Geochronologie, GeoPlasma Lab, Königsbrücker Landstraße 159, 01109, Dresden, Germany
[h] Department of Geology, Lund University, Sölvegatan 12, SE-223 62, Lund, Sweden
[i] The Swedish Museum of Natural History, SE-114 18, Stockholm, Sweden
[j] Mohammed VI Polytechnic University, Geology and Sustainable Mining Department, Hay Moulay Rachid, Ben Guerir, 43150, Morocco
[k] Géosciences Montpellier, Université de Montpellier 2, CNRS, Cc 60, Place Eugène Bataillon, 34095, Montpellier Cedex 05, France
[l] Managem Group, Twin Center, Tour A, Angle Boulevards Zerktouni & Al Massira Al Khadra, P.O. Box 5199, Casablanca, Morocco
[m] Department of Earth and Planetary Sciences, University of California, Riverside, CA, 92521, USA
[n] Department of Geology, University of Johannesburg, Auckland Park 2006, South Africa

ARTICLE INFO

Keywords:
Morocco
Anti-Atlas Belt
Proterozoic
Lower Anti-Atlas supergroup
U–Pb geochronology

ABSTRACT

U–Pb geochronology of magmatic and detrital zircons (Zenaga and Bou Azzer-El Graara inliers, Anti-Atlas Belt, Morocco) and a reassessment of the published constraints suggest a revised stratigraphic framework for the lower Anti-Atlas Supergroup. Five major unconformity-bounded lithostratigraphic packages are here distinguished: the two lower units of Paleoproterozoic age are named the Tasserda-Taghatine Group (2030–1706 Ma) and the Oumoula (Mimount) Formation (ca. 1745–1650 Ma); the third unit of Paleoproterozoic to Neoproterozoic age (ca. 1650 to >883 Ma) is the Tizi n'Taghatine Group; the fourth and fifth units of Neoproterozoic age are the ca. 883 Ma Tachdamt and the ca. 700 Ma Bleida formations. Implications of this revised stratigraphic framework include: 1) the Tasserda-Taghatine Group might be linked to the post-orogenic collapse after the Eburnean Orogeny; 2) the Tizi n'Taghatine Group might be ca. 1.1 Ga in age based on proposed correlation with the Taoudeni Basin succession in Mauritania; 3) the Bleida Formation likely reflects deposition in the foreland basin at the early stage of the Pan-African Orogeny; 4) the Oumoula (Mimount) Formation, Tizi n'Taghatine Group, and Tachdamt Formation potentially record extensional events within the Nuna/Columbia and Rodinia supercontinents; 5) the provenance of the lower Anti-Atlas Supergroup (based on our new detrital zircon dating) is mainly from the West African craton along with possible contributions from other cratons such as Amazonia and

* Corresponding author.
E-mail addresses: abdelhak.aitlahna@ced.uca.ma, aitlahna.abdelhak@gmail.com (A. Ait Lahna), youbi@uca.ac.ma (N. Youbi), ccgtassi@usp.br (C.C.G. Tassinari), baseimas@usp.br (M.A.S. Basei), Richard.Ernst@carleton.ca, Richard.Ernst@ernstgeosciences.com (R.E. Ernst), latifa_918@yahoo.fr (L. Chaib), barzoukabdelhafed@gmail.com (A. Barzouk), jmata@fc.ul.pt (J. Mata), Andreas.Gaertner@senckenberg.de (A. Gärtner), admou@uca.ac.ma (H. Admou), boumehdi@uca.ac.ma (M.A. Boumehdi), Ulf.Soderlund@geol.lu.se (U. Söderlund), bensalah@uca.ac.ma (M.K. Bensalah), JeanLouis.Bodinier@um6p.ma, bodin@gm.univ-montp2.fr (J.-L. Bodinier), L.maacha@managemgroup.com (L. Maacha), andrey.bekker@ucr.edu (A. Bekker).

https://doi.org/10.1016/j.jafrearsci.2020.103946
Received 11 December 2019; Received in revised form 28 June 2020; Accepted 30 June 2020
Available online 21 July 2020
1464-343X/© 2020 Elsevier Ltd. All rights reserved.

the Sahara Metacraton; 6) the flood basalt sequence of the Tachdamt Formation likely belongs to the ca. 885-883 Ma intraplate Iguerda-Taïfast Large Igneous Province (LIP) event defined by previously dated dykes in the Iguerda and Taïfast inliers; and 7) the 1650 Ma Zenaga LIP can be potentially linked with LIP magmatism in Baltica and Laurentia.

1. Introduction

Substantial advances in the understanding of the geological evolution of several major Precambrian accretionary orogens of North America and Baltica (Hoffman, 1988; Chacko et al., 2000; Corrigan et al., 2005, 2009; Pehrsson et al., 2013; Bogdanova et al., 2008, 2016) have been made in recent years. However, there is still a fundamental gap in the knowledge of Precambrian orogenic belts in Africa. Much of the uncertainty about the accretionary history of the Precambrian African orogens stems from the limited database of reliable radiometric ages on structurally important units, combined with a lack of detailed studies using modern kinematic analysis in these deformed regions as well as of cutting-edge research using sedimentology and sequence stratigraphy.

One of the crucial Neoproterozoic African orogens is exposed in the Anti-Atlas Belt of Morocco located in the northern part of the West African Craton (WAC, Fig. 1). Extensive outcrops of the Neoproterozoic Pan-African Belt and underlying Paleoproterozoic foreland (Michard et al., 2008; Gasquet et al., 2008; Soulaimani et al., 2018 and references therein) are well exposed and have been studied for a long time (e.g. Choubert, 1963). Traditionally, the Precambrian of the Anti-Atlas Belt has been divided into three broad lithosomes (e.g. Choubert, 1963): the P I (Archean to Paleoproterozoic), P II (early and middle Neoproterozoic), and P III (late Neoproterozoic) (Fig. 2). This lithostratigraphic subdivision has recently been challenged (Walsh et al., 2002, 2012; Thomas et al., 2002, 2004; Michard et al., 2008; Gasquet et al., 2008; Youbi et al., 2013). In the conventional interpretation, the oldest, Paleoproterozoic rocks (PI) of the Anti-Atlas Belt are subdivided into a series of complexes (e.g. the Zenaga and Kerdous complexes in the Siroua and Kerdous basement inliers, respectively). The rocks of the P II lithosome deposited on this basement have collectively been called the *Anti-Atlas Supergroup*, within which there are four groups of volcano-sedimentary units (e.g. Lkest-Taghdout, Bou Azzer, Iriri, and Saghro groups) and they are conventionally inferred to be Neoproterozoic in age. Various poorly-dated intrusive suites are also recognized (e.g. Ifzwane and Toudma Suites). These volcano-sedimentary units have been related to the earliest passive margin, oceanic, and island-arc settings with inferred ages between ca. 800 and 660-640 Ma. The earliest Pan-African deformation at 660-640 Ma resulted from closure of the ocean basin, SW-directed thrusting, and accretion of the island-arc remnants.

Recent studies provided new structural, geochronological, and geochemical data. However, many critical questions about the accretionary history of the Anti-Atlas Belt are still debated (e.g. Soulaimani et al., 2018 and references therein). Such questions include the age of obducted oceanic crust segments (Siroua and Bou Azzer El Graara ophiolites), relationship between arc terranes to the north with ophiolites and an associated blueschist facies belt to the south, the age and nature of the basement in these terranes, the degree of interaction of Neoproterozoic magmas with the basement, and the timing of accretion of these terranes to the West African Craton. Finally, discrimination between the post-Eburnean sedimentary succession, recently dated to be late Paleoproterozoic in age (Ikenne et al., 2017; Soulaimani et al., 2019; Youbi et al., 2019; this work), and the Neoproterozoic sedimentary sequence (Leblanc and Moussine-Pouchkine, 1994; Bouougri and Saquaque, 2004; Blein et al., 2014a,b; Soulaimani et al., 2018; Youbi et al., 2018) remains uncertain.

The lower Anti-Atlas Supergroup of the Anti-Atlas Belt (Lkest-Taghdout Group *sensu* Thomas et al., 2004, Figs. 1D, 2 and 3) is one of the most important Proterozoic lithostratigraphic units on the WAC, yet with poor age constraints. It consists essentially of basalts, quartzites, and stromatolitic/oolitic carbonates, intruded by dolerite dyke swarms and sill complexes (Ifzwane and Toudma Suites). The lower Anti-Atlas Supergroup was previously thought to be ca. 1000-800 Ma in age on the basis of (1) stromatolites characteristic for the Neoproterozoic carbonate successions (Choubert, 1962), and (2) the Rb/Sr age of the contact-metamorphosed host rocks associated with mafic dykes (789 ± 10 Ma) in the Tachdamt Subinlier of the Bou Azzer El Graara Inlier (Clauer, 1976; Cahen et al., 1984).

The present study is based on field observations and new U–Pb ages for igneous zircons from a dolerite sill intruding carbonates from the lower Anti-Atlas Supergroup in the Zenaga Inlier and detrital zircon grains from four samples from the lower, middle, and upper parts of the lower Anti-Atlas Supergroup in the Zenaga and Bou Azzer El Graara inliers. We propose a new lithostratigraphy for the Proterorozoic lower Anti-Atlas Supergroup of the Anti-Atlas Belt based on a discussion of our data in combination with the previously published data (Abati et al., 2010; Walsh et al., 2012; Letsch, 2018; Bouougri et al., 2020) and constrain the provenance for the five major unconformity-bounded herein-defined packages of the supergroup.

2. Geological background

2.1. The West African Craton

The West African Craton (WAC, Fig. 1) extends across northwestern Africa, and consists of two Archean basement shields, the Reguibat Shield to the north and the Leo-Man Shield to the south. The Archean nuclei (3.5–2.7 Ga in age) of these shields are juxtaposed against an array of Paleoproterozoic domains (2.35–2.00 Ga in age) made up of greenstone belts and regions of extensive tonalite-trondhjemite-granodiorite (TTG) plutons, which are overlain by Meso-to Neoproterozoic and younger sedimentary basins. Smaller basement inliers are composed of Paleoproterozoic rocks: the Kayes and Kedougou-Kenieba inliers to the west, and those of the Anti-Atlas Belt to the north (Ennih and Liégeois, 2008; Abati et al., 2012). The WAC remained largely stable since 2 Ga (Schofield et al., 2006; Jessell et al., 2016). The basement of the WAC has evolved through several major orogenic cycles: the Paleoarchean Leonian cycle (several episodes between 3.40 and 3.10 Ga with uncertain chronology, related to continental accretion; e.g. Thiéblemont et al., 2004; Koffi et al., 2020), the Liberian cycle (2.85–2.70 Ga; Key et al., 2008; Koffi et al., 2020), the Paleoproterozoic Eburnean and Birimian cycles (2.15–2.07 Ga and 2.27–1.96 Ga, respectively; Abouchami et al., 1990; Boher et al., 1992; Egal et al., 2002; Schofield et al., 2006; Baratoux et al., 2011; Grenholm et al., 2019; McFarlane et al., 2019) and the late Neoproterozoic Pan-African orogenic event (885-550 Ma; Thomas et al., 2002, 2004; Gasquet et al., 2005, 2008; Walsh et al., 2012; Youbi et al., 2018). The WAC hosts four major intracratonic basins: the large central Taoudeni Basin and the smaller Tindouf and Volta basins, to the north and southwest, respectively, and the Gourma aulacogen to the east (Moussine-Pouchkine and Bertrand-Sarfati, 1978; Villeneuve, 2005; Deynoux et al., 2006; Lottaroli et al., 2009). These basins comprise mostly Mesoproterozoic-Neoproterozoic to Devonian-Carboniferous sediments. The WAC is surrounded by Pan-African belts, including the Trans-Saharan and Anti-Atlas belts (Ennih and Liégeois, 2008; Liégeois et al., 2013; Toummite et al., 2013; Brahimi et al., 2018).

Early compilations of WAC lithostratigraphy suggested an absence of

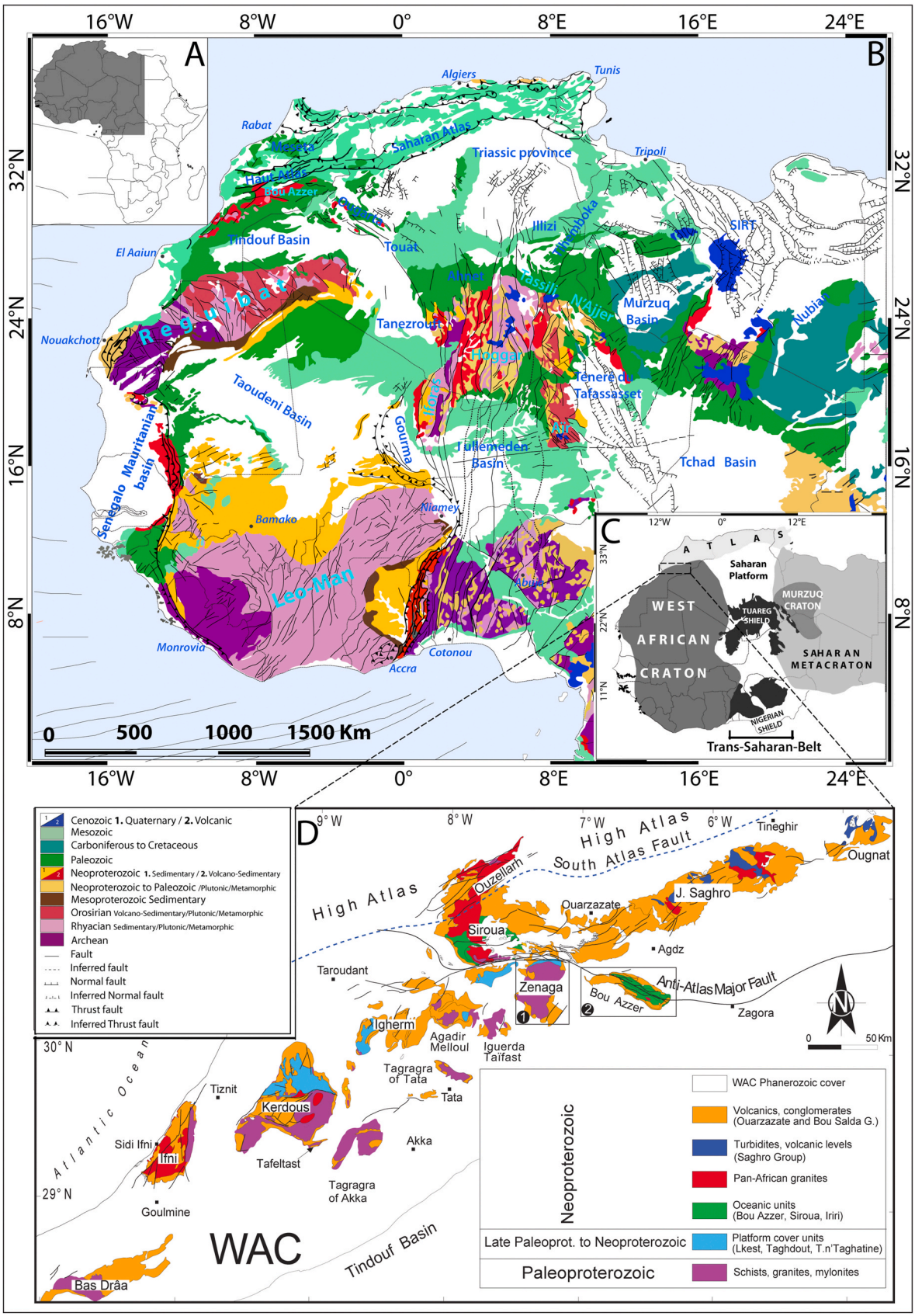

Fig. 1. (A) Location of Northwestern Africa; (B) geological map of Northwestern Africa (after Thiéblemont, 2016 and Brahimi et al., 2018); (C) distribution of main tectonic elements (after Brahimi et al., 2018); and (D) geological map of the Anti-Atlas Belt in southern Morocco showing the studied area in the Zenaga and Bou Azzer El Graara inliers (after Gasquet et al., 2008). Abbreviations: G.- Groups; J.- Jbel; Paleoprot.- Paleoproterozoic; T.-Tizi.

Mesoproterozoic events or rocks, indicating a tectonically quiescent period between 1.7 and 1.0 Ga (e.g. Ennih and Liégeois, 2008 and references therein). The lack of detrital zircons of that age in the pre-Cryogenian strata is considered characteristic of sediments sourced from the WAC (e.g. Abati et al., 2010; Gärtner et al., 2013, 2017; 2018). However, recent studies in the northern WAC (El Bahat et al., 2013; Kouyaté et al., 2013; Söderlund et al., 2013; Youbi et al., 2013; Ikenne et al., 2017) demonstrated important intraplate magmatic events based on dating of mafic dykes by the U–Pb method on baddeleyite and zircon. Six distinct events are distinguished throughout the inliers: ca. 2040 Ma Tagragra of Tata, 1750 Ma Tagragra of Akka, 1650 Ma Zenaga, 1416–1380 Ma Bas Drâa, and 885–883 Ma Iguerda-Taïfast events, and 612–600 Ma pulse of the Central Iapetus Magmatic Province (CIMP; Walsh et al., 2002; Gasquet et al., 2004; El Bahat et al., 2013; Kouyaté et al., 2013; Söderlund et al., 2013; Youbi et al., 2013; El Bahat et al., 2017; Ikenne et al., 2017; Bouougri et al., 2020; Youbi et al., 2020). Re–Os geochronology of the sedimentary succession of the Atar Group in the Taoudeni Basin of Mauritania indicated depositional ages ranging from 1109 ± 22 to 1105 ± 37 Ma (Rooney et al., 2010). These Mesoproterozoic ages are confirmed by the study of microfossils (Beghin et al., 2017) and chemostratigraphy (Kah et al., 2012). Recently, Baratoux et al. (2019) identified four new magmatic events 1.79–1.76, 1.58, 1.53, and 0.91–0.87 Ga in the southern WAC that add additional evidence for Mesoproterozoic mafic intrusive activity on this craton. Ar–Ar ages of ca. 1.24 Ga for the 1575 and 1520 Ma dyke swarms are considered to record a thermal overprint (Tapsoba et al., 2018).

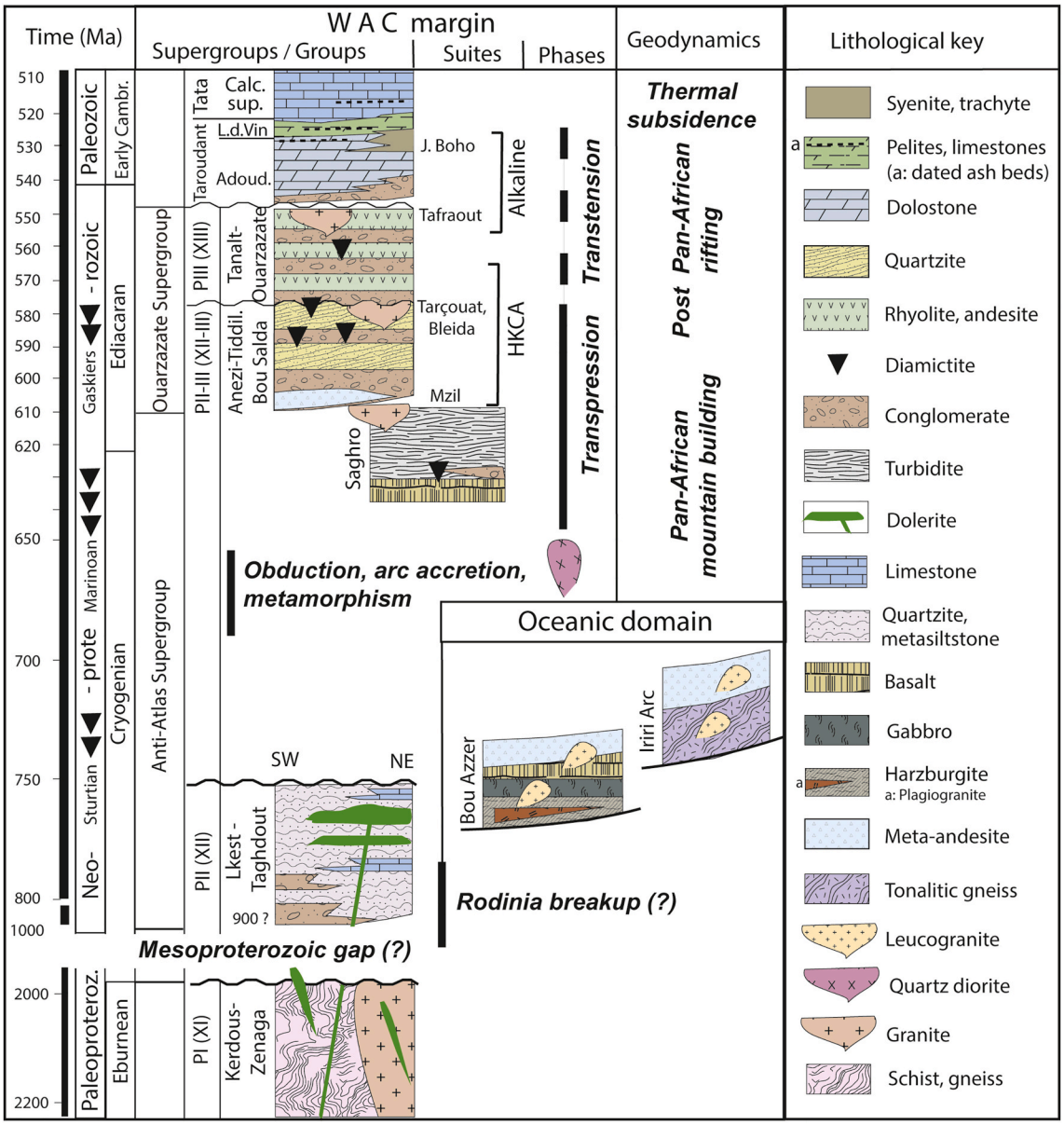

Fig. 2. Generalized lithostratigraphic column for the Anti-Atlas Pan-African orogen. After Thomas et al. (2004), modified by Gasquet et al. (2005, 2008) and Youbi et al. (2013), and taken from Youbi et al. (2013). The conventional viewpoint has been that there is a gap in magmatic activity between 1.7 and 1.0 Ga in the Anti-Atlas Belt (Mesoproterozoic gap). However, this interpretation was challenged with the results of Youbi et al. (2013), El Bahat et al. (2013), Kouyaté et al. (2013), Söderlund et al. (2013), which all indicated important intraplate magmatic events at ca. 1.75, 1.65, and 1.38–1.41 Ga. See the text for more explanation. This figure is the outdated correlation scheme for the Anti-Atlas Belt since it uses outdated chronology of the Anti-Atlas cover successions. Abbreviations: PI (XI), PII (XII), PII-III (XII-III) and PIII (XIII) are the classical stratigraphic symbols used on Anti-Atlas geological maps (Choubert, 1963). Adoud.- Adoudounien (or Adoudounian); Calc. Sup.- "Calcaires Supérieures" (Upper Limestones); Cambr.- Cambrian; HKCA- High-K calc-alkaline (granitoids); L. d. Vin - Lie de Vin (wine-coloured); Paleoproteroz.- Paleoproterozoic.

2.2. The Anti-Atlas Belt

The ENE-WSW trending Anti-Atlas Belt (800 km long and 200 km wide) of Morocco is the most important segment of the Neoproterozoic Pan-African Orogen in the northern part of the WAC (Fig. 1D). The Precambrian basement crops out in several erosional inliers ("boutonnières" in French), containing Late Ediacaran and younger units (Bas Drâa, Ifni, Kerdous, Tagragra of Akka, Tagragra of Tata, Igherm, Siroua, Zenaga, Bou Azzer, Saghro, and Ougnat; Fig. 1D) and distributed along two major fault systems (South Atlas Fault, SAF and Anti-Atlas Major Fault, AAMF; Fig. 1D).

The Anti-Atlas Belt contains the Paleoproterozoic basement (affected by the Eburnean Orogeny) unconformably overlain by the lower Anti-Atlas Supergroup (= Lkest-Taghdout Group *sensu* Thomas et al., 2004; = Tizi n'Taghatine Group *sensu* Bouougri and Saquaque, 2004), which is in turn unconformably overlain by the Ouarzazate Supergroup related to the Pan-African Orogeny. The two major periods of tectonothermal activity, associated with crustal accretion, have been recognized during the Proterozoic (Fig. 2) in the Anti-Atlas Belt and are described below.

(i) *The Paleoproterozoic Eburnean Orogeny (2.20–2.07 Ga*; Abouchami et al., 1990; Boher et al., 1992; Egal et al., 2002; Schofield et al., 2006; Baratoux et al., 2011; McFarlane et al., 2019*)*. The Paleoproterozoic basement rocks are found exclusively SW of the AAMF (Choubert, 1963), but they may also constitute the basement to the Pan-African Orogen to the NE (Ennih and Liégeois, 2001; Liégeois et al., 2006; Gasquet et al., 2008). The Paleoproterozoic basement is composed of metasedimentary rocks, granites, paragneisses, and migmatites, with U–Pb zircon ages ranging from 2200 to 2030 Ma (e.g. Aït Malek et al., 1998; Walsh et al., 2002; Thomas et al., 2002; Gasquet et al., 2004, 2008; O'Connor, 2010).

(ii) The Neoproterozoic Pan-African Orogeny (885–550 Ma). The Neoproterozoic sequences of the Anti-Atlas Belt are composed of units that were involved in the Pan-African Orogeny and the unconformably overlying post-collisional volcano-sedimentary rocks of the Ouarzazate Supergroup, which are a part of the Central Iapetus Magmatic Province (CIMP; Doblas et al., 2002; Maloof et al., 2005; Gasquet et al., 2005, 2008; Ernst and Youbi, 2017; Tuduri et al., 2018; Youbi et al., 2020). The Neoproterozoic rocks underlying the Ouarzazate Supergroup are subdivided into the lower units (Lkest--Taghdout, Bou-Azzer, and Iriri groups), affected by all Pan-African orogenic events, and the upper units (Saghro and Bou Salda groups), only affected by the latest stage of the Pan-African Orogeny (e.g. Walsh et al., 2002; Thomas et al., 2004; Gasquet et al., 2005, 2008; Alvaro et al., 2014).

The lower Anti-Atlas Supergroup consists essentially of basalt,

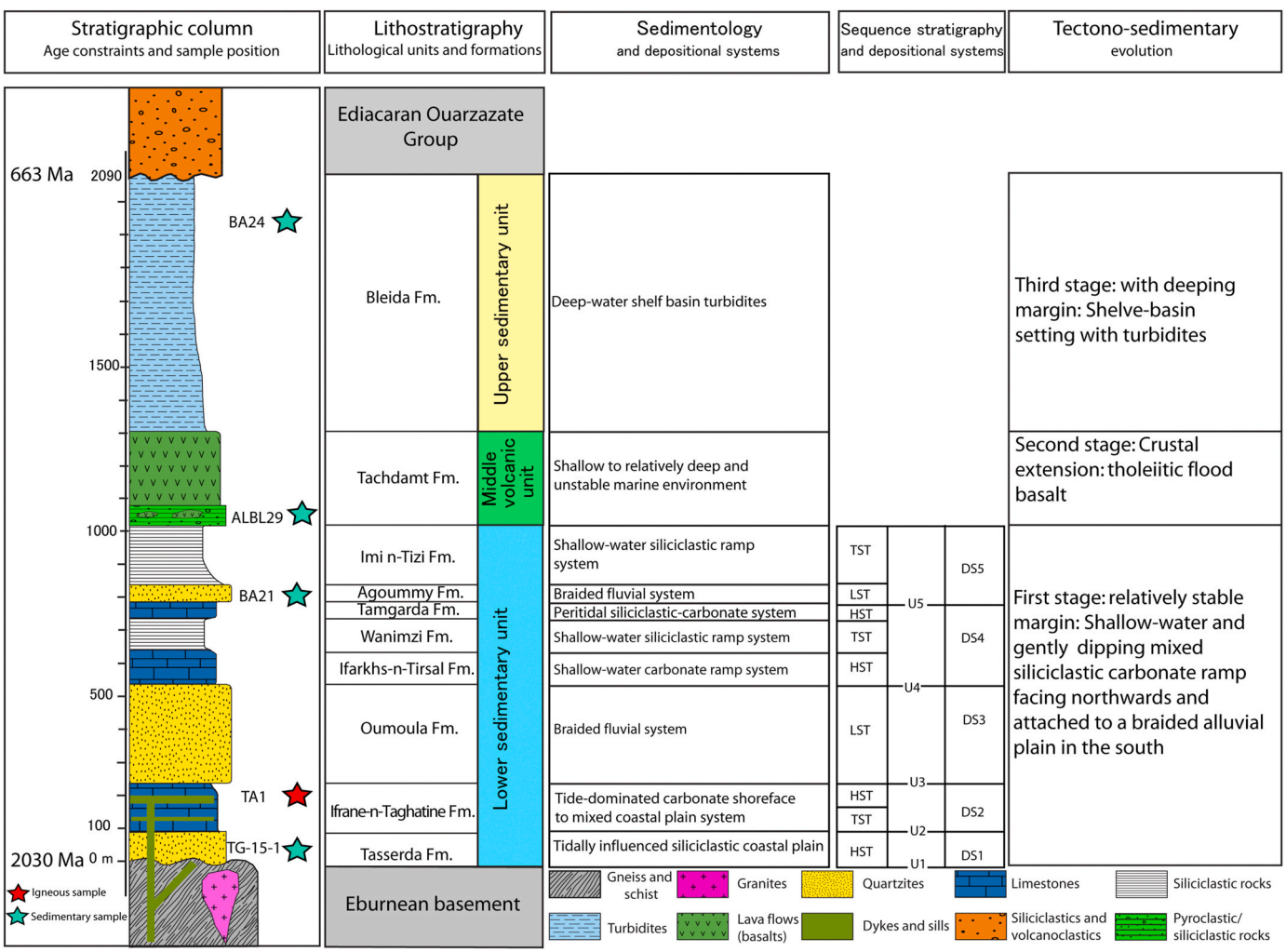

Fig. 3. Lithostratigraphic subdivision, sequence stratigraphy, and paleogeographic data for the lower Anti-Atlas Supergroup (modified after Bouougri and Saquaque, 2004). We use the name of the Ifrane-n-Taghatine Formation instead of the Taghdout Formation to ovoid confusion with the widely used name of the group - "the Taghdout Group" in the Zenaga Inlier. Abbreviations: systems tracts consist of (LST) lowstand system tracts, (TST) transgressive system tracts, and (HST) highstand system tracts. U1 to U5 are unconformities. DS1 to DS5 are depositional systems.

quartzite, and stromatolitic/oolitic carbonate, cut by undated dolerite dyke swarms and sill complexes (Thomas et al., 2004; Bouougri and Saquaque, 2004). It marks the onset of a period of rifting at the northern portion of the WAC during the late Neoproterozoic. The rifting culminated with the opening of an oceanic basin on the northern edge of the WAC. The relics of the oceanic crust (Bou-Azzer Group) are preserved in the Bou-Azzer and Siroua inliers as highly sheared allochthonous ophiolite complexes (El Hadi et al., 2010; Blein et al., 2014a and references therein). The ophiolitic assemblage is mainly made up of ultramafic rocks (serpentinites with few chromite pods), but also includes mafic meta-cumulates, meta-basaltic sheeted dykes, and, to a smaller extent, pillow lavas (Leblanc, 1975, 1981; Admou and Juteau, 1998). Their geochemical signatures point to emplacement in a supra-subduction zone (Bodinier et al., 1984; Naidoo et al., 1991; Ahmed et al., 2005; Hodel et al., 2017; Triantafyllou et al., 2019, 2020). Dating of plagiogranite intrusions in the Siroua Inlier indicated formation of an oceanic crust at ca. 760 Ma (U–Pb zircon age; Samson et al., 2004). Given the absence of reliable radiometric data on the age of the lower Anti-Atlas Supergroup, ca. 760 Ma was considered as the minimum age of its formation. The rifting might be associated with the late Neoproterozoic extension within the supercontinent Rodinia (Gasquet et al., 2008). Following the opening of the ocean basin, a subduction phase was initiated with island-arc development (the Iriri Group in the Siroua Inlier; Thomas et al., 2002; Triantafyllou, 2015, Triantafyllou et al., 2016). The cores and overgrowths of zircon grains from the Iriri Group migmatite yielded two U–Pb SHRIMP ages at 743 ± 14 and 663 ± 13 Ma, respectively (Thomas et al., 2002). The older age obtained from the cores is interpreted as the age of crystallization and emplacement of the migmatite protolith in an island–arc setting, whereas the younger age is thought to represent the timing of ophiolite obduction and arc accretion to the northern edge of the WAC in association with the regional metamorphism and the main orogenic event in the Anti-Atlas Belt (Thomas et al., 2002).

The development of the Anti-Atlas Belt oceanic arc complexes occurred during three magmatic flare-ups at ca. 750, 700, and 650 Ma that were interspersed with an early major tectonic episode between 730 and 700 Ma (Triantafyllou et al., 2018, 2020). A garnet Sm–Nd date of 647.2 ± 1.7 Ma was recently obtained for the Tasriwine ophiolite complex in the Siroua Inlier (Inglis et al., 2016). This age is more than 15 million years younger than the previous age estimate by Thomas et al. (2002). North of the AAMF in the eastern Anti-Atlas Belt (Figs. 1D and 2), the oldest rocks are thick deposits of basalt and turbidite of the Saghro Group, interpreted as either a distal-slope equivalent of the upper part of the lower Anti-Atlas Supergroup, deposited between the WAC to the south and an island arc (Saquaque et al., 1989; Thomas et al., 2002), or slivers of the stretched Eburnean crust (Hindermeyer, 1953; Ouguir et al., 1996; Fekkak et al., 2001, 2002; Massironi et al., 2007; Schiavo et al., 2007; Michard et al., 2017).

Preliminary detrital zircon data reported by Liégeois et al. (2006) and summarized in Gasquet et al. (2008) suggest that the sediments of the Saghro Group in the Kelaa Mgouna section were derived from sources ranging in age from about 880 to 615 Ma. The later post-collisional, extensional stage (605–542 Ma) is characterized by molasse deposition and magmatism of the Ouarzazate Supergroup, which was followed by the foreland development in the Saharan cratonic basin to the south (Taroudant and Tata groups; e.g. Doblas et al., 2002; Maloof et al., 2005; Gasquet et al., 2005, 2008; Hefferan et al., 2014; Karaoui et al., 2014, 2015; Tuduri et al., 2018; Geyer and Landing, 2006, 2020; Youbi et al., 2020).

2.3. The lower Anti-Atlas Supergroup

Since our study is focused on the lower Anti-Atlas Supergroup, we will give here an updated review of its lithology, stratigraphy, and nomenclature. The lower Anti-Atlas Supergroup, known in the Anti-Atlas literature as the Taghdout (Lkest/Tizi n'Taghatine) Group, contains a sedimentary succession deposited along the northern margin of the WAC (e.g. Thomas et al., 2002, 2004; Bouougri and Saquaque, 2004; Alvaro et al., 2014). The lower part of the lower Anti-Atlas Supergroup shows a progressive change of sedimentary facies from SW to NE representing a broad proximal to distal trend: conglomerates, sandstones, and quartz sandstones predominate in the Ifni and Kerdous inliers, while quartz sandstones, carbonates, shales, turbidites, and basaltic lava flows (the so called "Série des Calcaires et Quartzites"; see Choubert, 1962) developed in the Igherm, Siroua, Zenaga, and Bou Azzer El Graara inliers (Bouougri and Saquaque, 2004; Thomas et al., 2004; Alvaro et al., 2014). The scarcity of structural studies combined with modern sedimentology and sequence stratigraphy to test correlations between the groups in different inliers has led to a proliferation of synonymous names in the lithostratigraphic terminology: e.g. the Jbel Lkest Group in the Kerdous Inlier (Hassenforder, 1987; O'Connor, 2010), the Bleida-Tachdamt or Bleida Group in the Bou Azzer El Graara Inlier (Leblanc and Moussine-Pouchkine, 1994; Blein et al., 2014a), and the Taghdout Group (= Tizi n'Taghatine) in the Zenaga Inlier (Thomas et al., 2002, 2004; Bouougri and Saquaque, 2004). Correlation between these groups (recently combined into the Lkest-Taghdout Group, equivalent to the lower Anti-Atlas Supergroup; Gasquet et al., 2008; Álvaro et al., 2014) is both lithostratigraphic and structural. The only lithostratigraphic correlation linking the Siroua-Zenaga and Bou Azzer El Graara inliers was proposed by Bouougri and Saquaque (2004) who considered the section of the Tizi n'Taghatine mountain pass as a stratotype for the group named after this locality. Although their lithostratigraphy requires revision, we will refer to it in this work. Two reasons motivated this choice: (1) the dated samples of this study are from the same area that Bouougri and Saquaque (2004) focused on, and (2) the Siroua-Zenaga and Bou Azzer El Graara inliers are the only areas where modern sedimentology and sequence stratigraphy were applied (Fig. 1D). However, we will use the name of the lower Anti-Atlas Supergroup (an equivalent of the Lkest-Taghdout Group) because, although the latter group is widely known in the literature (Gasquet et al., 2008; Álvaro et al., 2014), it combines genetically unrelated sequences deposited in superimposed sedimentary basins and in different tectonic settings with long-lasted hiatuses along unconformities. Five major unconformity-bounded lithostratigraphic packages are further here distinguished: the lower Tasserda-Taghatine Group, the second Oumoula (Mimount) Formation, the third Tizi n'Taghatine Group, the fourth Tachdamt Formation, and the uppermost Bleida Formation.

For a long time, until 2013, available data on the lower Anti-Atlas Supergroup suggested that the continental passive margin developed during the Tonian between about 1000 Ma (based on stromatolite morphology pointing to a Neoproterozoic age; Choubert, 1963) and ca. 787 Ma (Rb–Sr isochron age of contact metamorphism of the host rocks associated with mafic dykes at Tachdamt; Clauer, 1976; Cahen et al., 1984). However, these age constraints are still debated (Gasquet et al., 2008; Alvaro et al., 2014; Ikenne et al., 2017; Soulaimani et al., 2018, 2019; Youbi et al., 2019). There are too few reliable geochronologic age constraints to tightly constrain the age of the lower Anti-Atlas Supergroup. It unconformably overlies the Eburnean basement, including the post-tectonic 2032 ± 5 Ma Azguemerzi granodiorite of the Zenaga Inlier, and in turn is unconformably overlain by the subhorizontal volcanic and sedimentary succession of the Late Ediacaran (ca. 606-541 Ma) Ouarzazate Supergroup (Fig. 6A and B). The lower Anti-Atlas Supergroup records a low-grade tectonometamorphic event related to the Pan-African Orogeny dated at 663 ± 13 Ma (Thomas et al., 2002) and 647.2 ± 1.7 Ma (Inglis et al., 2016) in the Siroua Inlier. Consequently, the depositional age of the lower Anti-Atlas Supergroup can be broadly bracketed between 2032 ± 5 Ma and 663 ± 13/647.2 ± 1.7 Ma.

The lower Anti-Atlas Supergroup sediments are intruded by abundant dolerite and gabbro dykes and sills, also found as dyke swarms and sill complexes in the Paleoproterozoic basement of the Zenaga (Fig. 4) and several other inliers (e.g. Igherm, Tagragra of Akka, Tagragra of Tata, Kerdous, and Bas Drâa). These rocks have been collectively called

the Ifzwane Suite in the Zenaga and Siroua inliers (Thomas et al., 2004), and the Toudma Suite in the Kerdous Inlier (Thomas et al., 2004; O'Connor, 2010).

Letsch (2018) showed that the quartzites of the Mimount Formation (*sensu* Thomas et al., 2002) and the Oumoula Formation (*sensu* Bouougri and Saquaque, 2004), overlying the basal, carbonate-quartzite-metapelite units near the Town of Taghdout at the northern margin of the Zenaga Inlier (see Thomas et al., 2002), do not contain detrital zircons younger than ca. 1987 Ma (Benziane, 2007; Walsh et al., 2012) and ca. 1809 Ma (Abati et al., 2010), respectively. Neoproterozoic detrital zircon grains only appear in the overlying formations of the Saghro and Bou Salda groups of the Siroua Inlier (Abati et al., 2010). Detrital zircons from the Mimount and Oumoula formations display exclusively Paleoproterozoic ages, suggesting a ca. 1890 Ma maximum depositional age for the upper parts of the formations. In the Ifni Inlier, detrital zircons from quartzites of the upper part of the

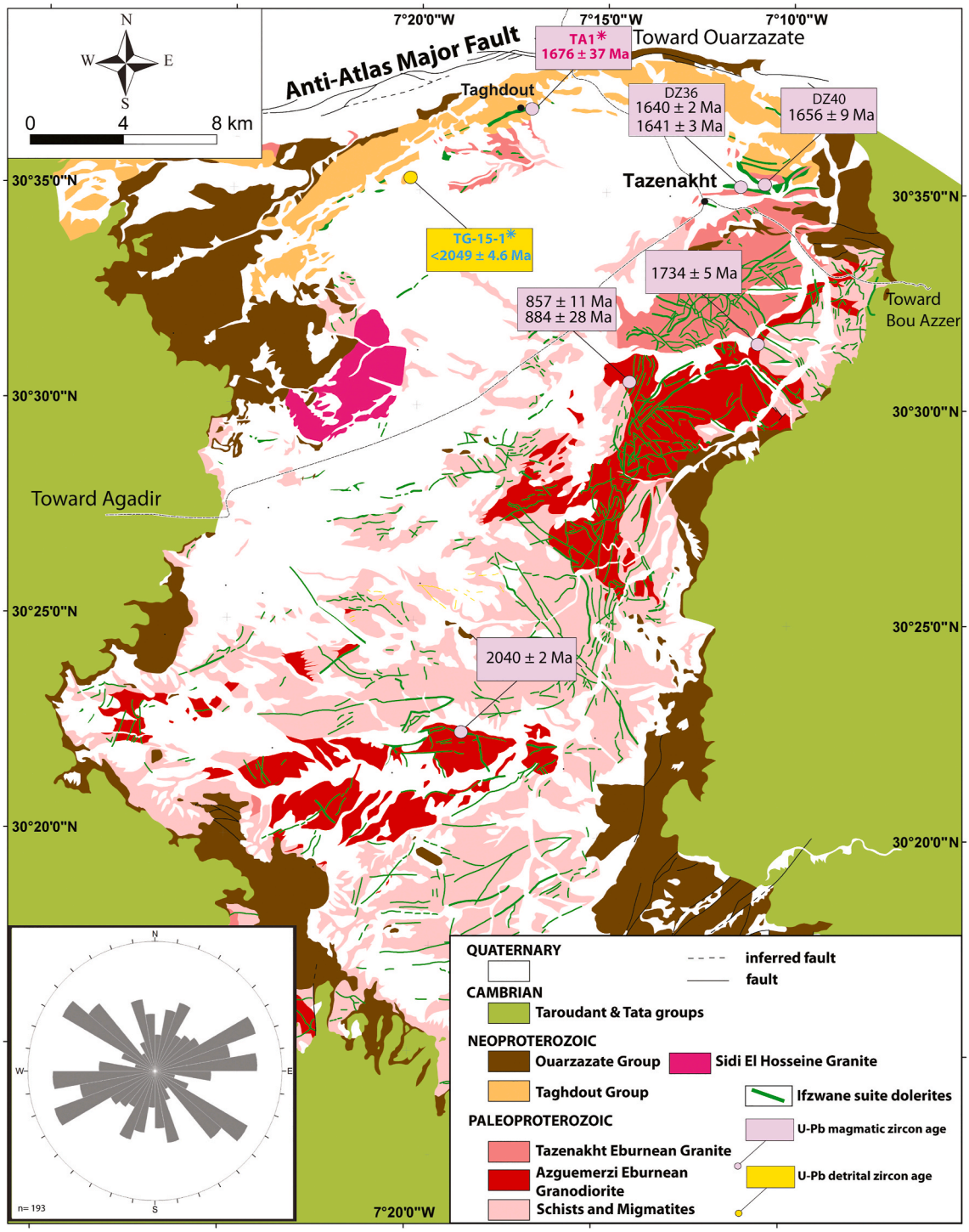

Fig. 4. Geology of the Zenaga Inlier (modified after Choubert, 1963; Ennih and Liégeois, 2001; Thomas et al., 2002; Kouyaté et al., 2013; Youbi et al., 2013). The Taghdout Group corresponds to the lower Anti-Atlas Supergroup (Thomas et al., 2004). Inset shows a rose diagram that summarizes mafic dyke trends measured from the map and Google Earth; n is the number of measurements. The U–Pb ages obtained in this study are indicated with asterisks; other age constraints are from literature (Kouyaté et al., 2013; Youbi et al., 2013).

Lkest Group (the basal group of the lower Anti-Atlas Supergroup) exhibit two main clusters in distribution of SHRIMP $^{207}Pb/^{206}Pb$ ages, 2060–1890 and 1810–1640 Ma (Schulte et al., 2016). The maximum depositional age is given by a weighted average $^{207}Pb/^{206}Pb$ date of 1744 ± 26 Ma based on four youngest concordant grains.

3. Sampling and analytical procedures

3.1. Sampling

In order to investigate the maximum depositional age of the lower Anti-Atlas Supergroup of the Anti-Atlas Belt, we collected five samples from two key inliers within the Anti-Atlas Orogen (Zenaga and Bou Azzer El Graara) for geochronological investigation. The Taghdout sill that intruded to the lower part of the lower Anti-Atlas Supergroup in the Zenaga Inlier was sampled for geochemistry and zircon U–Pb geochronology: sample TA1 was collected at the centre of the sill and herein dated at 1676 ± 37 Ma and sample TA2 is from the margin of the sill. Four metasedimentary samples were collected for detrital zircon U–Pb geochronology: one sample from metasiltstones of the Tasserda Formation of the Zenaga Inlier and three samples from the Agoummy, Tachdamt, and Bleida formations of the lower Anti-Atlas Supergroup in the Bou Azzer Inlier (Figs. 3–5). Sample site locations, a brief description of the samples, and their ages are provided in Table 1.

3.2. Analytical procedures

3.2.1. Whole-rock geochemistry

Elemental concentrations of whole rocks were obtained at "Service d'Analyse des Roches et des Minéraux" at the Geochemical and Petrographical Research Center in Nancy (SARM laboratory-CRPG-CNRS, Nancy, France). To avoid contamination, crushing and pulverizing were undertaken using agate mills. Powders were treated with $LiBO_2$, dissolved with HNO_3, and analyzed and calibrated with international geostandards (Basalt BE-N, Basalt BR, Dolerite WS-E, Microgabbro PM-S). Major and trace elements were analyzed using inductively coupled plasma atomic emission spectroscopy (ICP-AES) and Inductively Coupled Mass Spectrometry (ICP-MS), respectively. The analytical procedures are described in detail at http://helium.crpg.cnrs-nancy.fr/SARM/.

3.2.2. U–Pb geochronology

Zircon grains from all studied samples were separated from 3 to 5 kg of crushed rocks using conventional heavy liquid and magnetic separation techniques (jaw crusher, disk grinder, Wilfley table, Frantz isodynamic magnetic separator, and density separation using bromoform and methylene iodide) at the Centro de Pesquisas Geocronológicas, Universidade de São Paulo (CPGeo-USP), Brazil. About 20 to 100 zircon grains from each sample were mounted in epoxy resin, polished to approximately half of mean grain thickness for further imaging with transmitted light and cathodoluminescence to resolve internal grain texture. After coating with Au, cathodoluminescence (CL) images of zircon grains were obtained using a Quanta 250 FEG scanning electron microscope equipped with Mono CL3 + cathodoluminescence spectroscope (Centaurus) at the Centro de Pesquisas Geocronológicas of the University of São Paulo (CPGeo-USP), Brazil. The conditions used in CL analysis were as follows: 60 μA emission current, 15.0 kV accelerating voltage, 7 μm beam diameter, 200 μs acquisition time, and a resolution of 1024 × 884 pixels.

3.2.2.1. Sensitive High Resolution Ion Microprobe (SHRIMP II) analysis. Igneous zircon grains from the dolerite sample TA 1 and detrital zircon grains from the quartzite samples BA21 and BA24 were analyzed by the U–Pb isotopic technique using a SHRIMP II at CPGeo-USP following the analytical procedures of Williams (1998). The crystals were mounted, together with the TEMORA-2 reference zircon (Black et al., 2004), in epoxy and polished to expose the interior of the grains. Correction for common Pb was made based on ^{204}Pb measured, and the typical error

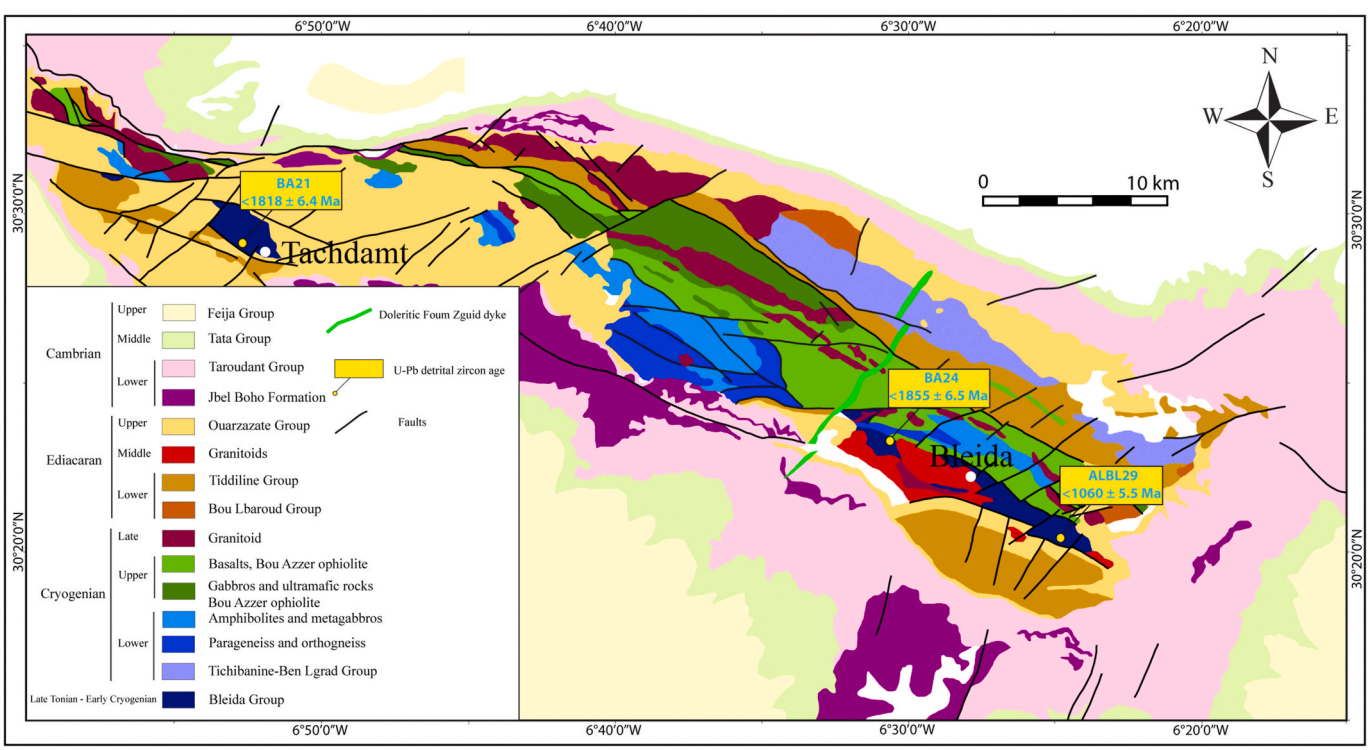

Fig. 5. Simplified geological map of the Bou Azer-El Graara Inlier showing the main lithotectonic units. The localities (Tachdamt and Bleida) mentioned in the text are indicated, as well as the location of samples used for U–Pb detrital geochronology (after Blein et al., 2014a). The Bleida Group corresponds to the lower Anti-Atlas Supergroup (Blein et al., 2014a).

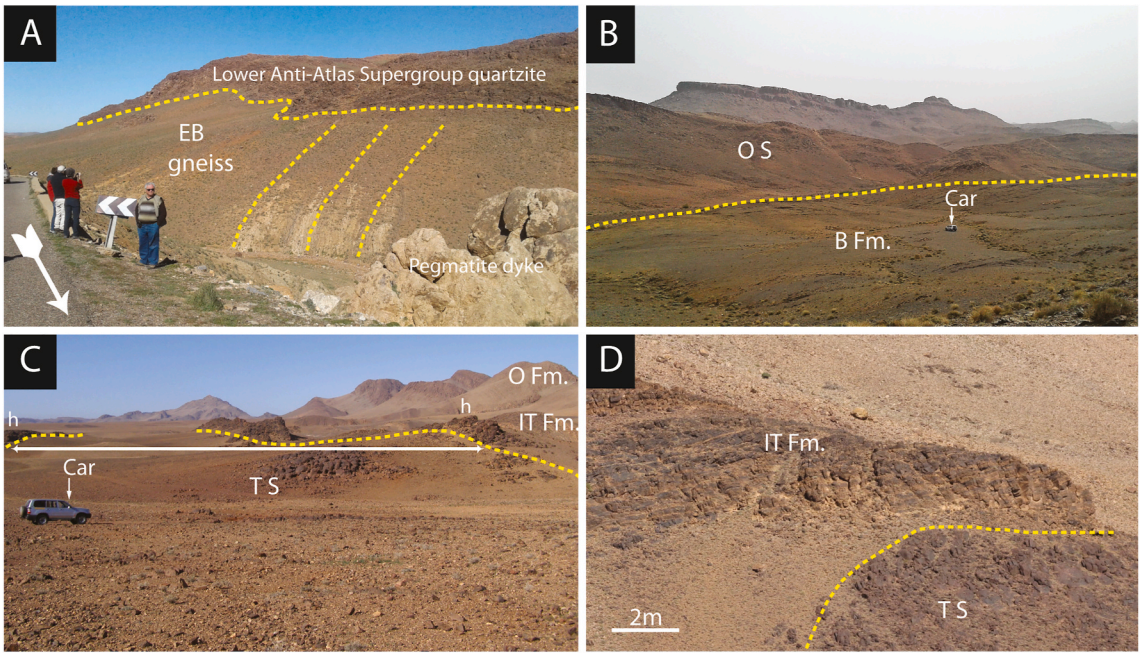

Fig. 6. (A) General view of the unconformity between the Eburnean basement and the overlying quartzites of Oumoula Formation (O Fm.) of the lower Anti-Atlas Supergroup at Tizi n'Taghatine locality. The Eburnean basement (EB: gneiss and schists) is crosscut by pegmatite dyke. The arrow indicates the road from Taliwine to Tazenakht. Geologists are Fida Medina, Maria Giuditta Fellin, Claudio Faccenna, and Riccardo Lanari; (B) View of the unconformity between the schists of the Bleida Formation (B Fm.) and the overlying volcanic rocks of the Ouarzazate Supergroup (OS); (C) View of the Taghdout sill (TS) crosscutting the mixed siliciclatic-carbonate succession of the Ifrane-n-Taghatine Formation (IT Fm.) in the Zenaga Inlier near the Taghdout Town. Note hornfels (h) at the baked margin of the sill. The Ifrane-n-Taghatine Formation is overlain by thick quartzites of Oumoula Formation (O Fm.); and (D) Detailed view of the upper contact between the Taghdout dolerite sill (TS) and limestones of the Ifrane-n-Taghatine Formation (IT Fm.) transformed into hornfels.

Table 1
Site location and summary of the data for the studied samples. The names of units and formations are sensu Bouougri and Saquaque (2004).

Sample ID	Coordinates (GPS WGS84)	Inlier/Subinlier	Lithology	Units/Formations/ Suites	Methods/ Mineral	Number of spots	U–Pb zircon Age (Ma)
BA24	N 30°23′7.90″, W 6°30′33.40″	Bou Azzer El Graara/Bleida	Fine-grained sandstone	Upper Unit/Bleida Formation	SHRIMPII/ Zircon	44 spots	1855 ± 6.5–977 ± 10[a]
ALBL29	N 30°20′19.28″, W 6°24′48.70″	Bou Azzer El Graara/Bleida	Medium to coarse-grained quartzite	Middle Unit/ Tachdamt Formation	LA-ICP-MS/ Zircon	96 spots	1060 ± 5.5–930 ± 12[a]
BA21	N 30°29′11.40″, W 6°52′44.00″	Bou Azzer El Graara/Tachdamt	Medium-grained quartzite	Lower Unit/Agoummy Formation	SHRIMPII/ Zircon	55 spots	1818 ± 6.4[a]
TA1	N 30°36′43.6″, W 7°17′13.4″	Zenaga	Coarse-grained to a fine-grained microlitic porphyric dolerite	Ifzwane Suite	SHRIMPII/ Zircon	18 spots	1676 ± 37[b]
TG-15-1	N 30°35′11.76″, W 7°20′06.92″	Zenaga	Purple coarse-grained and quartz rich metasiltstone	Lower Unit/Tasserda Formation	LA-ICP-MS/ Zircon	99 spots	2049.3 ± 4.6[a]

SHRIMPII: Sensitive High Resolution Ion Microprobe.
LA-ICP-MS: Laser Ablation Inductively Coupled Plasma Mass Spectrometry.
ID: Identification.
GPS WGS84: The Global Positioning System (GPS) uses the World Geodetic System (WGS84) as its reference coordinate system.
[a] U–Pb detrital zircon, maximum depositional age.
[b] U–Pb age emplacement.

for the $^{206}Pb/^{238}U$ ratio was less than 2%; uranium abundance and U/Pb ratios were calibrated against the TEMORA-2 reference material, and the ages were calculated using Isoplot® version 3.0 software application (Ludwig, 2003). Errors are reported as 1σ deviations and ages have been calculated at the 95% confidence level.

3.2.2.2. Laser ablation inductively coupled plasma mass spectrometry (LA-ICP-MS) analysis. U–Pb analyses of detrital zircon grains from the samples TG-15-1 and ALBL29 were performed using a Neptune multi-collector inductively coupled plasma mass spectrometer (MC-ICP–MS) and an Analyte G2 excimer laser ablation (LA) system at CPGeo-USP, Brazil. The U–Pb analysis was performed in the following order: two blanks, two 612 NIST standard glasses, three external standards, 13 unknown samples, two external standards, and two blanks. An interpolation of the four blank measurement sequences, using the bracketing method with two blanks before and two after the samples, was subtracted from all the seven measured masses (202, 204, 206, 207, 208, 232, and 238). The ^{235}U isotope was not measured, but calculated using the relative abundance $^{238}U/^{235}U = 137.88$. The ^{204}Hg interference on ^{204}Pb was corrected using ^{202}Hg and assuming $^{204}Hg/^{202}Hg = 4.350360$. Using the partially corrected $^{207}Pb/^{206}Pb$ ratio as an estimate for the age and the equations of Stacey and Kramers (1975), the $^{206}Pb/^{204}Pb$, $^{207}Pb/^{204}Pb$, and $^{208}Pb/^{204}Pb$ relative abundances were calculated and corrected for common (non-radiogenic) Pb fraction. Bracketing measurement of unknowns with NIST-612 standard glasses (two measurement sequences before and after) was used to convert the

total Pb, Th, and U signals to ppm concentrations.

A final bracketing (with three measurements before and two after unknown) with the GJ-1 reference zircon (Jackson et al., 2004) was used to correct the effect of the instrumental fractionation on four ratios ($^{206}Pb/^{238}U$, $^{207}Pb/^{235}U$, $^{207}Pb/^{206}Pb$, and $^{208}Pb/^{232}Th$) before they were used to calculate the respective ages. Errors in all arithmetic operations were algebraically propagated. Least squares fitting was used for the best line fit and all the data are reported at the 1σ level calculated with Isoplot 3.70 (Ludwig, 2008). A U–Pb analysis is concordant when it overlaps with the Concordia within uncertainty. So, it seems to be appropriate to exclude results with a low level of concordance ($^{206}Pb/^{238}U$ age/$^{207}Pb/^{206}Pb$ age × 100), but very large errors that overlap with the Concordia from interpretation. Thus, an interpretation with respect to the obtained ages was done for all grains within the concordance interval of 90–110% ($^{206}Pb/^{238}U$ age/$^{207}Pb/^{206}Pb$ age × 100) which is often used (e.g. Spencer et al., 2016). Discordant analyses were generally interpreted with caution. Analyses with discordance of more than 10% were discarded. For zircons younger than 1300 Ma, $^{206}Pb/^{238}U$ ages were preferred, while for older zircons the $^{207}Pb/^{206}Pb$ ages were used. The detrital zircon age distribution by probability density was performed using the AgeDisplay application (an EXCEL workbook to evaluate and display univariate geochronological data using binned frequency histograms and probability density distributions) (Sircombe, 2004).

4. Results

4.1. The great mafic sill of the Ifzwane Suite at Taghdout Town

4.1.1. Field observations

The Taghdout sill was collected near Taghdout Town, ca. 9 km NW of Tazenakht City (Table 1 and Figs. 3 and 4), from a 227 m thick, well-preserved, massive sill belonging to the Ifzwane Suite (dolerite dyke swarm and sill complex of the Zenaga Inlier, of likely multiple ages as discussed in Sec. 2.1). The sill intruded into the lower part of the lower Anti-Atlas Supergroup (Fig. 6C), which mainly consists of carbonate and mixed siliciclastic-carbonate sequence of the Ifrane-n-Taghatine Formation (Bouougri and Saquaque, 2004). The sill can be traced in outcrops for more than one km in length and has thick chilled margins of marble grading away from the intrusion into carbonate host rock (Figs. 3, 4., and 6D). The following new samples were used in this study: TA1 (centre of the sill) and TA2 (border of the sill) from the Taghdout sill of the Zenaga Inlier.

4.1.2. Petrographic features

Fresh samples of the Taghdout sill are dark-grey, but due to widespread hematitic alteration the rock appears reddish. However, the original texture and primary igneous mineralogy are usually well preserved. The texture varies from a coarse-grained doleritic texture in the centre of the sill to a fine-grained, microlitic porphyric texture at the border of the sill (Fig. 7).

The primary igneous minerals consist of clinopyroxene (augite and locally pigeonite), very rare orthopyroxene, plagioclase, and oxides. Apatite and zircon are present as accessory minerals; amphibole and, more rarely, biotite are found around pyroxene crystals or as irregular patches in the groundmass. Although tholeiitic mafic rocks are generally characterized by low alkaline content ($Na_2O + K_2O$), granophyric quartz/K-feldspar mesostasis was observed in coarse-grained portions of the sill, consistent with the examples previously described in literature (e.g. Fodor, 2009; Block et al., 2015). The secondary mineral assemblage includes albite, chlorite, actinolite, epidote, titanite, calcite, and quartz, which is characteristic for the greenschist facies of metamorphism.

4.1.3. Geochronology: U–Pb dating of the Great Taghdout sill

The zircon grains from the sample TA1 range in length from 120 to 150 μm. Cathodoluminescence (CL) images (Fig. S1 of supplementary data) show that most zircons are stubby sub-euhedral to euhedral, with a typical oscillatory zoning within a large uniform central zone, followed by much finer, poorly resolvable oscillatory zoned bands. Some grains lack any zoning (Fig. S1 of supplementary data). We analyzed 18 spots on 13 zircon grains (Table S1 of supplementary data). High Th/U ratios (between 1.18 and 3.38) support a magmatic origin for the zircons (Fig. 8) (cf. Möller et al., 2003; Hoskin and Schaltegger, 2003; Linnemann et al., 2007). Most of the analyzed spots with high U and Th concentrations show evidence for significant Pb loss. On the Wetherill diagram, these thirteen analyses are aligned along a discordia that shows two intercepts with the concordia (Fig. 9A): an upper intercept with an age of 1639 ± 34 Ma and a lower intercept with an age of 688 ± 65 Ma. The age of 1639 ± 34 Ma is interpreted to reflect the time of magmatic emplacement of the sill, whereas the 688 ± 65 Ma age is thought to correspond to the time of a metamorphic and/or thermal overprint event. However, these intercept ages have a very high Mean Square Weighted Deviation (MSWD = 6.8), making this age poorly constrained. In contrast, analyses with low Th and U concentrations (Th < 1000 ppm, spots 2.1, 7.1, and 13.1) produced nearly concordant $^{207}Pb/^{206}Pb$ ages. We therefore calculated the weighted mean average $^{207}Pb/^{206}Pb$ age for those spots characterized by low Th and U concentrations, obtaining a mean $^{207}Pb/^{206}Pb$ age of 1676 ± 37 Ma (n = 3, MSWD = 3.1; Fig. 9B).

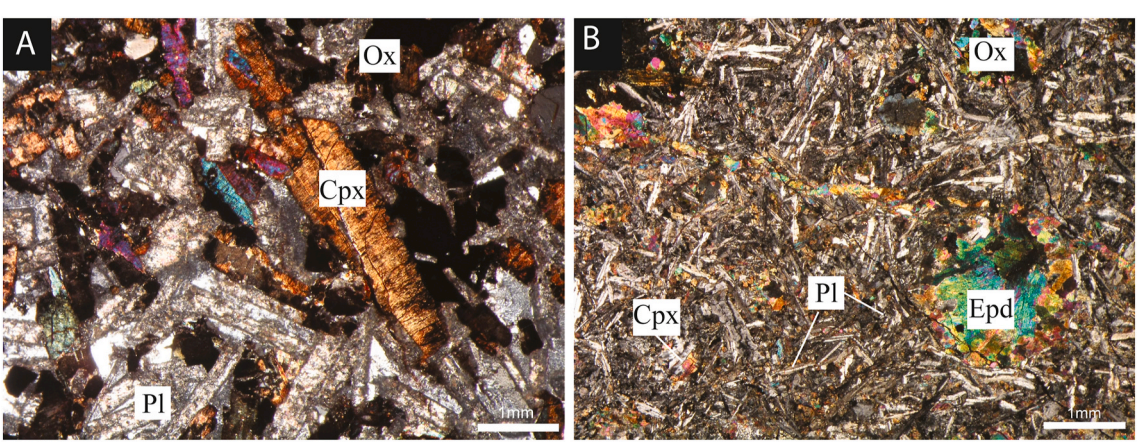

Fig. 7. Thin-section photomicrographs of the Great Taghdout sill. (A) coarse-grained dolerite in the centre of the sill with plagioclase (Pl) and clinopyroxene (Cpx) minerals and oxides (Ox), crossed nicols; (B) fine-grained, microlitic porphyric texture at the border of the sill with microlites (tiny crystals) of plagioclase (Pl) and clinopyroxene (Cpx) minerals and oxides (Ox). Epidote (Ep) is filling vesicles; crossed nicols.

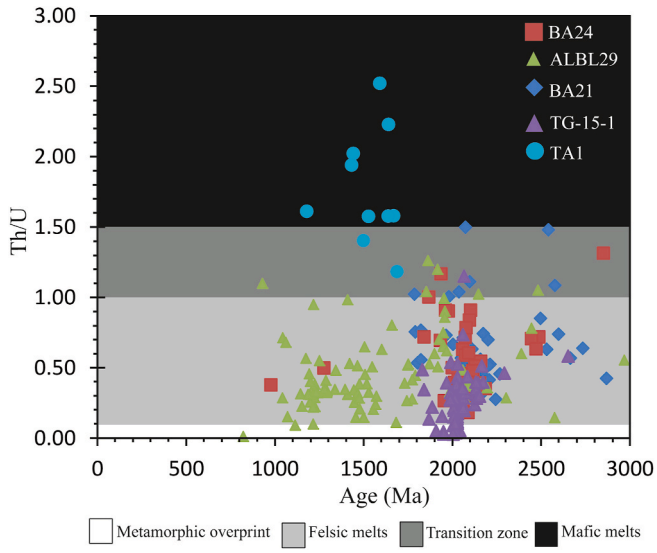

Fig. 8. Th/U ratios versus concordant U–Pb ages of igneous and detrital zircon grains of the lower Anti-Atlas Supergroup.

4.1.4. Geochemical characteristics

The major and trace element composition of previously studied and new samples (TA1 and TA2) are listed in Table 2. On the total alkali versus silica diagram (Fig. 10A), the studied samples TA1 and TA2 and the ca. 1.6 Ga doleritic dykes and sills previously analyzed by Youbi et al. (2013) plot in the subalkaline basalt field. These additional dolerites are: DZ 36 (dated at 1640 ± 2 Ma and 1641 ± 3 Ma; Kouyaté et al., 2013) and DZ 40 (dated at 1656 ± 9 Ma; Kouyaté et al., 2013) of the Zenaga Inlier (close to Tazenakht City), and doleritic dyke (AMHA069 dated at 1654 ± 16 Ma; Kouyaté et al., 2013) from the Agadir Melloul Inlier. This subalkaline affinity is also evident from Nb/Y ratios that are below 0.67 (cf. Pearce and Cann, 1973; Winchester and Floyd, 1977). Additionally, their non-orogenic tholeiitic character is shown in the Ti vs. V diagram of Shervais (1982) (Fig. 10B) with the data plotting exclusively within the Continental Flood Basalt (CFB) and Mid-Ocean Ridge Basalt (MORB) fields (20 < V/Ti < 50). When plotted on a multi-element variation diagram (spidergram; Fig. 11), the dated dykes display patterns similar to some continental tholeiites such as those of the Central Atlantic Magmatic Province (CAMP) with a moderate enrichment in large-ion lithophile elements (LILE) and distinct positive Pb and negative Nb anomalies (Bertrand et al., 1982; Youbi et al., 2003; Marzoli et al., 2004, 2019; Tegner et al., 2019). Nb anomalies have been related to crustal contamination or the influence of a subduction zone, which was either active during magma generation or earlier metasomatized lithospheric mantle with which asthenospheric magma interacted during ascent (e.g. Thompson et al., 1982; Dupuy and Dostal, 1984; Coish and Sinton, 1992; Dorais et al., 2005). Furthermore, the negative Nb anomaly is accompanied by negative P anomaly; this pattern is similar to some low-Ti CFB tholeiitic magmas contaminated by continental crust. This and the relatively high Ti/V ratios (see Fig. 10B) point to a non-orogenic origin of the mafic magmas, which were contaminated with continental crust during magma ascent/emplacement (Ikenne, 1997; Hafid, 1999; Hafid et al., 2001; El Aouli et al., 2004, 2010; El Bahat et al., 2013, 2017; Youbi et al., 2013).

4.2. Geochronology: detrital zircon study of the lower Anti-Atlas Supergroup

4.2.1. Metasiltstone of the Tasserda Formation: sample TG-15-1

The sample TG-15-1 (Table 1) is purple, coarse-grained quartz-rich metasiltstone collected from the Tasserda Formation near the village of Taghadout (Figs. 3 and 4). The Tasserda Formation consists of thick-to medium-bedded quartz arenites with few channels filled with conglomerates. The main mineral components of siltstone are quartz and feldspar embedded in a sericite-rich matrix (Fig. 12A).

The zircon grains of this sample exhibit mean lengths and widths of 120 and 60 μm, respectively. In most cases, they are sub-euhedral to euhedral in shape. The internal texture of zircon grains shows oscillatory concentric, sector, and banded zoning (Fig. S2 of supplementary data). The Th/U ratio ranges from 0.03 to 1.15 (Fig. 8). About 83% of the analyzed zircons have Th/U ratios larger than 0.1, potentially indicating that they were derived from intermediate to felsic igneous rocks (cf. Möller et al., 2003; Hoskin and Schaltegger, 2003; Linnemann et al., 2007). The other 17% have a Th/U ratio below 0.1 and could be of metamorphic origin. From the total of 99 measured spots, 74 yielded less than 10% discordant ages (Table S2 of supplementary data). About 99% of the zircon population is of Paleoproterozoic age (26% are Rhyacian and 73% are Orosirian), ranging from 2294 ± 32 Ma to 1831 ± 35 Ma, with a prominent peak at around 2022 Ma and three minor peaks at about 2294, 2142, and 1870 Ma. One remaining analysis, representing 1% of the concordant ages of this sample, yielded an age of 2653 ± 32 Ma (Fig. 13A and B). The dominance of the Paleoproterozoic ages indicates that almost all of the detrital zircon grains were derived from the Paleoproterozoic (Eburnean) crust. The seven youngest zircon grains yielded a concordia age of 2049.3 ± 4.6 Ma, which constrains the maximum depositional age of the Tasserda Formation (Fig. 13A and B).

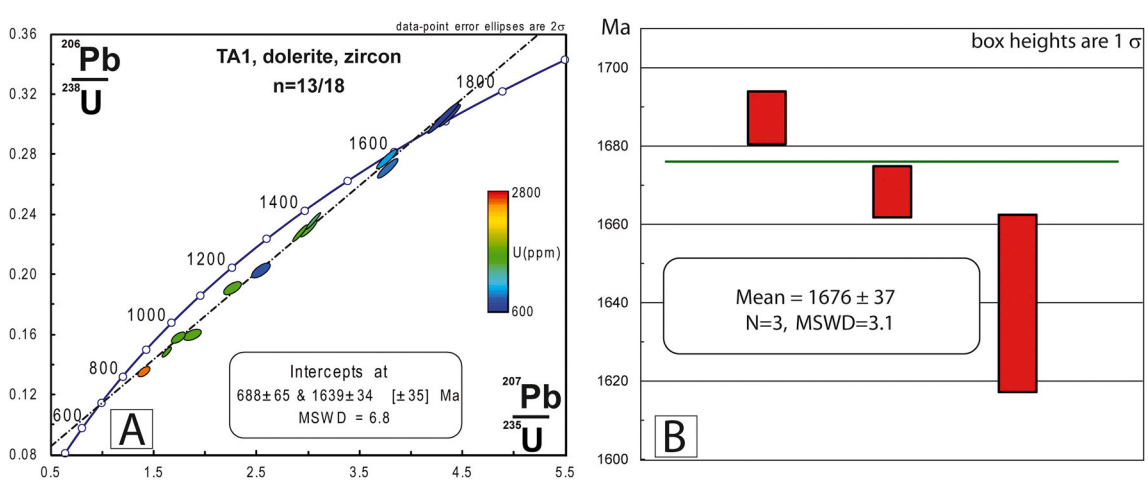

Fig. 9. Zircon U–Pb SHRIMP geochronology: (A) Wetherill concordia plots of U–Pb zircon data for the Taghdout sill (sample TA) of the Zenaga Inlier. (B) Weighted mean average $^{207}Pb/^{206}Pb$ age of analysis with low Th and U concentrations (spots 2.1, 7.1, and 13.1).

Table 2
Representative whole-rock major and trace element geochemical data for dykes and sills from the Zenaga, Agadir Melloul, Iguerda-Taïfast, and Tagragra of Akka inliers including the dated dykes, samples TA1 from the Zenaga Inlier (1676 ± 37 Ma; this work), DZ 36 (1640 ± 2 Ma and 1641 ± 3 Ma; Kouyaté et al., 2013) and DZ 40 (1656 ± 9 Ma; Kouyaté et al., 2013) from the Zenaga Inlier (Kouyaté et al., 2013), and AMHA069 (1654 ± 16 Ma; Kouyaté et al., 2013) from the Agadir Melloul Inlier. The geochemical data are from unpublished theses (Hafid, 1999; Mortaji, 1989) and published papers (Hafid et al., 2001; El Aouli et al., 2010; Youbi et al., 2013). Fe_2O_{3t} = total Fe expressed as Fe_2O_3. Loss-on-ignition (L.O.I.) determined by sample weight loss at 1000 °C.

Sample	TA1	TA2	DZ36	DZ40	AMHA69	ZEN-4	ZEN-13	ZEN-1	ZEN-11	IT-5	IT-7	IT-12	IT-13	NC40	NC379	NC314aMor	NC 361
Inlier	Zenaga	Zenaga	Zenaga	Zenaga	Agadir Melloul	Zenaga	Zenaga	Zenaga	Zenaga	Iguerda-Taïfast	Iguerda-Taïfast	Iguerda-Taïfast	Iguerda-Taïfast	Tagragra of Akka	Tagragra of Akka	Tagragra of Akka	Tagragra of Akka
Latitude N	30°36′43.6″	30°36′43.7″															
Longitude W	7°17′13.4″	7°17′13.3″															
Orientation	N45°	N45°	N125°	N140°		N170°	N125°	N85°	N170°		N00°	N30°	N45°	N50°-N110°	N50°-N110°	N30°-N160°	N30°-N160°
Ages (Ma)	1676 ± 37		1640 ± 2/1641 ± 3	1656 ± 9	1654 ± 16												
Reference	(this work)	(this work)	Kouyaté et al., 2013	Kouyaté et al. (2013)	Kouyaté et al. (2013)	Hafid (1999)	Hafid (1999)	Hafid (1999)	Hafid (1999)	Hafid (1999)	Hafid (1999)	Hafid (1999)	Hafid (1999)	Mortaji (1989)	Mortaji (1989)	Mortaji (1989)	Mortaji (1989)
SiO2	49.31	49.73	50.66	50.84	45.78	48.56	49.71	48.38	48.30	49.12	49.98	49.00	47.98	50.85	47.58	44.35	49.18
TiO2	1.64	1.58	0.85	0.73	0.79	2.66	2.09	1.98	1.64	2.05	2.52	2.17	2.06	0.91	1.93	2.86	2.99
Al2O3	13.79	13.48	14.55	14.61	13.73	13.58	14.08	13.97	13.97	13.50	13.67	13.06	13.20	14.72	13.62	15.25	12.75
Fe2O3t	14.51	14.35	10.27	9.78	9.50	14.43	14.83	13.71	13.16	15.17	15.02	14.87	15.54	12.60	15.63	16.53	16.06
MnO	0.23	0.23	0.16	0.18	0.25	0.17	0.19	0.16	0.20	0.26	0.17	0.23	0.26	0.19	0.20	0.18	0.12
MgO	6.34	6.68	7.31	7.55	9.87	6.61	5.76	6.55	7.73	5.28	5.24	5.91	6.24	6.69	6.29	5.95	5.21
CaO	6.70	6.20	10.01	11.27	12.18	8.71	8.51	10.18	10.34	8.52	6.98	10.04	8.40	7.22	8.82	7.16	4.36
Na2O	3.26	4.06	2.17	1.94	2.49	2.40	2.59	1.86	2.10	2.46	2.45	1.91	2.73	3.36	2.04	2.58	2.63
K2O	0.96	0.32	0.74	0.62	0.29	0.54	0.78	0.32	0.64	1.15	1.79	0.36	0.95	0.14	0.77	1.04	1.31
P2O5	0.14	0.19	0.07	0.08	0.06	0.24	0.33	0.18	0.15	0.43	0.36	0.19	0.17	0.14	0.24	0.69	0.50
L.O.I.	2.47	3.04	2.48	2.38	4.37	2.35	2.18	2.67	2.02	1.46	1.73	2.07	1.99	3.67	2.69	3.80	5.00
Total	99.34	99.84	99.49	100.25	99.68	100.25	101.05	99.96	100.25	99.40	99.91	99.81	99.52	100.49	99.81	100.39	100.11
V	343.24	317.91	240.00	233.70	223.00	326.90	317.14	306.30	332.92	290.97	339.52	400.00	413.57	278.00	367.00	189.00	367.00
Cr	18.95	18.83	307.70	410.10	802.70	189.80	96.76	197.10	181.59	114.14	126.86	113.12	180.31	139.00	114.00	180.00	118.00
Co	51.53	54.75	46.00	44.67	57.36	43.13	50.47	40.43	55.85	44.43	46.07	44.10	43.62	57.00	54.00	46.00	46.00
Ni	39.42	37.22	143.00	185.20	178.30	117.00	69.71	94.16	121.74	44.20	64.28	79.64	92.72	55.00	95.00	109.00	65.00
Zn	126.00	158.84	90.36	92.06	228.20	150.20	152.60	119.80	161.27	131.25	129.48	134.44	155.27		116.00	153.00	62.00
Rb	35.95	8.84	26.89	20.34	10.88	16.85	20.90	8.44	19.70	63.40	68.05	24.02	45.85	10.00	43.00	29.00	81.00
Sr	192.75	220.51	215.20	196.60	191.10	391.10	410.50	269.90	256.15	372.90	370.30	253.56	200.55	593.00	185.00	247.00	120.00
Y	23.11	23.50	16.27	14.16	12.11	28.80	30.91	27.12	22.87	37.00	28.97	29.81	28.79	19.46	30.85	41.74	26.22
Zr	88.44	93.50	69.43	56.11	40.35	151.90	123.40	87.81	75.23	142.31	178.72	111.29	108.45		122.00	293.00	167.00
Nb	6.80	7.02	4.56	3.64	2.99	13.10	7.60	4.62	3.77	8.57	15.77	7.74	8.29		10.00	36.00	20.00
Ba	238.53	148.42	146.60	342.30	43.29	169.70	482.90	70.51	113.54	762.92	700.14	224.48	425.88	103.00	274.00	528.00	418.00
La	8.50	9.31	9.45	7.77	3.82	18.75	25.71	8.90	8.06	26.09	30.90	7.84	8.38	10.47	9.79	31.79	18.87
Ce	20.35	22.54	20.54	16.79	8.92	50.90	63.10	23.08	19.89	59.41	70.09	21.36	21.78	27.83	28.15	70.15	45.07
Pr	2.87	3.24	2.51	2.06	1.24	5.75	6.45	3.18	2.75	7.76	8.92	3.23	3.28				
Nd	13.34	15.24	11.26	9.54	6.45	25.95	26.89	14.22	12.43	33.49	37.03	16.27	15.26	13.43	17.19	40.17	27.38
Sm	3.65	4.05	2.74	2.29	1.84	6.44	6.11	4.55	3.81	7.32	7.46	4.56	4.44	3.60	5.26	8.75	7.06
Eu	1.36	1.31	0.87	0.78	0.68	2.21	2.07	1.56	1.31	1.96	2.42	1.68	1.53	1.01	1.52	1.87	2.32
Gd	3.98	4.24	2.81	2.42	2.11	6.61	6.10	4.47	3.55	6.89	7.19	5.96	5.53	3.40	5.49	7.93	6.94
Tb	0.66	0.69	0.47	0.39	0.35	1.07	0.99	0.84	0.67	1.06	1.05	0.96	0.93				
Dy	4.27	4.38	2.87	2.44	2.14	5.68	5.75	5.02	4.05	6.69	5.91	5.58	5.70	3.35	5.65	7.94	5.55
Ho	0.89	0.93	0.57	0.49	0.43	1.11	1.16	1.03	0.83	1.41	1.18	1.13	1.19				
Er	2.38	2.41	1.61	1.39	1.19	2.68	3.00	2.66	2.24	3.66	2.99	3.04	3.08	1.99	2.97	4.35	2.55
Tm	0.34	0.34	0.24	0.21	0.18	0.37	0.44	0.39	0.32	0.56	0.42	0.45	0.46				
Yb	2.21	2.26	1.62	1.38	1.14	2.39	2.70	2.45	1.88	3.34	2.53	2.68	2.77	2.01	2.82	4.12	2.04
Lu	0.34	0.36	0.25	0.22	0.18	0.35	0.39	0.36	0.29	0.51	0.37	0.40	0.42	0.37	0.46	0.67	0.36
Cu	279.90	20.75	67.27	60.43	193.30	22.64	61.31	68.13	10.68	73.30	20.24	200.74	18.26	15.00	148.00	33.00	18.00
U	0.28	0.32	0.53	0.41	0.14	0.54	0.47	0.24	0.25	0.40	1.65	0.18	0.21				
Th	0.81	0.92	1.69	1.33	0.37	1.77	2.42	0.89	0.79	1.70	3.65	0.64	0.80				
Ta	0.51	0.54	0.36	0.28	0.23	0.82	0.24	0.19	0.20	0.48	1.00	0.59	0.59				
Hf	2.45	2.65	2.00	1.61	1.16	3.86	3.03	2.29	1.95	3.99	4.92	3.36	3.29				
Sc	48.93	48.88				32.09	41.73	39.63	48.49	38.97	28.38	38.58	41.10		45.00	35.00	30.00
Ga	20.82	19.25	16.88	15.52	13.62	21.02	21.94	18.46	19.54	21.78	22.31	19.06	18.76				
Pb	4.00	4.47	8.16	16.85	8.78	7.07	9.65	5.42	5.55	8.50	6.98	5.52	5.90				
Cs	0.87	0.45	1.17	0.65	0.30	1.05	1.15	0.73	1.21	7.09	1.39	1.41	2.00				

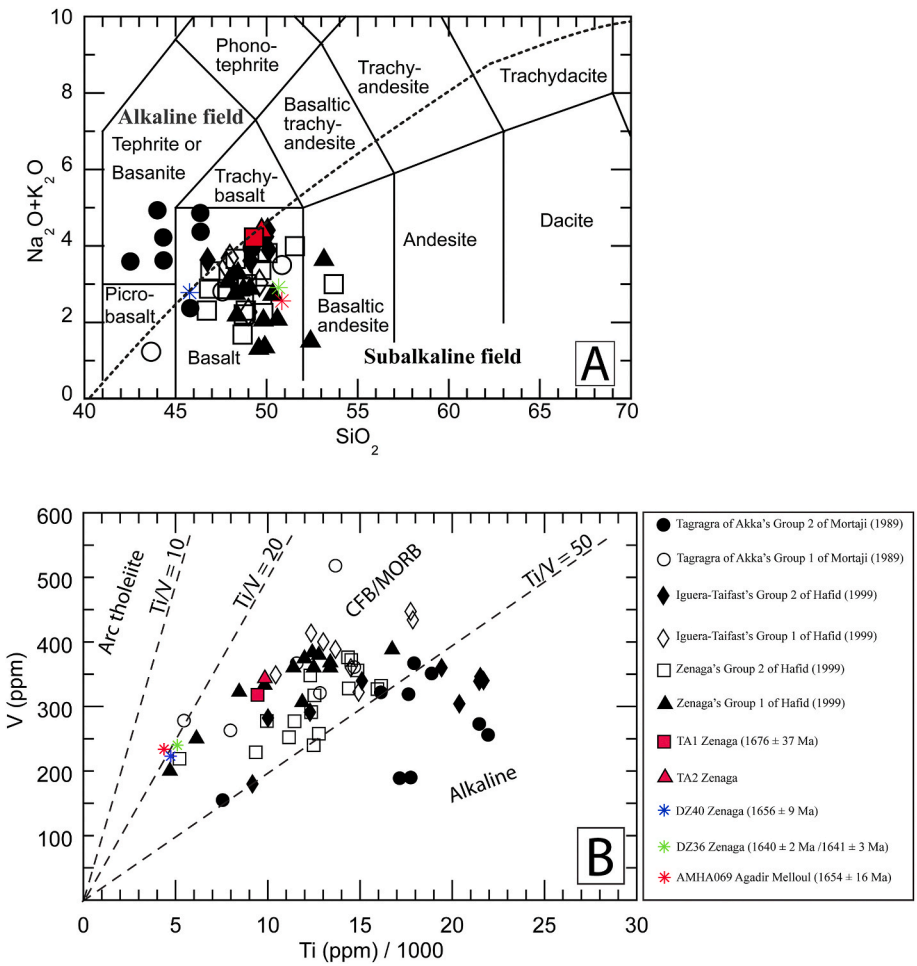

Fig. 10. (A) Total alkali vs. silica (TAS) diagram for the chemical classification and nomenclature (after LE Bas et al., 1986). Subalkaline vs. alkaline series boundary (dotted line) is from Irvine and Baragar (1971). (B) Ti vs. V variations in samples from the Zenaga, Agadir Melloul, Iguerda-Taïfast, and Tagragra of Akka inliers including four datasets reported by Mortaji (1989, unpublished thesis), Hafid (1999, unpublished thesis), Hafid et al. (2001) and El Aouli et al. (2010); diagram is after Shervais (1982). The studied samples TA1 (centre of the sill dated at 1676 ± 37 Ma; this work) and TA2 (border of the sill) and the 1.6 Ga dolerite dykes and sills from the Zenaga and Agadir Melloul inliers collected by Kouyaté et al. (2013) are also shown on this diagram.

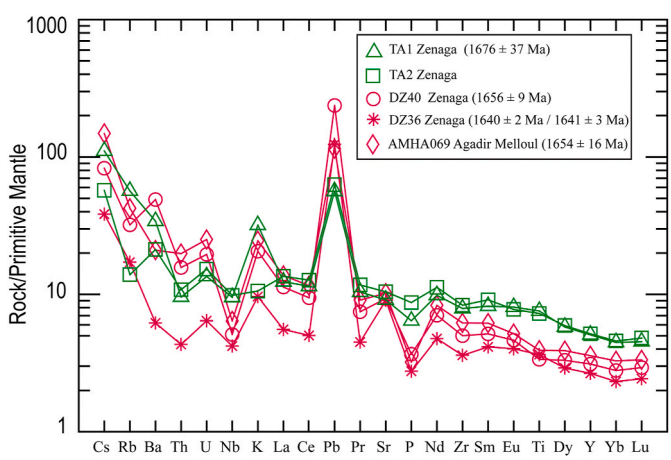

Fig. 11. Primitive mantle-normalized trace element 'spidergram' for the dated mafic sill and dykes of the Zenaga and Agadir Melloul inliers. Primitive mantle values used for normalization are from Sun and McDonough (1989).

4.2.2. *Quartzites of the Agoummy Formation: sample BA21*

The sample BA21 (Table 1) is a medium-grained quartzite collected from the Agoummy Formation at the Tachdamt section (Figs. 3 and 5). The Agoummy Formation consists of thick-to medium-bedded quartzites with few conglomerates nested in channels.

The quartzites are dominated by quartz that is mainly subrounded. Some quartz grains show overgrowth rims. The rock is moderately sorted with a matrix that consists of silt-sized quartz and mica minerals such as sericite. Intergranular voids are filled with secondary Fe–Ti oxides (Fig. 12B).

Zircons from this sample have a mean length and width of 110 and 70 μm, respectively. Zircon grains are mainly sub-rounded to rounded in shape with some euhedral crystals (Fig. S3 of supplementary data). Most of them show oscillatory zoning, suggesting that they are of igneous origin. This is corroborated by their Th/U ratios ranging from 0.19 to 1.50 (Fig. 8). The internal textures include oscillatory zoning, planar zoning, banded zoning, and a minor portion with sector zoning. A total of 55 spots have been analyzed (Table S3 of supplementary data), of which 50 yielded 90–110% concordant ages. About 84% are Paleoproterozoic (Statherian - 4%, Orosirian - 24%, Rhyacian - 54%, and Siderian - 2%), 12% of all ages are Neoarchean and 4% are Mesoarchean (2869 ± 8 Ma and 2857 ± 32 Ma). The Neoarchean ages range from 2735 ± 11 to 2531 ± 18 Ma, while the Paleoproterozoic ages range from 2498 ± 14 to 1786 ± 20 Ma. The probability-density plot is dominated by peaks at ca. 2205, 2080, 2035, and 1812 Ma. The six youngest grains, ranging from 1834 ± 24 Ma to 1786 ± 20 Ma, combined yield a concordia age of 1818 ± 6.4 Ma (MSWD = 1.5; probability = 0.22), which likely represents the maximum depositional age for the Agoummy Formation (Fig. 13C and D).

4.2.3. *Quartzites of the Tachdamt Formation: sample ALBL29*

The sample ALBL29 (Table 1) is a medium-to coarse-grained, poorly sorted quartz arenite from the lowermost part of the Tachdamt Formation at the Bleida section (Figs. 3 and 5). This formation consists of basaltic lava flows and interbedded volcanic breccias, lapilli tuffs, and volcanoclastic sediments. The mineral assemblage mainly consists of quartz with a small amount of feldspar and a matrix of silt-sized quartz

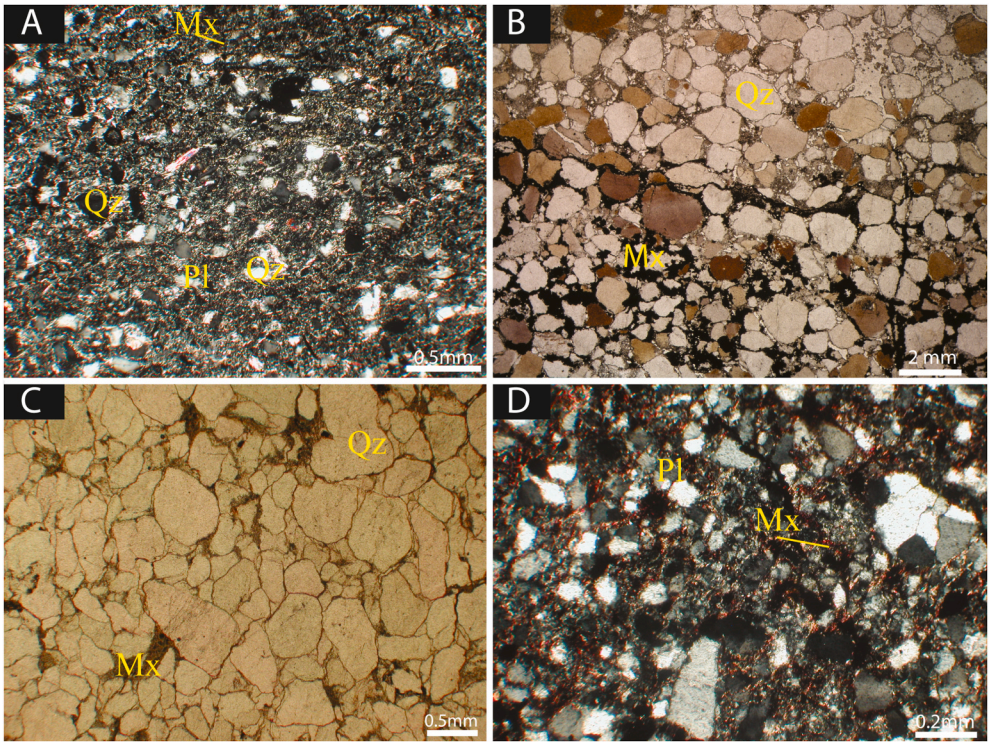

Fig. 12. Thin section photomicrographs of the sedimentary samples. (A) Metasiltstones of the Tasserda Formation: sample TG-15-1; purple, coarse-grained and quartz-rich metasiltstone with quartz (Qz) and feldspar (Pl) embedded in a sericite-rich matrix (Mx); crossed nicols. (B) Quartzites of the Agoummy Formation: sample BA21, with quartz grains that are mostly subrounded. (C) Quartzites of the Tachdamt Formation: sample ALBL29, with a mineral assemblage comprised mainly of quartz (Qz) associated to a small amount of feldspars (Pl) with a matrix (Mx) of silt-sized quartz and mica minerals. (D) Metasandstone of the Bleida Formation: sample BA24, fine-grained, moderately sorted metasandstone with quartz (Qz), plagioclase (Pl), and lithic fragments in mica matrix (Mx). (For interpretation of the references to colour in this figure legend, the reader is referred to the Web version of this article.)

and mica minerals (Fig. 12C).

Zircon grains from this sample exhibit a mean length and width of 160 and 90 μm, respectively. The grains are sub-rounded and euhedral (Fig. S4 of supplementary data). The internal textures predominantly show concentric zoning, with few grains lacking any zoning. The Th/U ratio ranges from 0.01 to 1.26, with a dominant population of likely igneous origin (98%; 0.1 to 1.26) and a minor population with a potentially metamorphic origin (2%; 0.01 to 0.1; Fig. 8). Out of 96 measured spots (Table S4 of supplementary data), 92 yielded less than 10% discordant ages (Fig. 14A and B). About 54% of the ages are Mesoproterozoic (Calymmian - 22%, Ectasian - 17%, and Stenian - 17%), 41.3% of the ages are Paleoproterozoic (Siderian - 4%, Rhyacian - 8%, Orosirian - 18%, and Statherian - 11%), 2% of the ages are Neoproterozoic (Tonian), 1% of the ages are Mesoarchean, and 1% of the ages are Neoarchean. Neoarchean and Mesoarchean ages are each represented by one analysis at 2577 ± 53 and 2969 ± 48 Ma, respectively. Paleoproterozoic ages range from 2482 ± 66 to 1603 ± 175 Ma with two prominent peaks at ca. 1978 and 1752 Ma. The Mesoproterozoic ages range from 1572 ± 55 to 1043 ± 12 Ma with four prominent peaks at ca. 1525, 1280, 1208, and 1060 Ma. The Neoproterozoic age at 822 ± 6 Ma is only 92% concordant and has a very low Th/U ratio of 0.01 indicating some overprint of the zircon grain. This grain is therefore not used to calculate a maximum depositional age. The inferred maximum age of deposition is set by a concordia age derived from the youngest population of concordant grains at 1060 ± 5.5 Ma (four grains), and 930 ± 12 Ma, a 100% concordant single grain analysis with a Th/U ratio of 1.10 (Fig. 14A and B).

4.2.4. Metasandstone of the Bleida Formation: sample BA24

The sample BA24 (Table 1) is a fine-grained, moderately sorted metasandstone from the middle part of the Bleida Formation (Figs. 3 and 5) at the Bleida section. The Bleida Formation consists of up to 600 m thick siliciclastic deposits interbedded with volcanoclastics. The sample contains quartz, plagioclase, and lithic fragments with matrix bearing clays, sericite, muscovite, and chlorite. The grains are subangular to subrounded indicating that the sediment is immature (Fig. 12D).

The zircon grains of this sample exhibit a mean length and width of 125 and 85 μm, respectively, and most of them are sub-rounded to subangular in shape. The internal texture of the zircons revealed by CL images comprise concentric and sector zoning, and some unzoned grains (Fig. S5 of supplementary data). The Th/U ratio ranges from 0.18 to 1.31, indicating a magmatic origin of the zircon grains (Fig. 8). Of 44 measured spots (Table S5 of supplementary data), 40 yielded less than 10% discordant ages. A total of 93% exhibits Paleoproterozoic ages (Siderian - 7%, Rhyacian - 49%, and Orosirian - 37%), Mesoarchean, Mesoproterozoic, and Neoproterozoic populations are each 2%. The Mesoarchean is represented by one age of 2852 ± 7 Ma, while the Paleoproterozoic ages range from 2487 ± 6 to 1841 ± 12 Ma with one prominent peak at ca. 2075 Ma and three minor peaks at ca. 2158, 1960, and 1852 Ma. The only Mesoproterozoic age is 1276 ± 14 Ma and the Neoproterozoic age is 977 ± 10 Ma. Two youngest grains, overlapping within errors, give a concordia age of 1855 ± 6.5 Ma (Fig. 14C and D).

In summary, the inferred maximum depositional ages based on concordia diagrams for the sedimentary succession of the lower Anti-Atlas Supergroup are 2049.3 ± 4.6 Ma for the Tasserda Formation, 1818 ± 6.4 Ma for the Agoummy Formation, 1060 ± 5.5 Ma for the Tachdamt Formation and 1855 ± 6.5 Ma for the Bleida Formation (Table 1). However, the latter formations could be younger (see Sec. 5.3)

5. Discussion

5.1. The 1.68–1.64 Ga Zenaga Event

The SHRIMP U–Pb geochronologic data for the Great Taghdout sill presented here shows a weighted mean average $^{207}Pb/^{206}Pb$ age of 1676 ± 37 Ma interpreted to date the magmatic emplacement of the sill (Fig. 9B). This age is similar within error to those obtained for other dolerite dykes and sills in the studied area (Zenaga Inlier), as well as in other inliers of the Anti-Atlas Belt (e.g. Agadir Melloul Inlier). Kouyaté et al. (2013) obtained ages of 1640 ± 2 Ma and 1641 ± 3 Ma (U–Pb baddeleyite) on the sill (DZ 36), which intrudes the Eburnean basement in the Zenaga Inlier (Fig. 4). They also obtained an age of 1656 ± 9 Ma (U–Pb baddeleyite) on another sill (DZ40), which is connected to a sill intruding the lowermost part of the lower Anti-Atlas Supergroup of the

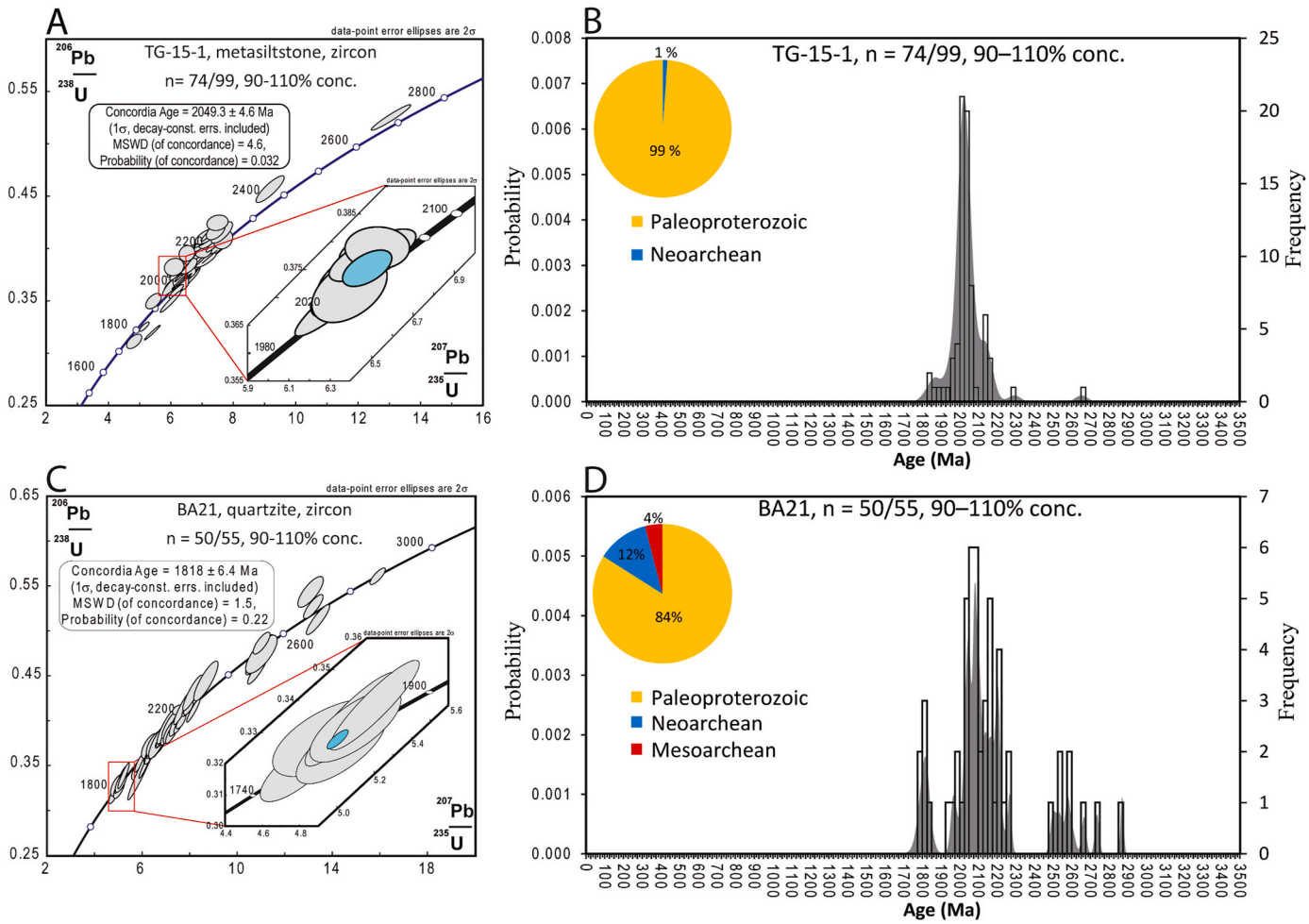

Fig. 13. U–Pb ages for detrital zircon grains from samples TG-15-1 (metasiltstones of the Tasserda Formation) and BA21 (quartzites of the Agoummy Formation) of the lower Anti-Atlas Supergroup. (A) and (C) are concordia diagrams; (B) and (D) are combined binned frequency and probability density plots of detrital zircon grains. Abbreviations: Conc.-Concordance; Decay-const. errs.- Decay-constant errors.

Zenaga Inlier (the Tasserda-Taghatine Group) and an age of 1654 ± 16 Ma (U–Pb baddeleyite) on a large NE-trending dyke, which crosscuts the Eburnean basement of the Agadir Melloul Inlier. More recently, Youbi et al. (2019) dated two sills intruding quartzites of the Lkest Group (equivalent of the Oumoula Formation) in the Kerdous Inlier. One of the sills yielded an upper intercept date of ca. 1640 Ma, constrained with ID-TIMS data for three zircon grains. LA-ICP-MS data for the same sample yielded a weighted mean average $^{207}Pb/^{206}Pb$ age of ca. 1650 Ma, identical within analytical uncertainties to the ID-TIMS date. Only a single baddeleyite grain has been analyzed from the second sill, producing a similar crystallization age of ca. 1650 Ma. All of these ages overlap within error with the newly obtained age from this study.

These ca. 1.68-1.64 Ga ages match the Rb–Sr dates, which were obtained for granitic rocks from the Anti-Atlas Belt; the Timrharbine granite (Zenaga Inlier), Tasserhert granite (Kerdous Inlier), and Oued Chaiba granite (Bas Drâa Inlier) dated at 1650 ± 50, 1680 ± 35, and 1640 ± 32 Ma, respectively (Charlot, 1976, 1982). This suggests an event of bimodal magmatism during the late Paleoproterozoic, post-dating the ca. 2.04 Ga Tagragra of Tata LIP extensional event (Kouyaté et al., 2013; Youbi et al., 2013), and confirms the polycyclic character of magmatism in the Anti-Atlas Belt, previously inferred in Kerdous and Tagragra of Akka inliers (Gasquet et al., 2004; Barbey et al., 2004). These ca. 1650 Ma ages are interpreted to belong to a single LIP event, which is termed the Zenaga Event (Kouyaté et al., 2013; Youbi et al., 2013; Ernst, 2014).

Globally, magmatism at ca. 1640–1656 Ma is also observed on other cratons (Fig. 15). In northwestern Greenland, the Melville Bugt dyke swarm extends for about 1000 km and is precisely dated at 1622–1635 Ma by the U–Pb method (1622 ± 3, 1629 ± 1, 1632 ± 1, and 1635 ± 3 Ma; Halls et al., 2011). Following upon previous work on the ca. 1630 Ma Melville Bugt dyke swarm along the NW coast of Greenland, Klausen and Nilsson (2019) confirmed its proposed continuation to the SE Greenland, indicating an extraordinary >2000 km long Trans-Greenlandic dyke swarm of Laurentia. This correlation was not only based on the swarm's continuous pattern, but also on a matching 1630 ± 4 Ma U–Pb baddeleyite age determination (Klausen and Nilsson, 2019) and similar whole-rock compositions as well as distinctive outcrop characteristics. In Laurentia, the bimodal Narakay Volcanic Complex in the Dease Arm of the Great Bear Lake, associated with deposition in the intracontinental Hornby Bay Basin, NWT, Canada, yielded TIMS U–Pb zircon age of 1663 ± 8 Ma (Bowring and Ross, 1985).

Corresponding magmatism on Baltica includes the ca. 1.64 Ga NW-trending dyke swarms of Häme, Sipoo, and Suomenniemi and the related rapakivi granite complexes exposed in the Svecofennian Domain of the Fennoscandian Shield in southeast Finland (Vaasjoki et al., 1991; Salminen et al., 2017). The most extensive of these dyke swarms is the 1642 ± 2 Ma Häme diabase dyke swarm (U–Pb ID-TIMS baddelleyite age; Salminen et al., 2017).

In Southern Siberia, the Nersa Sill Complex from the Biryusa Block of the Irkutsk Promontary has a 1641 ± 8 Ma U–Pb baddeleyite age (Ernst et al., 2016). Other potential matches are rejected. The Khibelen dykes

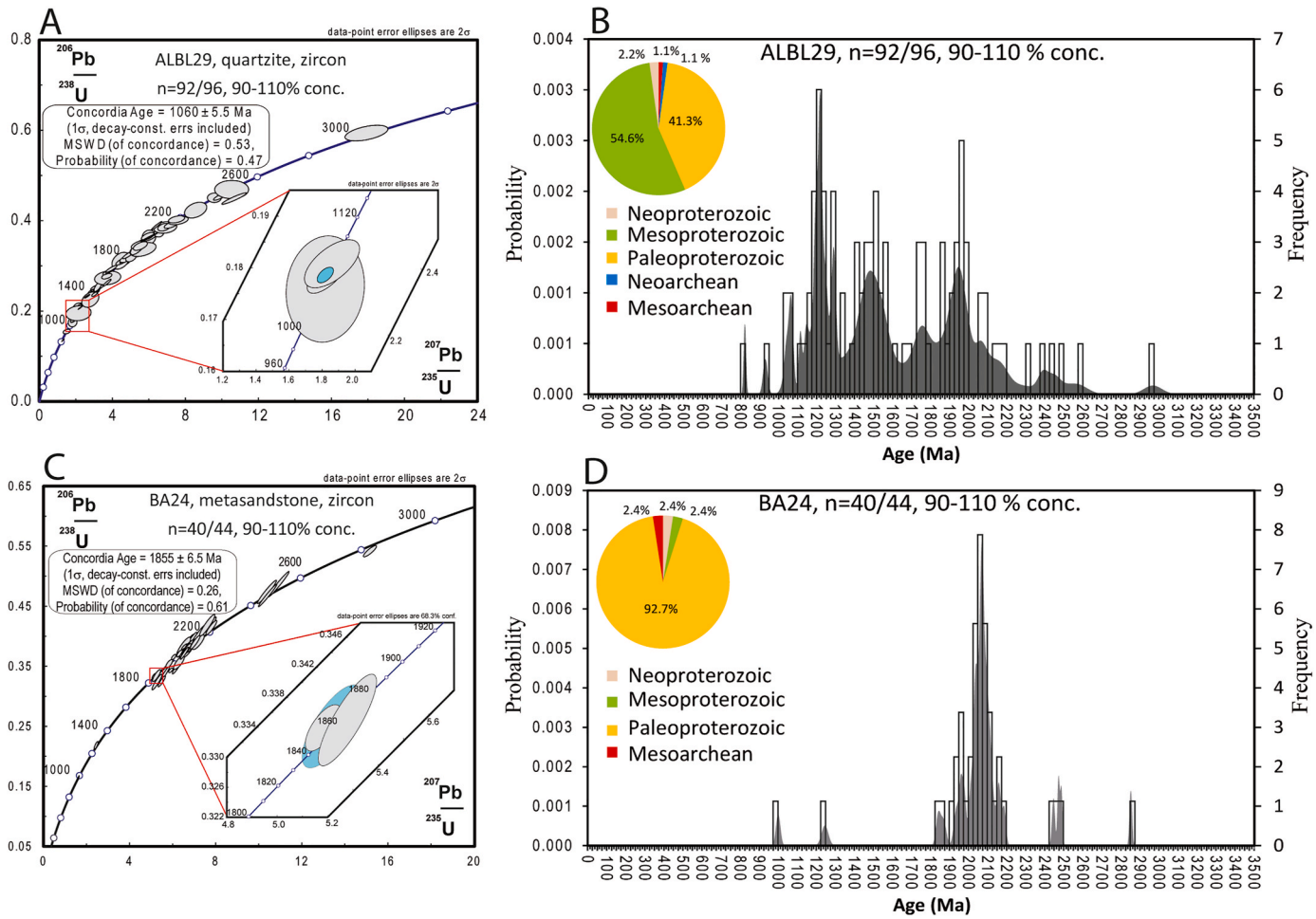

Fig. 14. U–Pb ages for detrital zircon grains from samples ALBL29 (quartzites of the Tachdamt Formation) and BA24 (metasandstone of the Bleida Formation) of the lower Anti-Atlas Supergroup. (A) and (C) are concordia diagrams; (B) and (D) are combined binned frequency and probability density plots of detrital zircon grains. Abbreviations: Conc.-Concordance; Decay-const. errs.- Decay-constant errors.

of the Baikal Uplift, Siberia have a 1674 ± 29 Ma Sm–Nd pyroxene, plagioclase, and whole-rock isochron age (Gladkochub et al., 2010). However, the Khiblelen dykes are on a trend from the SW-trending Chaya dyke subswarm, which has a 1752 ± 3 Ma U–Pb baddeleyite age (Gladkochub et al., 2010; Ernst et al., 2016), and so the Chaya and Khibelen dykes likely represent a single ca. 1750 Ma swarm. The type section for the Early Riphean, a major Russian stratigraphical division, in the South Urals Mountains, southeast Baltica, contains poorly-dated trachybasalts of the Navysh Subformation of the Ai Formation, which was originally thought to be of similar age. However, based on more recent high-precision SHRIMP U–Pb zircon dating these volcanics are 1752 ± 11 Ma in age (Krasnobaev et al., 2013a, b; Puchkov et al., 2014).

5.2. Stratigraphic implications arising from the U–Pb dating of the Great Taghdout sill

Based on the previously published data, the age of the lower Anti-Atlas Supergroup is bracketed between ca. 2032 and 647 Ma (see Sec. 2.3). The new U–Pb SHRIMP zircon age of 1676 ± 37 Ma obtained for the herein named Taghdout sill provides a new constraint on the minimum age for the lowermost part of the lower Anti-Atlas Supergroup in the Zenaga Inlier. The Taghdout sill intrudes into the lower Anti-Atlas Supergroup and is consequently younger than the intruded sedimentary rocks (that is the Tasserda and Ifrane-n-Taghatine formations) and most likely older than the unconformably overlying Oumoula Formation. The new age indicates that the lowermost part of the lower Anti-Atlas Supergroup was likely deposited during the late Paleoproterozoic (2.03-1.64 Ga). It could potentially be related to extension during the post-Eburnean orogenic collapse and if so should be close in age to ca. 2.0 Ga. In contrast, the much younger ca. 1.67 Ga Taghdout sill, likely related to the ca. 1.65 Ga Zenaga LIP, is a part of the mantle plume event/s that occurred at the late stage of the Nuna/Columbia supercontinent assembly (Fig. 15).

The new 1676 ± 37 Ma age for the sill in the Zenga Inlier is equivalent within uncertainty to the ca. 1706 ± 7 Ma age obtained for mafic intrusions crosscutting basal quartzites in the Igherm Inlier (Ikenne et al., 2017) and the ca. 1650 Ma age of the thick sills intruding the basal part of the lower Anti-Atlas Supergroup in the Kerdous Inlier (Youbi et al., 2019). Together, these ages indicate associated extension. Therefore, the post-Eburnean hiatus of one billion years on the WAC is no longer valid and the pre-Pan-African sediments and magmatic events are preserved along the northern margin of the craton. The 1640–1680 Ma (this study; Youbi et al., 2019) and the ca. 1706 Ma (Ikenne et al., 2017) magmatic events indicate that extension predated deposition of the thick quartzites of the Oumoula Formation, but postdated accumulation of the Tasserda and Ifrane-n-Taghatine formations. Further geochronological work is required to determine whether the ca. 1650 Ma, ca. 1676 Ma, and ca. 1706 Ma intrusions represent separate intraplate events on the WAC or belong to a single long-lived 1.70–1.65 Ga LIP event across the WAC and potentially representing an event extending into Baltica and Laurentia (Fig. 15). Regardless, all these ages for mafic sills are additional evidence that the lower part of the lower

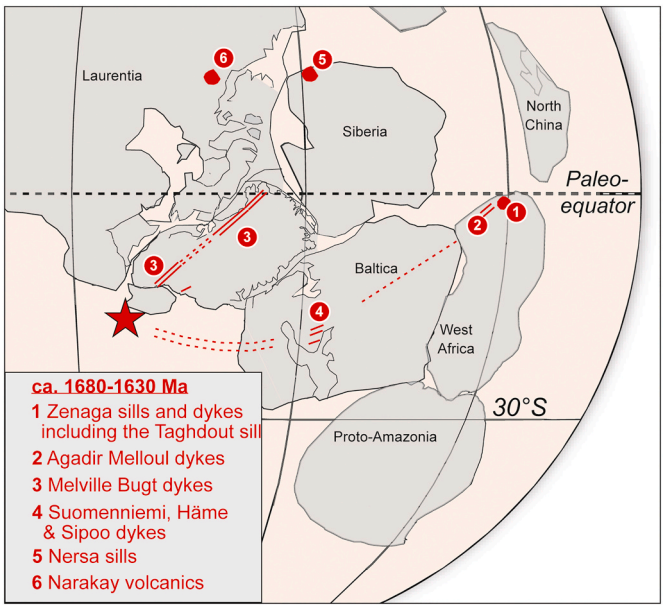

Fig. 15. Paleomagnetically and geologically informed reconstruction of WAC, Amazonia, and Baltica cratons (SAMBA connection) along with Laurentia and Siberia in the core of the Nuna supercontinent (modified after Evans and Mitchell, 2011); additional ca. 1640–1680 Ma dyke swarms include the 1641 ± 8 Ma Nersa sill complex of Southern Siberia (U–Pb baddeleyite TIMs age; Metelkin et al., 2011; Ernst et al., 2016), 1635.0 ± 2.7 to 1622.1 ± 3.2 Ma Melville Bugt dykes of western Greenland (U–Pb baddeleyite TIMS age; Halls et al., 2011; Klausen and Nilsson, 2019), 1663 ± 8 Ma bimodal Narakay Volcanic Complex of Canada (U–Pb zircon TIMS age; Bowring and Ross, 1985), and 1642 ± 2 Ma dyke swarms of Häme, Sipoo, and Suomenniemi of the Fennoscandian Shield in southeast Finland (U–Pb ID-TIMS baddelleyite age; Vaasjoki et al., 1991; Salminen et al., 2017). Star locates mantle plume centre, proposed for the Melville Bugt swarm by Klausen and Nilsson (2019).

Anti-Atlas Supergroup has an upper Paleoproterozoic age and, therefore, nearly one billion years older than previously thought.

5.3. Constraints from detrital zircons on the depositional age of the lower Anti-Atlas supergroup

The youngest detrial zircons from the sample TG-15-1 (the Tasserda Formation) are ca. 2049 Ma old (Fig. 13A and B), providing a maximum depositional age for the formation. This is in agreement with the geological context of the lower Anti-Atlas Supergroup: (i) the age of the succession is bracketed between 2032 ± 5 Ma and 647 ± 2 Ma; (ii) the 1676 ± 37 Ma Taghdout sill indicates that the intruded sedimentary rocks (that is the Tasserda and Ifrane-n-Taghatine formations) are older than 1676 ± 37 Ma, consistent with the minimum age constraints of ca. 1650 Ma in the Kerdous Inlier (Youbi et al., 2019) and ca. 1710 Ma in the Igherm Inlier (Ikenne et al., 2017).

The six youngest zircon grains in the sample BA21 (the Agoummy Formation) yielded a late Paleoproterozoic concordia age of 1818 ± 6.4 Ma (Fig. 13C and D), providing the maximum age for deposition of this formation. The U–Pb detrital zircon data obtained from this sample are consistent with the U–Pb zircon data for quartzites of the Mimount Formation in the Siroua Inlier (*sensu* Thomas et al., 2002), which is the stratigraphic equivalent of the Oumoula Formation (*sensu* Bouougri and Saquaque, 2004) of the lower Anti-Atlas Supergroup. For the Mimount Formation, Abati et al. (2010) obtained LA-ICP-MS $^{207}Pb/^{206}Pb$ zircon ages from ca. 2936 to ca. 1809 Ma, with major peaks at ca. 2200 and 2086 Ma and a number of minor peaks (ca. 2005, 1950, and 1818 Ma). The youngest zircon in the Oumoula Formation gave a concordant age of 1809 ± 15 Ma (Abati et al., 2010), while the youngest population age is ca. 1818 Ma, providing a maximum age for deposition of the Oumoula Formation. For the Mimount Formation, Walsh et al. (2012) obtained a range of SHRIMP $^{207}Pb/^{206}Pb$ zircon ages from about 2182 to 1987 Ma, with a major peak at ca. 2050 Ma. The similarity between detrital zircon age distribution in our sample BA21 from the Agoummy Formation and that of the Mimount Formation in Abati et al. (2010) and Walsh et al. (2012) indicates a similar provenance for the Mimount (= Oumoula) and Agoummy formations.

The lack of ca. 1.67 Ga zircon grains in samples from the Mimount and Agoummy formations is worth a note given the prominence of the 1650 Ma Zenaga event (see Sec. 5.1). However, mafic melts are usually poor in zircons; this may explain their relative absence in these formations.

The youngest detrital zircon grains from the Tachdamt Formation which overlap within errors are ca. 1060 Ma old (Fig. 14A and B). However, there are two younger single zircon grains with ages at 930 ± 12 and 822 ± 6 Ma. The latter age has a concordance of only 92% and a very low Th/U ratio, therefore the maximum age of sedimentation is constrained by ca. 1060 Ma and ca. 930 dates, consistent with ca. 883 Ma U–Pb SHRIMP zircon ages for two tuff horizons interbedded in the basal part of the Tachdamt Formation in the Siroua Inlier (Youbi et al., 2018; Bouougri et al., 2020). The youngest concordant zircon dates that overlap within errors in the sample BA24 from the Bleida Formation yield a concordia age of 1855 ± 6.5 Ma. The two youngest zircon grains provide dates at 1276 ± 14 Ma and 977 ± 10 Ma (Fig. 14C and D). However, Letsch (2018) reported a pronounced bimodal age distribution for a greywacke from the Bleida Formation in the Bou Azzer Inlier with a major Paleoproterozoic population (peaked at ca. 2060 Ma) and a minor Neoproterozoic one (with a prominent mode at ca. 690 Ma); the latter defines, along with the 697.3 ± 2.2 Ma maximum depositional age of the metasiltstone from the most basal part of the Bleida Formation (Bouougri et al., 2020), a Cryogenian maximum depositional age for this formation (although the minimum depositional age is younger than 883 Ma). These data imply a significant hiatus (697 to <883 Ma) in time of deposition between the Tachdamt and Bleida formations.

Both the Bleida and Tachdamt formations contain Mesoproterozoic detrital zircon ages (Fig. 14), however these ages are less abundant in the Bleida Formation, suggesting a change in the provenance consistent with a major hiatus in the time of deposition for these units. Importantly, detrital zircon ages indicate that the provenance for the lower Anti-Atlas Supergroup was overwhelmingly Paleoproterozoic and Mesoproterozoic in age with a much smaller contribution from Archean and Neoproterozoic sources.

5.4. Interpretation of detrital zircon age clusters

Four major detrital zircon age clusters have been obtained in this study: 3.0–2.4, 2.3–1.74, 1.7–1.4, and 1.25–0.95 Ga (Fig. 16). The few Archean zircon grains, forming a poorly defined cluster, were likely derived from the Reguibat and Leo-Man shields (Rocci et al., 1991; Thiéblemont et al., 2004; Key et al., 2008; Koffi et al., 2020). The second cluster (2.30–1.74 Ga) reflects contribution from mafic and felsic magmatic intrusions emplaced during the Eburnean Orogeny and its aftermath along the northern margin of the WAC (Abouchami et al., 1990; Boher et al., 1992; Egal et al., 2002; Schofield et al., 2006; Kouyaté et al., 2013; Youbi et al., 2013 Baratoux et al., 2011, 2019; McFarlane et al., 2019). The third cluster (1.7–1.4 Ga) is likely linked to the emplacement of dykes and sills accompanying the protracted rifting and the breakup of the Nuna/Columbia supercontinent (Youbi et al., 2013; Evans et al., 2013). Zircons of the fourth cluster (1.25–0.95 Ga) are common in the early Neoproterozoic sedimentary rocks. It is thought that these zircons were derived from the 1.25–0.95 Ga Grenvillian arcs (Rino et al., 2008) that underwent uplift and erosion during and in the aftermath of the amalgamation of the Rodinia supercontinent, and they may have been transported for thousands of kilometres inside the supercontinent by rivers (Rainbird et al., 1997). Interestingly, metamorphic and intrusive units with these ages are common in the Sunsás

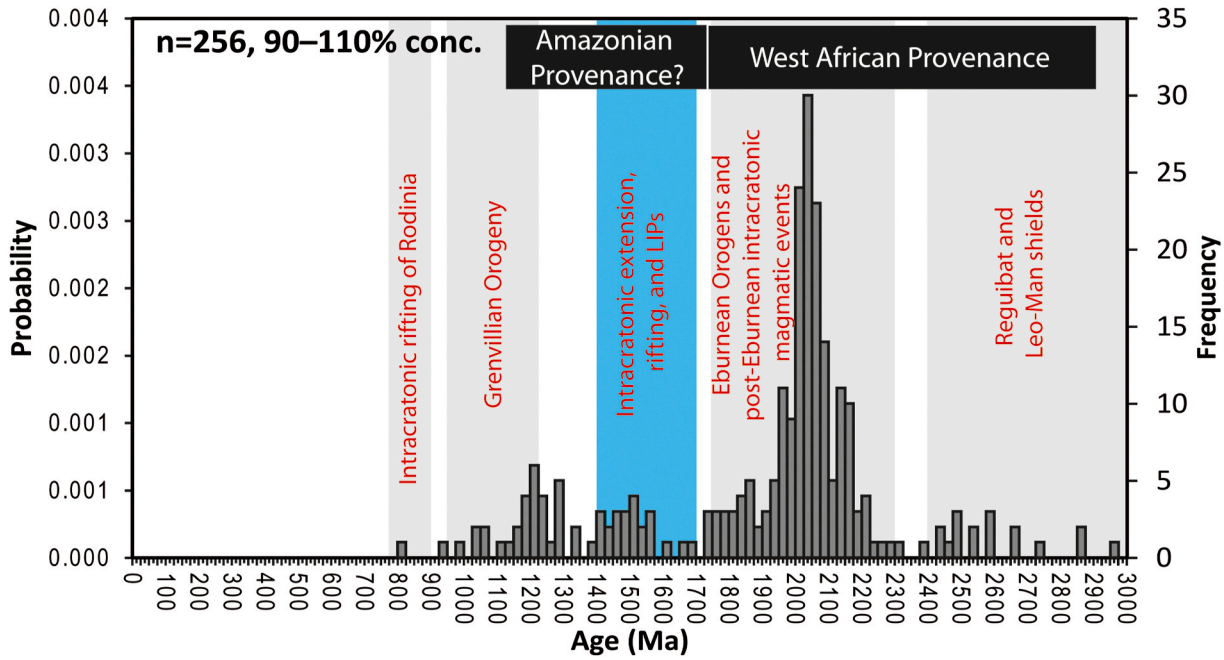

Fig. 16. Age compilation for detrital zircon grains from four samples collected from the lower Anti-Atlas Supergroup in the Zenaga and Bou Azzer El Graara inliers. Ages older than 1.7 Ga indicate the West African provenance (modified from Linnemann et al., 2010 and Abubaker et al., 2017). See the text for more explanation. Abbreviations: Conc.-Concordance.

Orogen (e.g. Sadowski and Bettencourt, 1996; Santos et al., 2008), which borders the Andean side of the Amazonian Craton (Fig. 17), and the Sveconorwegian Orogen of the northwestern part of Baltica (e.g. Andersson et al., 2007; Christoffel et al., 1999; Cosca et al., 1998) that were adjacent to the WAC in the Rodinia supercontinent configuration.

5.5. Speculations on the provenance and paleogeographic reconstruction

The main feature of our detrital zircon populations is the general absence or scarcity of Mesoproterozoic ages (Figs. 13 and 14), which is consistent with the earlier studies that argued for a tectonomagmatically quiescent period between ca. 1.7 and 1.0 Ga (e.g. Ennih and Liégeois, 2008). The absence or scarcity of Mesoproterozoic ages has been considered diagnostic in distinguishing the WAC provenance as a possible source (e.g. Nance and Murphy, 1994; Friedl et al., 2000; Linnemann et al., 2004; Abati et al., 2010; Bahlburg et al., 2010; Gärtner et al., 2013, 2016, 2017). How could this be reconciled with the U–Pb geochronological evidence for major mafic magmatic events at ca. 1.75, 1.65, and 1.41–1.38 Ga (e.g. Youbi et al., 2013)? The simplest explanation is that the mafic magmatism does not produce a significant detrital zircon population, and hence these major LIP events are not reflected in the detrital zircon record.

Samples from the upper part of the lower Anti-Atlas Supergroup (the Tachdamt and Bleida formations) contain Mesoproterozoic detrital zircons. Considering that in most reconstructions of the Nuna-Columbia and Rodinia supercontinents, the Amazonian Craton and Baltica were adjacent to the WAC (e.g. Hoffman, 1991; Dalziel, 1991, 1997; Weil et al., 1998; Evans, 2013; Li et al., 2013; Johansson, 2009, 2014; Merdith et al., 2017) and had their sources of Mesoproterozoic zircons far from their borders with the WAC (Fig. 15), both of these cratons could have been potential sources of detrital zircons as long as a long-distance fluvial transport was involved. However, the Amazonian Craton (Tassinari and Macambira, 1999) is characterized by a continuous range of Mesoproterozoic ages since it undergone several late Paleoproterozoic to Mesoproterozoic orogenic events, and igneous and metamorphic units with the ages ranging from 2000 to 1000 Ma are common there (e.g. Santos et al., 2000; Tassinari et al., 2000). While the sample ALB29 is indeed characterized by a continuous range of Mesoproterozoic ages, the sample BA24 has only few Mesoproterozoic zircons. Tantalizingly, similar to the sample ALB29 range of Mesoproterozoic detrital zircon ages was observed for the ca. 1.1 Ga Polissya Series in the western part of the Ukrainian Shield (SW part of Baltica (Sarmatia); Shumlyanskyy et al., 2015) that was positioned adjacent to the WAC in the configuration of Fig. 15, but equally lacks sources for the Mesoproterozoic detrital zircons. A long-distance transport from NW Baltica has thus been inferred for this mode in detrital zircon ages based on the combined ages and Hf isotope systematics. Mesoproterozoic detrital zircon ages were also found in the Neoproterozoic sedimentary units in the Mauritanides and in the Taoudeni Basin (Straathof, 2011; Nicoll et al., 2010; Bradley et al., 2015; see for compilation Gärtner et al., 2017), indicating long-distance fluvial transport of Mesoproterozoic zircons in the aftermath of the Grenville Orogeny (cf. Rainbird et al., 1997).

5.6. Refining proterozoic stratigraphy of the Anti-Atlas Belt

Fig. 18 shows a tentative correlation of the lower Anti-Atlas Supergroup (*sensu* Thomas et al., 2004) among the Anti-Atlas inliers. Based on our own geochronologic data and on published U–Pb geochronology, as well as on lithostratigraphy, we propose to abandon the Lkest-Taghdout Group name since it combines genetically unrelated successions deposited in different, superimposed basins recording different tectonic settings and bracketed by long-lasted hiatuses. Instead, we propose to use the lower Anti-Atlas Supergroup as the highest stratigraphic hierarchy unit for the Proterozoic, pre-Pan-African successions of the Anti-Atlas Belt that can be further subdivided in five unconformity-bounded lithostratigraphic units.

(1) The lower lithostratigraphic unit is Paleoproterozoic in age (ca. 2030-1706 Ma) and comprises the Tasserda and Ifrane-n-Taghatine formations, named here the Tasserda-Taghatine Group. Our maximum depositional age for the Tasserda Formation (<2049 Ma) agrees well with the only other detrital zircon study for the Tasserda and Ifrane-n-Taghatine formations by Letsch (2018), who inferred <2038–1975 Ma maximum

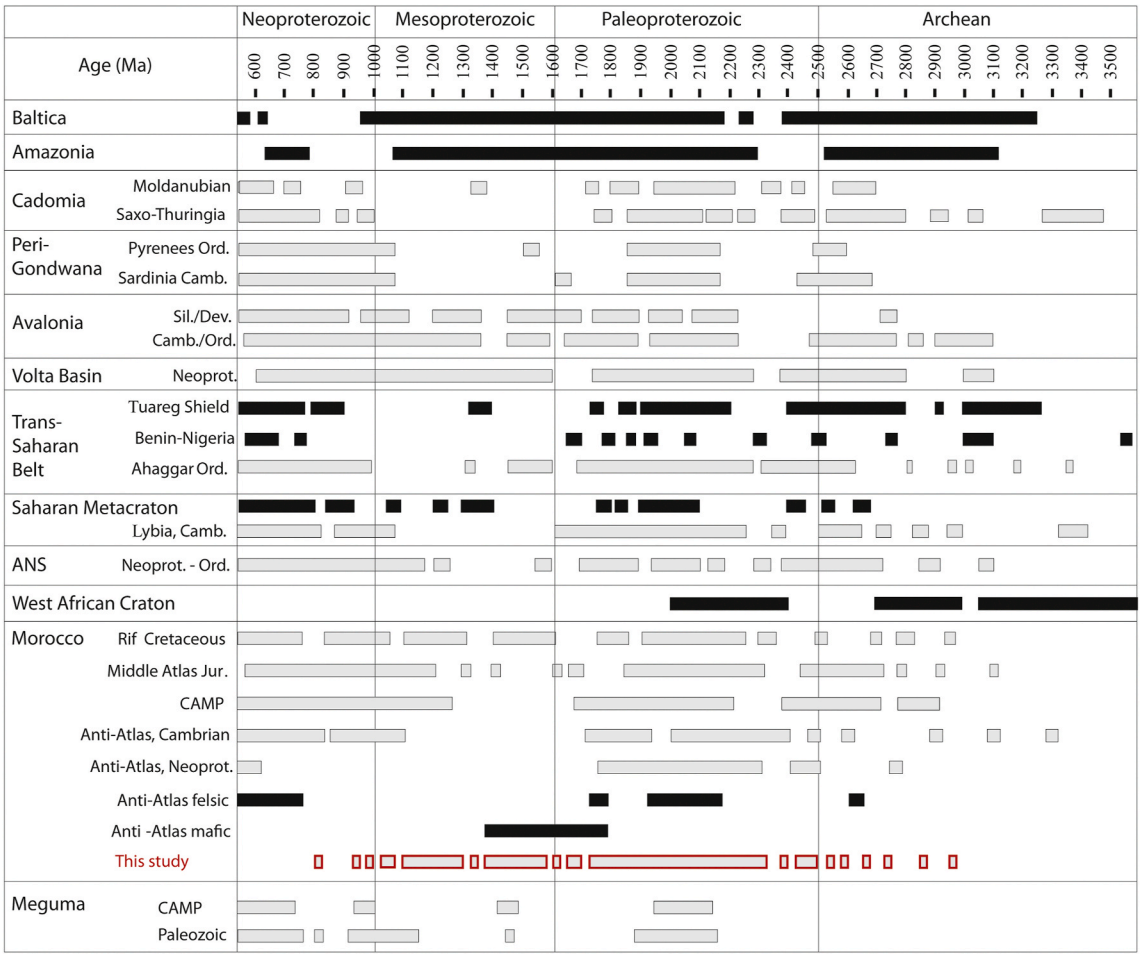

Fig. 17. Distribution of U–Pb ages for detrital zircon grains analyzed in this study from the lower Anti-Atlas Supergroup in the Zenaga and Bou Azzer El Graara inliers (all grouped together) and potential sources compiled from the literature. Grey stripes: detrital zircons; black stripes: zircons from magmatic rocks. Detrital zircon data sources: Pyrenees (Margalef et al., 2016); Lybia (Altumi et al., 2013); Algeria, Ahaggar (Linnemann et al., 2011); Meguma, Ganderia, and Avalonia detrital zircons (Fyffe et al., 2009; Gärtner et al., 2016; Henderson et al., 2016; Murphy et al., 2004a, 2004b; Waldron et al., 2009 and references therein); Anti-Atlas and Sardinia Cambrian (Avigad et al., 2012); Anti-Atlas Neoproterozoic (Abati et al., 2010; Karaoui et al., 2015). Anti-Atlas mafic rocks (Youbi et al., 2013 and references therein). Modified after Linnemann et al. (2011), Pratt et al. (2015), and Marzoli et al. (2017), and references therein. Abbreviations: ANS = Arabian–Nubian Shield; CAMP-Central Atlantic Magmatic Province; Camb.-Cambrian; Dev.- Devonian; Jur., Jurassic; Neoprot.- Neoproterozoic; Ord.- Ordovician; Sil.-Silurian.

depositional age for this succession. The lower group is herein related to the Eburnean Orogen collapse at ca. 2.0 Ga and deposition in extensional intracratonic basins.

(2) The second lithostratigraphic unit is also Paleoproterozoic in age (ca. 1745–1650 Ma) and comprises the Oumoula (=Mimount) Formation. In the Ifni Inlier, the stratigraphic equivalent of the lower Anti-Atlas Supergroup, the "Groupe des Quartzites" (Jeannette et al., 1981), consists of quartzites and metasiltstones that have been subdivided into three units that unconformably overlie the Eburnean basement. U–Pb dating of the Eburnean basement in this inlier yielded 2042 ± 5 Ma and 2026 ± 7 Ma ages for the Alouzad and Sahel granites, respectively (Schulte et al., 2016). The detrital zircons from the Ifni Inlier quartzites yielded ages ranging between ca. 2020 and 1745 Ma with no evidence of the Mesoproterozoic ages (Benziane et al., 2016). We tentatively correlate the Ifni Inlier succession with the Oumoula Formation based on a similar detrital zircon distribution patterns.

In the Agadir Melloul and south Siroua inliers, the stratigraphic equivalents of the lower Anti-Atlas Supergroup are the Iguiguil-Tizi n'Taghatine and Ahmamad formations, that both unconformably overlie the Eburnean granites and diorites with ca. 2.04–2.03 Ga U–Pb zircon ages (Choubert et al., 1992; Blein et al., 2014b). The Iguiguil-Tizi n'Taghatine Formation (Fig. 18) contains the Jbel Iguiguil quartzites that are sedimentologically similar to the quartzites of the Oumoula Formation (*sensu* Bouougri and Saquaque, 2004) and Mimount Formation (*sensu* Thomas et al., 2002, 2004). The Ahmamad Formation (Fig. 18) consists of quartzites and locally developed carbonate rocks exposed along the strike-slip faults in the southeastern part of the Azaghar-Izazen Inlier (Blein et al., 2014b and references therein). Both the Iguiguil-Tizi n'Taghatine and Ahmamad formations appear to have a similar age, although spatial (and structural) relationships are not clear (Choubert et al., 1992; Blein et al., 2014b). The Ahmamad Formation is similar to the Oumoula Formation in Jbel Iguiguil. The Iguiguil-Tizi n'Taghatine Formation is intruded by 570 ± 7 Ma dyke swarms and sill complexes of dolerites and gabbros (U–Pb zircon age; Blein et al., 2014b).

The Agadir Melloul Inlier has several ridges with nearly vertical conglomeratic quartzite beds sandwiched in Paleoproterozoic granites. Detrital zircon dates from the quartzites yielded the major peak at ca. 2.0 Ga and the youngest ages at ca. 1.8–1.7 Ga (Soulaimani et al., 2019), similar to the distribution trend shown by detrital zircons from the Oumoula Formation.

In the Kerdous Inlier, the stratigraphic equivalent of the lower Anti-Atlas Supergroup is the Jbel Lkest Group and includes the whole section of the "PII" quartzites in the Anzi District (Hassenforder, 1987;

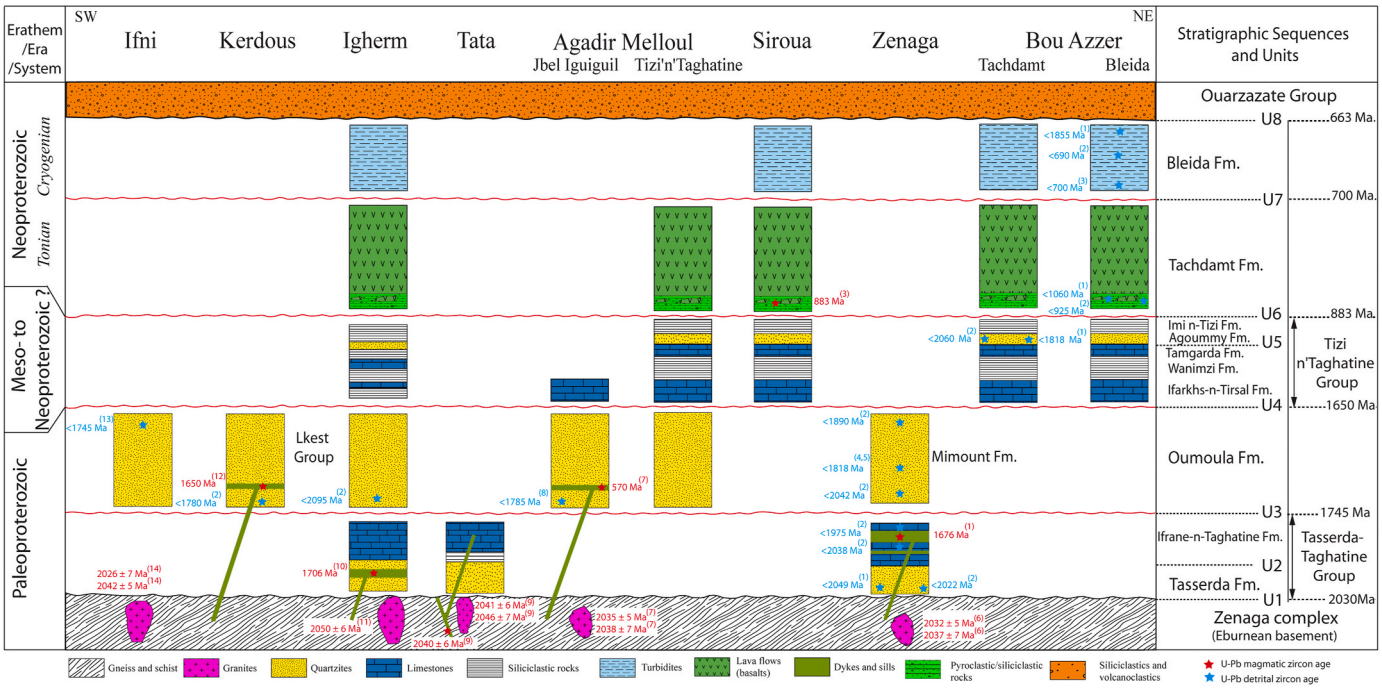

Fig. 18. A tentative correlation scheme of the lower Anti-Atlas Supergroup and its stratigraphic equivalents in the Anti-Atlas inliers. U1 to U8 are unconformities. U–Pb geochronology data are from (1) this study, (2) Letsch (2018), (3) Youbi et al. (2018) and Bouougri et al. (2020)Bouougri et al. (2020), (4) Abati et al. (2010), (5) Walsh et al. (2012), (6) Thomas et al. (2002), (7) Soulaimani et al. (2013), Hafid et al. (2013), Blein et al. (2014b), (8) Soulaimani et al. (2019), (9) Walsh et al. (2002), (10) Ikenne et al. (2017), (11) Aït Malek et al. (1998), (12) Youbi et al. (2019), (13) Benziane et al. (2016), and (14) Schulte et al. (2016).

O'Connor et al., 2010). The thick, hematite-rich quartzite sequence is not subdivided because of its monotonous nature and the lack of preservation of original textures due to extensive recrystallization, however it seems to correspond to the same depositional facies as the Oumoula Formation (*sensu* Bouougri and Saquaque, 2004) and Mimount Formation (*sensu* Thomas et al., 2002, 2004) quartzites. The great thickness of this formation and its homogeneity imply a constant supply of sediment sustained for a long period of time balanced by a continuous subsidence. Letsch (2018) constrained the maximum depositional age for the quartzite to be 1780 Ma based on U–Pb LA-ICP-MS detrital zircon data. As noted above (Sec. 5.2), Youbi et al. (2019) recently dated two mafic sills emplaced into the quartzite. One of the sills yielded an upper intercept date of ca. 1640 Ma, constrained by ID-TIMS data on three zircon fractions. LA-ICP-MS data for the same sample yielded a weighted mean average $^{207}Pb/^{206}Pb$ date of ca. 1650 Ma, identical within analytical uncertainties to the ID-TIMS date. Only a single fraction of baddeleyite has been analyzed from the second sill, indicating a similar crystallization age of ca. 1650 Ma.

The unconformably bounded Oumoula Formation is thus bracketed in age between ca. 1745 and 1650 Ma (Fig. 18). The data suggest that there was a pronounced change in the provenance across the unconformity between the Oumoula and the underlying Tasserda-Taghatine Group. Furthermore, the underlying units show a different structural pattern from the Oumoula Formation in the Zenaga Inlier (cf. Choubert et al., 1951; Brabers, 1988; Letsch, 2018), suggesting that they were deposited in different basins. Discontinuous distribution of the lower group formations and the Oumoula Formation, combined with geochemical composition of the 1.75–1.64 Ga mafic dykes and sills akin to continental flood basalts (Sec. 4.1.4.), indicate deposition of the Oumoula Formation at ca. 1.75–1.64 Ga in the compartmentalized extensional basins (rifts).

(3) The third lithostratigraphic unit is Paleoproterozoic to Neoproterozoic in age (<ca. 1706–1640 Ma to > ca. 883 Ma). It incorporates the Ifarkhs-n-Tirsal, Wanimzi, Tamgarda, Agoummy, and Imi n-Tizi formations. This lithostratigraphic unit is named here the Tizi n'Taghatine Group. Our detrital zircon ages for the Agoummy Formation provide the first maximum depositional age for this succession (<1818 Ma), but unfortunately it does not improve independent age constraints for this group. Ca. 1650 Ma sills and dykes that intrude the underlying Oumoula Formation, but not the Tizi n'Tghatine Group provide the maximum depositional age and ca. 883 volcanics in the unconformably overlying Tachdamt Formation set the minimum depositional age for this succession. The succession was likely deposited in the intracratonic basin related to the rifting within the assembling Rodinia supercontinent.

(4) The fourth lithostratigraphic unit is the ca. 883 Ma Tachdamt Formation. The Tachdamt Formation consists of a succession of basaltic lava flows interbedded with subordinate pyroclastic rocks. Youbi et al. (2018) and Bouougri et al. (2020) dated two tuff horizons, interbedded in the basal part of the Tachdamt Formation in the Siroua Inlier, at 885 ± 5.9 Ma and 883 ± 2.3 Ma (U–Pb SHRIMP on zircon). The NE30°-trending Iguerda-Taïfast mafic dyke swarm in the Zenaga and Iguerda-Taïfast inliers and the coeval volcanics of the Tachdamt Formation are part of the ca. 885-883 Ma Iguerda-Taïfast Large Igneous Province (LIP) in the Anti-Atlas Belt of Morocco (Kouyaté et al., 2013; Söderlund et al., 2013; Youbi et al., 2013, 2018; Bouougri et al., 2020), related to the rifting within the Rodinia supercontinent. The formation was likely deposited in the rift basin at the late stage in the assembly of the supercontinent Rodinia, but it remains uncertain whether this basin evolved into a passive continental margin setting along the northern margin of the WAC. Similar-age LIP events have been recognized in the southern part of the WAC (Baratoux et al., 2019), and on the Tarim Terrane of North China (Wang et al., 2015; Zhang et al., 2019) and the Congo Craton (Armstrong et al., 2005; Johnson et al., 2007).

(5) The uppermost unit, the ca. 700 Ma Bleida Formation is characterized by fine-grained and thin-bedded siliciclastic turbidites,

interbedded with minor basaltic lava flows, exhalative facies (jasper and ironstone), and black shales. Depositional setting of the Bleida Formation and the minimum age of its detrital zircons point to deposition in a foreland basin developed in the lead of the ca. 660–680 Ma Pan-African Orogeny (Thomas et al., 2004; Bouougri et al., 2020).

5.7. Potential correlation with the Taoudeni Basin succession in Mauritania

Our study indicates that the lower Anti-Atlas Supergroup records Mid-Proterozoic protracted and episodic deposition in intracontinental basins developed in association with extension and LIPs events on the WAC. Considering that these conditions, likely linked to far-distant tectonic stresses and emplacement of mantle plumes, could also have affected other parts of the WAC, we explore here correlation with another Mid-Proterozoic basin on the WAC, the Taoudeni Basin, located approximately 500 km to the south of the Anti-Atlas Belt (Fig. 1). It contains three unconformity-bounded successions in the ascending order: the Char, Atar, and Assabet el Hassiane groups.

The lower part of the sedimentary fill of the Taoudeni Basin, the Hodh Supergroup (Super-groupe du Hodh), is subdivided into the three unconformity-bound groups: the Char, Atar, and de l'Assabet el Hassiane (Moussine-Pouchkine and Bertrand-Sarfati, 1997; Benan and Deynoux, 1998). The mixed carbonate-siliclastic Char Group was deposited in a fault-bounded, compartmentalized basin developed on the deeply weathered Eburnean basement with aeolean and fluvial redbeds grading upsection to tidally influenced, marine siliciclastic and carbonate deposits with some evidence (halite pseudomorphs, mudcracks and mudchips, dessication cracks) for warm and arid climate. The depositional and tectonic setting of the Char Group is similar to that of the Tasserda-Taghatine Group (lithostratigraphic unit 1 in the Anti-Atlas Belt). Similarly, both successions carry detrital zircons with youngest ages corresponding to the Eburnean basement with an additional contribution in case of the Zenaga Inlier of the Anti-Atlas Belt of slightly younger, ca. 2042–1975 Ma provenance (Bradley et al., 2015; Straathof, 2011; Letsch, 2018; this study). We provisionally correlate these successions and link the development of their corresponding basins to the post-Eburnean orogen collapse.

We recognize no correlative stratigraphic interval in the Taoudeni Basin to the ca. 1745-1650 Ma Oumoula Formation (lithostratigraphic unit 2 of the Anti-Atlas Belt), which we link to extension and LIP emplacement on the WAC at the final stage in the assembly of the Nuna supercontinent. Importantly, ca. 1750 and 1650 Ma mafic magmatism, linked with deposition of the Oumoula Formation, was not so far recognized in the Taoudeni Basin and the surrounding Reguibat Craton.

The next potentially correlative stratigraphic intervals in the Anti-Atlas Belt and the Taoudeni Basin are the Tizi n'Tghatine (lithostraigraphic unit 3) and Atar groups, respectively. Both are mixed carbonate-siliciclastic successions deposited in intracratonic basins in warm and arid climate (Leblanc and Moussine-Pouchkine, 1994; Moussine--Pouchkine and Bertrand-Sarfati, 1997). Our youngest detrital zircon ages for the Agoummy Formation (ca. 1818 Ma) correspond well with the youngest detrital zircon ages reported for the Atar Group (1804 ± 33 Ma, Straathof, 2011; Nicoll et al., 2010; Bradley et al., 2015). Re–Os isochron ages for black shales from the Atar Group yielded the late Mesoproterozoic depositional age (1106 ± 12 Ma, 1109 ± 22 Ma, and 1105 ± 37 Ma; Rooney et al., 2010). These Mesoproterozoic ages are confirmed by the study of microfossils (Beghin et al., 2017) and chemostratigraphy (Kah et al., 2012). Carbonates of the Tizi n'Tghatine Group have highly negative to near zero carbon isotope values (−5.0 to +1.5‰; Alvaro et al., 2014). In comparison, carbonates of the Atar Group show large carbon isotope oscillations from −6.0 to +4.0‰ (Fairchild et al., 1990; Shields et al., 2007; Kah et al., 2012) that are characteristic of the latest Mesoproterozoic to early Neoproterozoic seawater.

It is uncertain whether there is a stratigraphic equivalent of either the ca. 883 Ma Tachdamt Formation/Bleida formation (lithostratigraphic units 4 and 5) in the Taoudeni Basin, but the siliciclastic Assabet el Hassiane Group yielded youngest ages for detrital zircons of 952 ± 38 Ma and 965 ± 29 Ma (Straathof, 2011; Bradley et al., 2015), which are consistent with the youngest ages for detrital zircons from the Tachdamt Formation (see Fig. 18). More importantly, both the Tachdamt Formation and the Assabet el Hassiane Group show influx of Mesoproterozoic detrital zircons in the aftermath of the Grenville Orogeny. A similar pattern for the Laurentia has been related to giant fluvial systems that delivered material from the Grenville Orogen inside the Rodinia supercontinent (Rainbird et al., 1997, 2012; Rainbird and Young, 2009). Kuznetsov et al. (2017) suggested the Rodinia supercontinent configuration ringed by continental arcs and with predominantly internal runoff that seems to fit well to the detrital zircon patterns of the WAC.

6. Concluding remarks

The main conclusions of our study are summarized below.

(1) The lower Anti-Atlas Supergroup was considered as a late Neoproterozoic passive continental margin sequence deposited during rifting and breakup on the northern margin of the WAC, culminating with opening of an oceanic basin between the northern edge of the WAC and an unknown terrane at ca. 760 Ma. Based on U–Pb geochronology data (this work and literature data) and lithostratigraphic constraints, we propose a new lithostratigraphic framework for the Proterorozoic lower Anti-Atlas Supergroup of the Anti-Atlas Belt. U–Pb geochronologic data indicate that deposition of the lower Anti-Atlas Supergroup lasted from the middle Paleoproterozoic to late Neoproterozoic with significant hiatuses along unconformities. Five major unconformity-bounded lithostratigraphic units are distinguished in the lower Anti-Atlas Supergroup. The lower unit is the ca. 2030-1706 Ma Tasserda-Taghatine Group and comprises the Tasserda and Ifrane-n-Taghatine formations. The second unit is the ca. 1745-1650 Ma Oumoula (Mimount) Formation. The third unit is Paleoproterozoic to Neoproterozoic in age (the ca. 1706-1640 Ma to > ca. 883 Ma Tizi 'n'Taghatine Group that incorporates the Ifarkhs-n-Tirsal, Wanimzi, Tamgarda, Agoummy, and Imi n-Tizi formations. The fourth unit is the ca. 883 Ma Tachdamt Formation and the uppermost unit is the ca. 700 Ma Bleida Formation.

Using this lithostratigraphic framework in combination with ages of LIPs on the WAC and herein developed correlation with the Taoudeni Basin succession highlights protracted and yet episodic mid-Proterozoic sedimentation in intracratonic basins on the WAC in association with extensional events and far-distance plate-boundary stresses that lasted from the early stage in the Nuna/Columbia assembly to the early stage in the breakup of the Rodinia supercontinent. Deposition of the Tasserda-Taghatine Group is potentially linked to the post-Eburnean orogenic collapse. The Oumoula (Mimount) Formation might reflect the intracontinental extension within the Nuna/Columbia supercontinent in response to either ca. 1750 Ma and/or 1650 Ma LIP events. The Tizi 'n'Taghatine Group might be correlative to the ca. 1.1 Ga Atar Group (Taoudeni Basin). The Tachdamt Formation records rifting within the Rodinia supercontinent, but it is uncertain whether this event led to the development of the passive continental margin along the northern boundary of the WAC. Finally, the Bleida Formation deposited in the foreland basin records the early stage in the assembly of the Gondwana supercontinent. The WAC formed the core of the Nuna/Columbia supercontinent and transited to the Rodinia supercontinent directly unaffected by the supercontinent breakup and subsequent assembly.

(2) The maximum depositional age and provenance of the lower Anti-Atlas Supergroup are constrained by new detrital zircon ages from the lower, middle, and upper parts of the sedimentary successions at the Zenaga and Bou Azzer El Graara inliers. The inferred maximum depositional ages are: ca. 2049 Ma for the Tasserda Formation, ca. 1818 Ma for the Agoummy Formation, ca. 1060 Ma for the Tachdamt Formation, and ca. 700 Ma for the Bleida Formation. Four detrital zircon age clusters have been defined in this study: ca. 3.0–2.4, 2.3–1.74, 1.7–1.4, and 1.25–0.95 Ga.

The provenance of detrital zircon was mainly on the WAC (that is the Reguibat and Leo-Man shields), but other cratons such as Amazonia, Baltica, and the Sahara Metacraton (Hoggar, Mali) cannot be excluded as possible subsidiary source areas. Importantly, we find that subsequent to the Grenville Orogeny, long-distance transport by fluvial systems delivered onto the WAC Mesoproterozoic zircons either from the Fennoscandia of Baltica or the Sunsas Belt of Amazonia (see Fig. 15). Transport from either of these two areas requires giant fluvial systems directed inward of the Rodinia supercontinent.

(3) The Tachdamt Formation (lithostratigraphic unit 4) consists mainly of a succession of basaltic lava flows. A ca. 885 Ma mafic dyke swarm in the Zenaga and Iguerda-Taïfast inliers and the coeval volcanics of the Tachdamt Formation constitute a LIP in the Anti-Atlas Belt of Morocco, named the Iguerda-Taïfast LIP. Similarly aged LIPs also occur on other cratons such as the Tarim Terrane (North China) and Congo Craton (Central Africa) and might reflect rifting at the late stage in the assembly of the Rodinia supercontinent.

Declaration of competing interest

The authors declare that they have no known competing financial interests or personal relationships that could have appeared to influence the work reported in this paper.

Acknowledgements

Most of this work was carried out at the Department of Geology of the Faculty of Sciences-Semlalia, Cadi Ayyad University of Marrakech and the "Centro de Pesquisas Geocronológicas (CPGeo), Instituto de Geociências (IG), Universidade de São Paulo-USP, São Paulo (SP), Brazil" within the framework of the scientific and technical agreement between the São Paulo University and the Cadi Ayyad University (responsibles Colombo Celso Gaeta Tassinari and Nasrrddine Youbi). We acknowledge the Academy Hassan II for Science and Technology for funding studentship for Abdelhak Ait Lahna in 2016–2018. Financial support for this work was also provided by several research projects: (i) the Academy Hassan II for Science and Technology (HIIAST/SDU/2016.02) to Nasrrddine Youbi and co-workers; (ii) Medyna; and (iii) FCT (Portugal)-CNRST (Morocco) to Nasrrddine Youbi and João Mata. Richard E. Ernst was partially supported from Mega-Grant 14. Y26.31.0012 of the Russian Federation. João Mata acknowledges the financial FCT support through project UIDB/50019/2020 – IDL. The Editor Prof. Damien Delvaux is gratefully acknowledged for his comments, patience, and support. We greatly appreciate thoughtful comments of reviewers Prof. David Evans and Dr. Shuan-Hong Zhang that helped to improve the manuscript.

Appendix A. Supplementary data

Supplementary data to this article can be found online at https://doi.org/10.1016/j.jafrearsci.2020.103946.

References

Abati, J., Aghzer, A.M., Gerdes, A., Ennih, N., 2010. Detrital zircon ages of Neoproterozoic sequences of the Moroccan Anti-Atlas belt. Precambrian Res. 181 (1), 115–128. https://doi.org/10.1016/j.precamres.2010.05.018.

Abati, J., Aghzer, A.M., Gerdes, A., Ennih, N., 2012. Insights on the crustal evolution of the West African craton from Hf isotopes in detrital zircons from the Anti-Atlas belt. Precambrian Res. 212–213, 263–274. https://doi.org/10.1016/j.precamres.2012.06.005.

Abouchami, W., Boher, M., Michard, A., Albarede, F., 1990. A Major 2.1 Ga event of mafic magmatism in West Africa: an early stage of crustal accretion. J. Geophys. Res. 95, 17605–17629. https://doi.org/10.1029/jb095ib11p17605.

Abubaker, A., Hofmann, M., Gärtner, A., Linnemann, U., Elicki, O., 2017. First U–Pb geochronology on detrital zircons from Early-Middle Cambrian strata of the Torgau-Doberlug Syncline (eastern Germany) and palaeogeographic implications. Int. J. Earth Sci. 106, 2445–2459. https://doi.org/10.1007/s00531-016-1440-y.

Admou, H., Juteau, T., 1998. Découverte d'un système hydrothermal océanique fossile dans l'ophiolite antécambrienne de Khzama (massif du Siroua, Anti-Atlas marocain). C. R. Acad. Sci. Ser II, Earth Planet Sci. Acad. Sci. 327 (5), 335–340. https://doi.org/10.1016/s1251-8050(98)80052-9.

Ahmed, A., Arai, S., Abdelaziz, Y., Rahimi, A., 2005. Spinel composition as a petrogenetic indicator of the mantle section in the Neoproterozoic Bou Azzer ophiolite, Anti Atlas, Morocco. Precambrian Res. 138 (3–4), 225–234. https://doi.org/10.1016/j.precamres.2005.05.004.

Aït Malek, H.A., Gasquet, D., Bertrand, J.M., Leterrier, J., 1998. Geochronologie U–Pb sur zircon de granitoïdes éburnéens et panafricains dans les boutonnières protérozoïques d'Igherm, du Kerdous et du Bas Draâ (Anti-Atlas Occidental, Maroc). C. R. Acad. Sci., Ser. II: Sci. Terre Planetes 327 (12), 819–826. https://doi.org/10.1016/s1251-8050(99)80056-1.

Altumi, M.M., Elicki, O., Linnemann, U., Hofmann, M., Sagawe, A., Gärtner, A., 2013. U–Pb LA-ICP-MS detrital zircon ages from the Cambrian of Al Qarqaf Arch, central-western Libya: provenance of the West Gondwanan sand sea at the dawn of the early Palaeozoic. J. Afr. Earth Sci. 79, 74–97. https://doi.org/10.1016/j.jafrearsci.2012.11.007.

Alvaro, J.J., Pouclet, A., Ezzouhairi, H., Soulaimani, A., Bouougri, E.H., Imaz, A.G., Fekkak, A., 2014. Early neoproterozoic rift-related magmatism in the anti-atlas margin of the west african craton, Morocco. Precambrian Res. 255, 433–442. https://doi.org/10.1016/j.precamres.2014.10.008.

Andersson, U.B., Rutanen, H., Johansson, Å., Mansfeld, J., Rimša, A., 2007. Characterization of the Paleoproterozoic mantle beneath the Fennoscandian shield: geochemistry and isotope Geology (Nd, Sr) of ~ 1.8 Ga mafic plutonic rocks from the transscandinavian igneous belt in southeast Sweden. Int. Geol. Rev. 49 (7), 587–625. https://doi.org/10.2747/0020-6814.49.7.587.

Armstrong, R.A., Master, S., Robb, L.J., 2005. Geochronology of the Nchanga granite, and constraints on the maximum age of the Katanga supergroup, Zambian copperbelt. J. Afr. Earth Sci. 42 (1–5), 32–40. https://doi.org/10.1016/j.jafrearsci.2005.08.012.

Avigad, D., Gerdes, A., Morag, N., Bechstädt, T., 2012. Coupled U–Pb–Hf of detrital zircons of Cambrian sandstones from Morocco and Sardinia: implications for provenance and precambrian crustal evolution of North Africa. Gondwana Res. 21, 690–703. https://doi.org/10.1016/j.gr.2011.06.005.

Bahlburg, H., Vervoort, J.D., DuFrane, S.A., 2010. Plate tectonic significance of middle Cambrian and Ordovician siliciclastic rocks of the Bavarian facies, Armorican terrane assemblage, Germany: U–Pb and Hf isotope evidence from detrital zircons. Gondwana Res. 17, 223–235. https://doi.org/10.1016/j.gr.2009.11.007.

Baratoux, L., Metelka, V., Naba, S., Jessell, M.W., Grégoire, M., Ganne, J., 2011. Juvenile Paleoproterozoic crust evolution during the Eburnean orogeny (~2.2–2.0Ga), western Burkina Faso. Precambrian Res. 191 (1–2), 18–45. https://doi.org/10.1016/j.precamres.2011.08.010.

Baratoux, L., Söderlund, U., Ernst, R.E., De roever, E., Jessell, M.W., Kamo, S., Naba, S., Perrouty, S., Metelka, V., Yatte, D., Grenholm, M., Diallo, D.P., Ndiaye, P.M., Dioh, E., Cournède, C., Benoit, M., Baratoux, D., Youbi, N., Rousse, S., Bendaoud, A., 2019. New U–Pb baddeleyite ages of mafic dyke swarms of the west african and Amazonian cratons: implication for their configuration in supercontinents through time. In: Srivastava, R.K., et al. (Eds.), Dyke Swarms of the World: A Modern Perspective, Springer Geology. Springer Nature Singapore Pte Ltd., pp. 263–314. https://doi.org/10.1007/978-981-13-1666-1_7

Barbey, P., Oberli, F., Burg, J.-P., Nachit, H., Pons, J., Meier, M., 2004. The Palaeoproterozoic in western Anti-Atlas (Morocco): a clarification. J. Afr. Earth Sci. 39, 39–245. https://doi.org/10.1016/j.jafrearsci.2004.07.044.

Beghin, J., Storme, J.-Y., Blanpied, C., Gueneli, N., Brocks, J.J., Poulton, S.W., Javaux, E. J., 2017. Microfossils from the late Mesoproterozoic-early neoproterozoic Atar/el Mreïti group, Taoudeni Basin, Mauritania, northwestern Africa. Precambrian Res. 291, 63–82. https://doi.org/10.1016/j.precamres.2017.01.009.

Benan, C.A.A., Deynoux, M., 1998. Facies analysis and sequence stratigraphy of neoproterozoic Platform deposits in Adrar of Mauritania, Taoudeni basin, West Africa. Geol. Rundsch. 87 (3), 283–302. https://doi.org/10.1007/s005310050210.

Benziane, F., Yazidi, A., Schulte, B., Boger, S., Stockhammer, S., Lehmann, A., Saadane, A., Yazidi, M., 2016. Carte géologique du Maroc, feuille au 1/50 000 Tlata Al Akhçaç. Notes Mém. Serv. Géol. (Morocco). Rabat n° 543bis.

Benziane, F., 2007. Lithostratigraphie et évolution géodynamique de l'Anti-Atlas (Maroc) du Paléoprotérozoïque au Néoprotérozoïque: exemples de la boutonnière de Tagragra de Tata et du Jbel Saghro. Ph.D. Univ. Savoie, France.

Bertrand, H., Dostal, J., Dupuy, C., 1982. Geochemistry of early Mesozoic tholeiites from Morocco. Earth Planet Sci. Lett. 58 (2), 225–239. https://doi.org/10.1016/0012-821x(82)90196-0.

Black, L.P., Kamo, S.L., Allen, C.M., Davis, D.W., Aleinikoff, J.N., Valley, J.W., Mundil, R., Campbell, I.H., Korsch, R.J., Williams, I.S., Foudoulis, C., 2004. Improved 206Pb/238U microprobe geochronology by the monitoring of a trace-element relatedmatrix effect: SHRIMP, ID-TIMS, ELA-ICP-MS and oxygen isotope documentation for a series of zircon standards. Chem. Geol. 205, 115–140. https://doi.org/10.1016/j.chemgeo.2004.01.003.

Blein, O., Baudin, T., Chèvremont, P., Soulaimani, A., Admou, H., Gasquet, P., Cocherie, A., Egal, E., Youbi, N., Razin, P., Bouabdelli, M., Gombert, P., 2014a. Geochronological constraints on the polycyclic magmatism in the bou Azzer-el Graara inlier (central anti-atlas Morocco). J. Afr. Earth Sci. 99, 287–306. https://doi.org/10.1016/j.jafrearsci.2014.04.021.

Blein, O., Baudin, T., Soulaimani, A., Cocherie, A., Chèvremont, P., Admou, H., Ouanaimi, H., Hafi, A., Razin, P., Bouabdelli, M., Roger, J., 2014b. New geochemical, geochronological and structural constraints on the Ediacaran evolution of the south Sirwa, Agadir-Melloul and Iguerda inliers, Anti-Atlas, Morocco. J. Afr. Earth Sci. 98, 47–71. https://doi.org/10.1016/j.jafrearsci.2014.06.019.

Block, K.A., Steiner, J.C., Puffer, J.H., Jones, K.M., Goldstein, S.L., 2015. Evolution of late stage differentiates in the Palisades Sill, New York and New Jersey. Lithos 230, 121–132. https://doi.org/10.1016/j.lithos.2015.05.018.

Bodinier, J.L., Dupuy, C., Dostal, J., 1984. Geochemistry of precambrian ophiolites from bou Azzer, Morocco. Contrib. Mineral. Petrol. 87 (1), 43–50. https://doi.org/10.1007/bf00371401.

Bogdanova, S.V., Bingen, B., Gorbatschev, R., Kheraskova, T.N., Kozlov, v. I., Puchkov, v. N., Volozh, Y.A., 2008. the east European craton (Baltica) before and during the assembly of Rodinia. Precambrian Res. 160 (1–2), 23–45. https://doi.org/10.1016/j.precamres.2007.04.024.

Bogdanova, S.V., Gorbatschev, R., Garetsky, R.G., 2016. Europe/East European Craton. Reference Module in Earth Systems and Environmental Sciences. Elsevier, pp. 1–18. https://doi.org/10.1016/b978-0-12-409548-9.10020-x.

Boher, M., Abouchami, W., Michard, A., Albarede, F., Arndt, N.T., 1992. Crustal growth in West Africa at 2.l Ga. J. Geophys. Res. 97, 345–369. https://doi.org/10.1029/91jb01640.

Bouougri, E.H., Saquaque, A., 2004. Lithostratigraphic framework and correlation of the neoproterozoic northern western african craton passive margin sequence (Siroua-Zenaga bou Azzer el Graarara inliers, central anti-atlas, Morocco): an integrated approach. J. Afr. Earth Sci. 39, 227–238. https://doi.org/10.1016/j.jafrearsci.2004.07.045.

Bouougri, E.H., Ait Lahna, A., Tassinari, C.C.G., Basei, M.A.S., Youbi, N., Admou, H., Maacha, L., 2020. Time constraints on early Tonian rifting and Cryogenian arc terrane-continent convergence along the northern margin of the west african craton: insights from SHRIMP and LA-ICP-MS zircon geochronology in the pan-african anti-atlas belt (Morocco). Gondwana Res. 85, 169–188. https://doi.org/10.1016/j.gr.2020.03.011.

Bowring, S.A., Ross, G.M., 1985. Geochronology of the Narakay volcanic complex: implications for the age of the Coppermine Homocline and Mackenzie igneous events. Can. J. Earth Sci. 22 (5), 774–781. https://doi.org/10.1139/e85-082.

Brabers, P.M., 1988. A plate tectonic model for the Panafrican Orogeny in the Anti-Atlas, Morocco. Lect. Notes Earth Sci. 61–80. https://doi.org/10.1007/bfb0011586.

Bradley, D.C., O'Sullivan, P., Cosca, M.A., Motts, H.A., Horton, J.D., Taylor, C.D., Beaudoin, G., Lee, G.K., Ramezani, J., Bradley, D.B., Jones, J.V., Bowring, S., 2015. Synthesis of geological, structural, and geochronologic data (phase V, deliverable 53): chapter A of Taylor CD. In: Second Projet de Renforcement Institutionnel du Secteur Minier de la République Islamique de Mauritanie (PRISM-II). U.S. Geological Survey Open-File Report 2013-12080-A, p. 328. https://doi.org/10.3133/ofr20131280A.

Brahimi, S., Liégeois, J.-P., Ghienne, J.-F., Munschy, M., Bourmatte, A., 2018. The Tuareg shield terranes revisited and extended towards the northern Gondwana margin: magnetic and gravimetric constraints. Earth Sci. Rev. 185, 572–599. https://doi.org/10.1016/j.earscirev.2018.07.002.

Cahen, L., Snelling, N.J., Delhal, J., Vail, J.R., 1984. The Geochronology and Evolution of Africa. Clarendon Press, Oxford, United Kingdom, p. 512.

Chacko, T., De, S.K., Creaser, R.A., Muehlenbachs, K., 2000. Tectonic setting of the Taltson magmatic zone at 1.9–2.0 Ga: a granitoid-based perspective. Can. J. Earth Sci. 37 (11), 1597–1609. https://doi.org/10.1139/e00-029.

Charlot, R., 1976. The precambrian of the Anti-Atlas (Morocco): a geochronologic synthesis. Precambrian Res. 3, 273–299. https://doi.org/10.1016/0301-9268(76)90013-9.

Charlot, R., 1982. Caracterisation des evenements eburneens et panafricains dans l'Anti-Atlas marocain; apport de la methode geochronologique Rb–Sr. Notes Mém. Ser. Géol. (Morocco) 313, 106p.

Choubert, G., 1962. Réflexions sur les parallélismes probables des formations quaternaires atlantiques du Maroc avec celles de la Méditerranée. Quaternaria 5, 137–175.

Choubert, G., 1963. Histoire géologique de l'Anti-Atlas de l'archéen à l'aurore des temps primaries. Notes Mém. Ser. Géol. (Morocco) 62, 350–352.

Choubert, G., Faure-Muret, A., Dahmani, M., Mouatani, E.A., Horrenberger, J.C., Salem, M., 1992. Carte géologique du Maroc à 1/100 000 feuille Agadir Melloul. Notes et Mémoires n° 359. Ministère de l'Energie et des Mines, Rabat.

Choubert, G., Termier, H., Termier, G., 1951. Les calcaires précambriens de Taghdout et leures organismes problématiques. Notes Mém. Ser. Géol. (Morocco) 85 (5), 9–34.

Christoffel, C.A., Connelly, J.N., Åhäll, K.-I., 1999. Timing and characterization of recurrent pre-Sveconorwegian metamorphism and deformation in the Varberg–Halmstad region of SW Sweden. Precambrian Res. 98 (3–4), 173–195. https://doi.org/10.1016/s0301-9268(99)00046-7.

Clauer, N., 1976. Grochimie isotopique du strontium des milieux sédimentaires. Application à la géochronologie du craton ouest-africain. Sciences géologiques, Strasbourg, 45, p. 256.

Coish, R.A., Sinton, C.W., 1992. Geochemistry of mafic dikes in the Adirondack Mountains: implications for late Proterozoic continental rifting. Contrib. Mineral. Petrol. 110, 500–514. https://doi.org/10.1007/bf00344084.

Corrigan, D., Hajnal, Z., Németh, B., Lucas, S.B., 2005. Tectonic framework of a Paleoproterozoic arc-continent to continent-continent collisional zone, Trans-Hudson Orogen, from geological and seismic reflection studies. Can. J. Earth Sci. 42 (4), 421–434. https://doi.org/10.1139/e05-025.

Corrigan, D., Pehrsson, S., Wodicka, N., de Kemp, E., 2009. The Palaeoproterozoic Trans-Hudson Orogen: a prototype of modern accretionary processes. Geol. Soc., London, Spec. Publ. 327 (1), 457–479. https://doi.org/10.1144/sp327.19.

Cosca, M.A., Mezger, K., Essene, E.J., 1998. The Baltica-Laurentia connection: Sveconorwegian (Grenvillian) metamorphism, cooling, and unroofing in the Bamble sector, Norway. J. Geol. 106 (5), 539–552. https://doi.org/10.1086/516040.

Dalziel, I.W.D., 1991. Pacific margins of Laurentia and East Antarctica–Australia as a conjugate rift pair: evidence and implications for an Eocambrian supercontinent. Geology 19, 598–601. https://doi.org/10.1130/0091-7613(1991)019<0598:pmolae>2.3.co;2.

Dalziel, I.W.D., 1997. Neoproterozoic–Paleozoic geography and tectonics: review, hypothesis and environmental speculation. Bull. Geol. Soc. Am. 109, 16–42. https://doi.org/10.1130/0016-7606(1997)109<0016:onpgat>2.3.co;2.

Deynoux, M., Affaton, P., Trompette, R., Villeneuve, M., 2006. Pan-African tectonic evolution and glacial events registered in Neoproterozoic to Cambrian cratonic and foreland basins of West Africa. J. Afr. Earth Sci. 46, 397–426. https://doi.org/10.1016/j.jafrearsci.2006.08.005.

Doblas, M., Lopez-Ruiz, J., Cebria, J.M., Youbi, N., Degroote, E., 2002. Mantle insulation beneath the west african craton during the precambrian-Cambrian transition. Geology 30, 839–842. https://doi.org/10.1130/0091-7613(2002)030<0839:mibtwa>2.0.co;2.

Dorais, M.J., Harper, M., Larson, S., Nugroho, H., Richardson, P., Roosmawati, N., 2005. A comparison of Eastern North America and Coastal New England magma suites: implications for subcontinental mantle evolution and the broad terrane hypothesis. Can. J. Earth Sci. 42, 1571–1587. https://doi.org/10.1139/e05-056.

Dupuy, C., Dostal, J., 1984. Trace element geochemistry of some continental tholeiites. Earth Planet Sci. Lett. 67 (1), 61–69. https://doi.org/10.1016/0012-821x(84)90038-4.

Egal, E., Thiéblemont, D., Lahondère, D., Guerrot, C., Adi Coseta, C., Iliescu, D., Delor, C., Goujou, J.-C., Lafon, J.M., Tegyey, M., Diaby, S., Kolié, P., 2002. Late Eburnean granitization and tectonics along the western and northwestern margin of the Archean Kénéma-Man domain (Guinea, West African Craton). Precambrian Res. 117, 57–84. https://doi.org/10.1016/s0301-9268(02)00060-8.

El Aouli, E.H., Ikenne, M., Amaouain, H., 2010. Petrographic and geochemical characterization of Cryogenian mafic dykes of the Iguerda–Taïfast inlier (central anti-atlas, Morocco). Int. J. Geomat. Geosci. 1, 355–371.

El Aouli, E.H., Ikenne, M., Beraaouz, E.H., Mortaji, A., 2004. Les roches basiques des boutonnières d'Agadir Melloul et d'Iguerda-Taïfast: témoins de l'histoire préorogénique de la chaîne panafricaine de l'Anti-Atlas (Maroc). Estud. Geol. 60, 11–20. https://doi.org/10.3989/egeol.04601-269.

El Bahat, A., Ikenne, M., Cousens, B., Söderlund, U., Ernst, R., Klausen, M., B, Youbi, N., 2017. New constraints on the geochronology and Sm-Nd isotopic characteristics of Bas-Drâa mafic dykes, Anti-Atlas of Morocco. J. Afr. Earth Sci. 127, 77–87. https://doi.org/10.1016/j.jafrearsci.2016.09.003.

El Bahat, A., Ikenne, M., Söderlund, U., Cousens, B., Youbi, N., Ernst, R., Soulaimani, A., Janati, M., Ahmid Hafid, A., 2013. U–Pb baddeleyite ages and geochemistry of dolerite dykes in the Bas Drâa inlier of the anti-atlas of Morocco: newly identified 1380 Ma event in the west african craton. Lithos 174, 85–98. https://doi.org/10.1016/j.lithos.2012.07.022.

El Hadi, H., Simancas, J.F., Martínez-Poyatos, D., Azor, A., Tahiri, A., Montero, P., Fanning, C.M., Bea, F., González-Lodeiro, F., 2010. Structural and geochronological constraints on the evolution of the bou Azzer neoproterozoic ophiolite (Anti-Atlas, Morocco). Precambrian Res. 182, 1–14. https://doi.org/10.1016/j.precamres.2010.06.011.

Ennih, N., Liégeois, J.P., 2008. The Boundaries of the West African Craton, with Special Reference to the Basement of the Moroccan Metacratonic Anti-Atlas Belt, vol. 297. Geological Society, London, Special Publications, pp. 1–17 (1).

Ennih, N., Liégeois, J.P., 2001. The Moroccan Anti-Atlas: the West African craton passive margin with limited pan-african activity. Implications for the northern limit of the craton. Precambrian Res. 112, 289–302. https://doi.org/10.1016/S0301-9268(01)00195-4.

Ernst, R.E., 2014. Large Igneous Provinces. Cambridge University Press, p. 653. https://doi.org/10.1017/CBO9781139025300.

Ernst, R.E., Hamilton, M.A., Söderlund, U., Hanes, J.A., Gladkochub, D.P., Okrugin, A.V., Kolotilina, T., Mekhonoshin, A.S., Bleeker, W., LeCheminant, A.N., Buchan, K.L., Chamberlain, K.R., Didenko, A.N., 2016. Long-lived connection between southern Siberia and northern Laurentia in the Proterozoic. Nat. Geosci. 9, 464–469. https://doi.org/10.1038/ngeo2700.

Ernst, R.E., Youbi, N., 2017. How large igneous provinces affect global climate, sometimes cause mass extinctions, and represent natural markers in the geological record. Palaeogeogr. Palaeoclimatol. Palaeoecol. 478, 30–52. https://doi.org/10.1016/j.palaeo.2017.03.014.

Evans, D.A.D., 2013. Reconstructing pre-Pangean supercontinents. Geol. Soc. Am. Bull. 125, 1735–1751. https://doi.org/10.1130/b30950.1.

Evans, D.A.D., Mitchell, R.N., 2011. Assembly and breakup of the core of Paleoproterozoic–Mesoproterozoic supercontinent Nuna. Geology 39, 443–446. https://doi.org/10.1130/g31654.1.

Fairchild, I.J., Marshall, J.D., Bertrand-Sarfati, J., 1990. Stratigraphic shifts in carbon isotopes from Proterozoic stromatolitic carbonates (Mauritania): influence of primary mineralogy an diagenesis. Am. J. Sci. 290A, 46–79.

Fekkak, A., Pouclet, A., Badra, L., 2002. The pre-pan-african rifting of Saghro (Anti-Atlas, Morocco): example of the middle neoproterozoic Basin of Boumalne. Bull. Soc. Geol. Fr. 173 (1), 25–35. https://doi.org/10.2113/173.1.25.

Fekkak, A., Pouclet, A., Ouguir, H., Ouazzani, H., Badra, L., Gasquet, D., 2001. Géochimie et signification géotectonique des volcanites du Cryogénien inférieur du Saghro (Anti-Atlas oriental, Maroc)/Geochemistry and geotectonic significance of Early Cryogenian volcanics of Saghro (Eastern Anti-Atlas, Morocco). Geodin. Acta 14 (6), 373–385. https://doi.org/10.1080/09853111.2001.10510730.

Fodor, R.V., 2009. Diorite segregations in gabbro: geochemical characteristics and conditions for origin assessed at diorite-gabbro contacts. J. Geol. 117 (2), 109–125. https://doi.org/10.1086/596506.

Friedl, G., Finger, F., McNaughton, N.J., Fletcher, I.R., 2000. Deducing the ancestry of terranes: SHRIMP evidence for South America-derived Gondwana fragments in central Europe. Geology 28, 1035–1038. https://doi.org/10.1130/0091-7613(2000)28<1035:dtaots>2.0.co;2.

Fyffe, L.L., Barr, S.M., Johnson, S.C., McLeod, M.J., McNicoll, V.J., Valverde-Vaquero, P., van Staal, C.R., White, C.E., 2009. Detrital zircon ages from Neoproterozoic and Early Paleozoic conglomerate and sandstone units of New Brunswick and coastal Maine: implications for the tectonic evolution of Ganderia. Atl. Geol. 45, 110–144. https://doi.org/10.4138/atlgeol.2009.006.

Gärtner, A., Villeneuve, M., Linnemann, U., El Archi, A., Bellon, H., 2013. An exotic terrane of Laurussian affinity in the Mauritanides and Souttoufides (Moroccan Sahara). Gondwana Res. 24, 687–699. https://doi.org/10.1016/j.gr.2012.12.019.

Gärtner, A., Villeneuve, M., Linnemann, U., Gerdes, A., Youbi, N., Hofmann, M., 2016. Similar crustal evolution in the western units of the Adrar Souttouf Massif (Moroccan Sahara) and the Avalonian terranes: insights from Hf isotope data. Tectonophysics 681, 305–317. https://doi.org/10.1016/j.tecto.2015.11.030.

Gärtner, A., Youbi, N., Villeneuve, M., Linnemann, U., Sagawe, A., Hofmann, M., Zieger, J., Mahmoudi, A., Boumehdi, M.A., 2018. Provenance of detrital zircon from siliciclastic rocks of the Sebkha Gezmayet unit of the Adrar Souttouf massif (Moroccan Sahara) – palaeogeographic implications. Compt. Rendus Geosci. https://doi.org/10.1016/j.crte.2018.06.004.

Gärtner, A., Youbi, N., Villeneuve, M., Sagawe, A., Hofmann, M., Mahmoudi, A., Boumehdi, M.A., Linnemann, U., 2017. The zircon evidence of temporally changing sediment transport—the NW Gondwana margin during Cambrian to Devonian time (Aoucert and Smara areas, Moroccan Sahara). Int. J. Earth Sci. 106 (8), 2747–2769. https://doi.org/10.1007/s00531-017-1457-x.

Gasquet, D., Chevremont, P., Baudin, T., Chalot-Prat, F., Guerrot, C., Cocherie, A., Roger, J., Hassenforder, B., Cheilletz, A., 2004. Polycyclic magmatism in the Tagragra and Kerdous-Tafeltast inliers (western anti-atlas, Morocco). J. Afr. Earth Sci. 39, 267–275. https://doi.org/10.1016/j.jafrearsci.2004.07.062.

Gasquet, D., Ennih, N., Liégeois, J.-P., Soulaimani, A., Michard, A., 2008. The Pan-African belt. In: Michard, A., Saddiqi, O., Chalouan, A., Frizon de Lamotte, D. (Eds.), Continental Evolution: the Geology of Morocco. Lecture Notes in Earth Sciences, vol. 116. Springer-Verlag, Berlin Heidelberg, pp. 33–64. https://doi.org/10.1007/978-3-540-77076-3_2 (Chapter 2).

Gasquet, D., Levresse, G., Cheilletz, A., Azizi-Samir, M.R., Mouttaqi, A., 2005. Contribution to a geodynamic reconstruction of the Anti-Atlas (Morocco) during Pan-African times with the emphasis on inversion tectonics and metallogenic activity at the Precambrian-Cambrian transition. Precambrian Res. 140, 157–182. https://doi.org/10.1016/j.precamres.2005.06.009.

Geyer, G., Landing, E., 2006. Ediacaran–Cambrian depositional environments and stratigraphy of the western Atlas regions. In: Geyer, G., Landing, E. (Eds.), Morocco 2006 – Ediacaran–Cambrian depositional environments and stratigraphy of the western Atlas regions. UCL Maghreb Petroleum Research Group, Infracambrian/Early Palaeozoic Field Guide Series 1 und Beringeria Special Issue, vol. 6, pp. 47–120.

Geyer, G., Landing, E., 2020. Cambrian deposition in northwestern Africa: relationship of Tamlelt massif (Moroccan–Algerian border region) succession to the Moroccan Meseta. J. Afr. Earth Sci. 103772. https://doi.org/10.1016/j.jafrearsci.2020.103772.

Gladkochub, D.P., Pisarevsky, S.A., Donskaya, T.V., Ernst, R.E., Wingate, M.T.D., Söderlund, U., Mazukabzov, A.M., Sklyarov, E.V., Hamilton, M.A., Hanesg, J.A., 2010. Proterozoic mafic magmatism in Siberian craton: an overview and implications for paleocontinental reconstruction. Precambrian Res. 183, 660–668. https://doi.org/10.1016/j.precamres.2010.02.023.

Grenholm, M., Jessell, M., Thébaud, N., 2019. A geodynamic model for the Paleoproterozoic (ca. 2.27–1.96 Ga) Birimian Orogen of the southern West African Craton – insights into an evolving accretionary-collisional orogenic system. Earth Sci. Rev. https://doi.org/10.1016/j.earscirev.2019.02.006.

Hafid, A., 1999. Magmatisme basique filonien Néoproterozoique (Précambrien II inferieur) dans l'Anti-Atlas central et Occidental. Minéralogie, géochimie, pétrogenèse et implication geodynamique. Unpublished Thèse de Doctorat d'Etat, Faculté des Sciences-Semlalia. Université Cadi Ayyad.

Hafid, A., Sagon, J.P., Julivert, M., Arboleya, M.L., Saquaque, A., El Boukhari, A., Saidi, A., Soler, J.M.F., 2001. Neoproterozoic basic dykes of the Zenaga Inlier, central Anti-Atlas, Morocco: petrology, geochemistry and geodynamic significance. J. Afr. Earth Sci. 32, 707–721. https://doi.org/10.1016/S0899-5362(02)00050-7.

Hafid, A., Blein, O., Admou, H., Soulaimani, A., Razin, P.H., Simon, B., Ouanaimi, H., El janati, M., Chevemont, P.H., Baudin, T., Bouabdelli, M., Abia, E.H., Beni Akhy, R., 2013. Notice explicative carte géol. Maroc (1/50 000), feuille Assaragh. Notes Mém. Serv. Géol. Morroco n°550, MEM/BRGM.

Halls, H.C., Hamilton, M., Denyszyn, S.W., 2011. The Melville Bugt dyke swarm of Greenland: a connection to the 1.5 - 1.6 Ga Fennoscandian rapakivi granite province? In: Srivastava (Ed.), Dyke Swarms: Keys for Geodynamic Interpretation, pp. 509–535. https://doi.org/10.1007/978-3-642-12496-9_27.

Hassenforder, B., 1987. La tectonique panafricaine et varisque de l'Anti-Atlas dans le massif de Kerdous (Maroc). Ph.D. thesis. Universite Strasbourg, Strasbourg, France, p. 249.

Hefferan, K., et al., 2014. A reconsideration of Pan African orogenic cycle in the Anti-Atlas Mountains, Morocco. J. Afr. Earth Sci. 98, 34–46. https://doi.org/10.1016/j.jafrearsci.2014.03.007.

Henderson, B.J., Collins, W.J., Murphy, J.B., Gutierrez-Alonso, G., Hand, M., 2016. Gondwanan basement terranes of the Variscan–Appalachian orogen: Baltican, Saharan and West African hafnium isotopic fingerprints in Avalonia, Iberia and the Armorican terranes. Tectonophysics 681, 278–304. https://doi.org/10.1016/j.tecto.2015.11.020.

Hindermeyer, J., 1953. Le Précambrien III du Sarhro. C. R. Hebd. Séances Acad. Sci. 237 (17), 1024–1026.

Hodel, F., Macouin, M., Triantafyllou, A., Carlut, J., Berger, J., Rousse, S., Ennih, N., Trindade, R.I.F., 2017. Unusual massive magnetite veins and highly altered Cr-spinels as relics of a Cl-rich acidic hydrothermal event in Neoproterozoic serpentinites (Bou Azzer ophiolite, Anti-Atlas, Morocco). Precambrian Res. 300, 151–167. https://doi.org/10.1016/j.precamres.2017.08.005.

Hoffman, P.F., 1988. United plates of America, the birth of a craton: early Proterozoic assembly and growth of Laurentia. Annu. Rev. Earth Planet Sci. 16 (1), 543–603. https://doi.org/10.1146/annurev.ea.16.050188.002551.

Hoffman, P.F., 1991. Did the breakout of Laurentia turn Gondwana inside out? Science 252, 1409–1412. https://doi.org/10.1126/science.252.5011.1409.

Hoskin, P.W.O., Schaltegger, U., 2003. The composition of zircon and igneous and metamorphic petrogenesis. In: Hanchar, J.M., Hoskin, P.W.O. (Eds.), Zircon; Reviews in Mineralogy and Geochemistry, 53, pp. 27–62. https://doi.org/10.2113/0530027.

Ikenne, M., 1997. La boutonnière précambrienne du bas Draa (Anti-Atlas Occidental, Maroc): caractérisation pétrologique et géochimique des roches magmatiques et métamorphiques et leurs relations avec la déformation. Ph.D. thesis. University of Agadir, p. 259.

Ikenne, M., Söderlund, U., Ernst, R.E., Pin, C., Youbi, N., El Aouli, E., Hafid, A., 2017. A c. 1710 Ma mafic sill emplaced into a quartzite and calcareous series from Ighrem, Anti-Atlas – Morocco: evidence that the Taghdout passive margin sedimentary group is nearly 1 Ga older than previously thought. J. Afr. Earth Sci. 127, 62–76. https://doi.org/10.1016/j.jafrearsci.2016.08.020.

Inglis, J.D., Hefferan, K., Samson, S.D., Admou, H., Saquaque, A., 2016. Determining age of Pan-African metamorphism using Sm-Nd garnet-whole rock geochronology and phase equilibria modeling in the Tasriwine ophiolite, Sirwa, Anti-Atlas Morocco. J. Afr. Earth Sci. 127, 88–98. https://doi.org/10.1016/j.jafrearsci.2016.06.021.

Irvine, T.N., Baragar, W.R.A., 1971. A guide to the chemical classification of the common volcanic rocks. Can. J. Earth Sci. 8, 523–548. https://doi.org/10.1139/e71-055.

Jackson, S.E., Pearson, N.J., Griffin, W.L., Belousova, E.A., 2004. The application of laser ablation-inductively coupled plasma-mass spectrometry to in situ U–Pb zircon geochronology. Chem. Geol. 211 (1–2), 47–69. https://doi.org/10.1016/j.chemgeo.2004.06.017.

Jeannette, D., Benziane, F., Yazidi, A., 1981. Lithostratigraphie et datation du Proterozoique de la boutonniere d'Ifni (Anti-Atlas, Maroc). Precambrian Res. 14 (3), 363–378. https://doi.org/10.1016/0301-9268(81)90045-0.

Jessell, M.W., Begg, G.C., Miller, M.S., 2016. The geophysical signatures of the west African craton. Precambrian Res. 274, 3–24. https://doi.org/10.1016/j.precamres.2015.08.010.

Johansson, Å., 2009. Baltica, Amazonia and the SAMBA connection - 1000 million years of neighbourhood during the Proterozoic? Precambrian Res. 175, 221–234. https://doi.org/10.1016/j.precamres.2009.09.011.

Johansson, Å., 2014. From Rodinia to Gondwana with the 'SAMBA' model – a distant view from Baltica towards Amazonia and beyond. Precambrian Res. 244, 226–235. https://doi.org/10.1016/j.precamres.2013.10.012.

Johnson, S.P., De Waele, B., Evans, D., Banda, W., Tembo, F., Milton, J.A., Tani, K., 2007. Geochronology of the Zambezi supracrustal sequence, Southern Zambia: a record of neoproterozoic divergent processes along the southern margin of the Congo Craton. J. Geol. 115 (3), 355–374. https://doi.org/10.1086/512757.

Kah, L.C., Bartley, J.K., Teal, D.A., 2012. Chemostratigraphy of the late Mesoproterozoic atar group, Taoudeni Basin, Mauritania: muted isotopic variability, facies correlation, and global isotopic trends. Precambrian Res. 200–203, 82–103. https://doi.org/10.1016/j.precamres.2012.01.011.

Karaoui, B., Breitkreuz, C., Mahmoudi, A., Youbi, N., 2014. Physical volcanology, geochemistry and basin evolution of the Ediacaran volcano-sedimentary succession in the Bas Draâ inlier (Ouarzazate supergroup, western anti-atlas, Morocco). J. Afr. Earth Sci. 99 (2), 307–331. https://doi.org/10.1016/j.jafrearsci.2014.06.022.

Karaoui, B., Breitkreuz, C., Mahmoudi, A., Youbi, N., Hofmann, M., Gärtner, A., Linnemann, U., 2015. U-Pb zircon ages from volcanic and sedimentary rocks of the Ediacaran Bas Draa inlier (Anti-Atlas Morocco): chronostratigraphic and provenance implications. Precambrian Res. 263, 43–58. https://doi.org/10.1016/j.precamres.2015.03.003.

Key, R.M., Loughlin, S.C., Horstwood, M.S.A., Gillespie, M., Pitfield, P.E.J., Henney, P.J., Crowley, Q.G., Del Rio, M., 2008. Two Mesoarchaean terranes in the Reguibat shield of NW Mauritania. In: Ennih, N., Liégeois, J.-P. (Eds.), Boundaries of the West African Craton, vol. 297. Special Publication of the Geological Society, London, pp. 33–52. https://doi.org/10.1144/sp297.3.

Klausen, M.B., Nilsson, M.K.M., 2019. The Melville Bugt Dyke Swarm across SE Greenland: A Closer Link to Mesoproterozoic AMCG-Complexes, 329, pp. 88–107. https://doi.org/10.1016/j.precamres.2018.06.001.

Koffi, G.R.-S., Kouamelan, A.N., Allialy, M.E., Coulibaly, Y., Peucat, J.-J., 2020. Re-evaluation of Leonian and Liberian Events in the Geodynamical Evolution of the Man-Leo Shield (West African Craton). Precambrian Research, p. 105582. https://doi.org/10.1016/j.precamres.2019.105582.

Kouyaté, D., Söderlund, U., Youbi, N., Ernst, R., Hafid, A., Ikenne, M., Soulaimani, A., Bertrand, H., El Janati, M., Chaham, K.R., 2013. U–Pb baddeleyite and zircon ages of 2040 Ma, 1650 Ma and 885 Ma on dolerites in the west african craton (Anti-Atlas inlier): possible links to break-up of precambrian supercontinents. Lithos 174, 71–84. https://doi.org/10.1016/j.lithos.2012.04.028.

Krasnobaev, A., Kozlov, V.I., Puchkov, V.N., Busharina, S.V., Sergeeva, N.D., Paderin, I. P., 2013a. Zircon geochronology of the Mashak volcanic rocks and the problem of the age of the lower middle Riphean boundary (Southern Urals). Stratigr. Geol. Correl. 21, 465–481. https://doi.org/10.1134/s0869593813050055.

Krasnobaev, A., Puchkov, V.N., Kozlov, V.I., Sergeeva, N.D., Busharina, S.V., Lepekhina, E.N., 2013b. Zirconology of Navysh volcanic rocks of the Ai suite and the problem of the age of the lower Riphean boundary in the southern Urals. Dokl. Earth Sci. 448, 185–190. https://doi.org/10.1134/s1028334x13020050.

Kuznetsov, A.B., Bekker, A., Ovchinnikova, G.V., Gorokhov, I.M., Vasilyeva, I.M., 2017. Unradiogenic strontium and moderate-amplitude carbon isotope variations in early Tonian seawater after the assembly of Rodinia and before the Bitter Springs Excursion. Precambrian Res. 298, 157–173. https://doi.org/10.1016/j.precamres.2017.06.011.

Le Bas, M.J., Maitre, R.W.L., Streckeisen, A., Zanettin, B., 1986. A chemical classification of volcanic rocks based on the total alkali-silica diagram. J. Petrol. 27 (3), 745–750. https://doi.org/10.1093/petrology/27.3.745.

Leblanc, M., 1975. Ophiolites précambriennes et gîtes arsénites de cobalt (Bou Azzer, Maroc). Ph.D. thesis. université, Paris VI, p. 329.

Leblanc, M., 1981. The late Proterozoic ophiolites of bou Azzer (Morocco): evidence for Pan-African plate tectonics. In: Kroner, A. (Ed.), Precambrian Plate Tectonics. Elsevier, Amsterdam, pp. 435–451. https://doi.org/10.1016/s0166-2635(08)70022-7.

Leblanc, M., Moussine-Pouchkine, A., 1994. Sedimentary and volcanic evolution of a Neoproterozoic continental margin (Bleida, Anti-Atlas, Morocco). Precambrian Res. 70 (1–2), 25–44. https://doi.org/10.1016/0301-9268(94)90019-1.

Letsch, D., 2018. The Anti-Atlas Belt (Morocco) during the Proterozoic – A Sedimentary Perspective. Ph.D. thesis. ETH Zurich, p. 201. https://doi.org/10.3929/ethz-b-000296186.

Li, Z.X., Evans, D.A.D., Halverson, G.P., 2013. Neoproterozoic glaciations in a revised global palaeogeography from the breakup of Rodinia to the assembly of Gondwanaland. Sediment. Geol. 294, 219–232. https://doi.org/10.1016/j.sedgeo.2013.05.016.

Liégeois, J.-P., Abdelsalam, M.G., Ennih, N., Ouabadi, A., 2013. Metacraton: nature, genesis and behavior. Gondwana Res. 23, 220–237. https://doi.org/10.1016/j.gr.2012.02.016.

Liégeois, J.-P., Fekkak, A., Bruguier, O., Errami, E., Ennih, N., 2006. The Lower Ediacaran (630–610 Ma) Saghro group: an orogenic transpressive basin development during the early metacratonic evolution of the Anti-Atlas (Morocco). In: Proceedings of the IGCP485 4th Meeting, Algiers, Algeria, 2 September 2006, p. 57.

Linnemann, U., Gerdes, A., Drost, K., Buschmann, B., 2007. The continuum between Cadomian Orogenesis and opening of the Rheic Ocean: constraints from LA-ICP-MS U–Pb zircon dating and analysis of plate-tectonic setting (Saxo-Thuringian Zone, NE Bohemian massif, Germany). In: Linnemann, U., Nance, D., Kraft, P., Zulauf, G. (Eds.), The Evolution of the Rheic Ocean: from Avalonian–Cadomian Active Margin to Alleghenian–Variscan Collision, 423. Memoir of Geological Society of America, pp. 61–96. https://doi.org/10.1130/2007.2423(03.

Linnemann, U., Hofmann, M., Romer, R.L., Gerdes, A., 2010. Transitional stages between the Cadomian and Variscan orogenies: basin development and tectonomagmatic evolution of the southern margin of the Rheic ocean in the Saxo-Thuringian zone (north Gondwana shelf). In: Linnemann, U., Romer, R.L. (Eds.), Pre-Mesozoic Geology of Saxo-Thuringia-From the Cadomian Active Margin to the Variscan Orogen. Schweizerbart Science Publishers, Stuttgart, pp. 59–98.

Linnemann, U., McNaughton, N.J., Romer, R.L., Gehmlich, M., Drost, K., Tonk, C., 2004. West African provenance for Saxo-Thuringia (Bohemian massif): did Armorica ever leave pre-Pangean Gondwana? U/Pb-SHRIMP zircon evidence and the Nd-isotopic record. Int. J. Earth Sci. 93, 683–705. https://doi.org/10.1007/s00531-004-0413-8.

Linnemann, U., Ouzegane, K., Drareni, A., Hofmann, M., Becker, S., Gärtner, A., Sagawe, A., 2011. Sands of West Gondwana: an archive of secular magmatism and plate interactions—a case study from the Cambro-Ordovician section of the Tassili Ouan Ahaggar (Algerian Sahara) using U–Pb LA-ICP-MS detrital zircon ages. Lithos 123, 188–203. https://doi.org/10.1016/j.lithos.2011.01.010.

Lottaroli, F., Craig, J., Thusu, B., 2009. Neoproterozoic–early Cambrian (Infracambrian) hydrocarbon prospectivity of North Africa: a synthesis. In: Craig, J., Thurow, J., Thusu, B., Whitham, A., Abutarruma, Y. (Eds.), Global Neoproterozoic Petroleum Systems: the Emerging Potential in North Africa, 326. Geological Society of London, Special Publication, pp. 137–156. https://doi.org/10.1144/sp326.7.

Ludwig, K.R., 2003. Isoplot 3. In: A Geochronological Toolkit for Microsoft Excel. Berkeley Geochronology Centre Special Publication 1a.

Maloof, A., Schrag, D., Crowley, J., Bowring, S., 2005. An expanded record of early Cambrian carbon cycling from the Anti-Atlas margin, Morocco. Can. J. Earth Sci. 42 (12), 2195–2216. https://doi.org/10.1139/e05-062.

Margalef, A., Castiñeiras, P., Casas, J.M., Navidad, M., Liesa, M., Linnemann, U., Hofmann, M., Gärtner, A., 2016. Detrital zircon from the Ordovician rocks of the Pyrenees: geochronological constraints and provenance. Tectonophysics 681, 121–134. https://doi.org/10.1016/j.tecto.2016.03.015.

Marzoli, A., Bertrand, H., Knight, K., Cirilli, S., Buratti, N., Verati, C., Nomade, S., Renne, P.R., Youbi, N., Martini, R., Allenbach, K., Neuwerth, R., Rapaille, C., Zaninetti, L., Bellieni, G., 2004. Synchrony of the central Atlantic magmatic province and the Triassic–Jurassic boundary climatic and biotic crisis. Geology 32, 973–976. https://doi.org/10.1130/g20652.1.

Marzoli, A., Bertrand, H., Youbi, N., Callegaro, S., Merle, R., Reisberg, L., Chiaradia, M., Brownlee, S., Jourdan, F., Zanetti, A., Davies, J.H.F.L., Cuppone, T., Mahmoudi, A., Medina, F., Renne, P.R., Bellieni, G., Crivellari, S., El Hachimi, H., Bensalah, M.K., Meyzen, C.M., Tegner, C., 2019. The central Atlantic magmatic province (CAMP) in Morocco. J. Petrol. 60 (5), 945–996. https://doi.org/10.1093/petrology/egz021. May 2019.

Marzoli, A., Davies, J.H.F.L., Youbi, N., Merle, R., Dal Corso, J., Dunkley, D.J., Fioretti, A. M., Bellieni, G., Medina, F., Wotzlaw, J.-F., McHone, G., Font, E., Bensalah, M.K., 2017. Proterozoic to Mesozoic evolution of North-West Africa and Peri-Gondwana microplates: detrital zircon ages from Morocco and Canada. Lithos 278–281, 229–239. https://doi.org/10.1016/j.lithos.2017.01.016. DOI: 10.1016/j.lithos.2017.01.016.

Massironi, M., Moratti, G., Algouti, A., Benvenuti, M., Dal Piaz, G.V., Eddebbi, A., El Boukhari, A., Laftouhi, N., Ouanaimi, H., Schiavo, A., Taj-Eddine, K., Visonà, D., 2007. Carte géologique au 1/50 000, Feuille Boumalne. Notes Mém. Serv. Géol. (Morroco) 521, 80.

McFarlane, H.B., Ailleres, L., Betts, P., Ganne, J., Baratoux, L., Jessell, M.W., Block, S., 2019. Episodic collisional orogenesis and lower crust exhumation during the Palaeoproterozoic Eburnean orogeny: evidence from the Sefwi greenstone belt, West African craton. Precambrian Res. 325, 88–110. https://doi.org/10.1016/j.precamres.2019.02.012.

Merdith, A.S., Williams, S.E., Müller, R.D., Collins, A.S., 2017. Kinematic constraints on the Rodinia to Gondwana transition. Precambrian Res. 299, 132–150. https://doi.org/10.1016/j.precamres.2017.07.013.

Metelkin, D.V., Ernst, R.E., Hamilton, M.A., 2011. A Ca. 1640 Ma Mafic Magmatic Event in Southern Siberia, and Links with Northern Laurentia. Geological Society of America Annual Meeting, abstract, Minneapolis, USA.

Michard, A., Saddiqi, O., Chalouan, A., Frizon de La Motte, D. (Eds.), 2008. Continental Evolution: the Geology of Morocco. Springer-Verlag Berlin Heidelberg, p. 404. https://doi.org/10.1007/978-3-540-77076-3.

Michard, A., Soulaimani, A., Ouanaimi, H., Raddid, Y., Aït Brahim, L., Rjimati, E., Baidder, L., Saddiqi, O., 2017. Saghro group in the Ougnat massif (Morocco), an evidence for a continuous Cadomian basin along the northern West African craton. C. R. Geosci. 349 (2), 81–90. https://doi.org/10.1016/j.crte.2017.01.001.

Möller, A., O'Brien, P.J., Kennedy, A., Kröner, A., 2003. Linking Growth Episodes of Zircon and Metamorphic Textures to Zircon Chemistry: an Example from the Ultrahigh-Temperature Granulites of Rogaland (SW Norway), vol. 220. Geological Society, London, Special Publications, pp. 65–81. https://doi.org/10.1144/gsl.sp.2003.220.01.04.

Mortaji, A., 1989. La boutonniere prébcambrienne de Tagragra d'Akka (Anti-Atlas Occidental, Maroc), Pérologie et géochimie des granitoides. filons basiques et métamorphites associées. Thése 3éme Cycle. Université Nancy I, p. 211.

Moussine-Pouchkine, A., Bertrand-Sarfati, J., 1978. Le Gourma; un aulacogene du Precambrien superieur? Bull. Soc. Geol. Fr. S7-XX (6), 851–855. https://doi.org/10.2113/gssgfbull.s7-xx.6.851.

Moussine-Pouchkine, A., Bertrand-Sarfati, J., 1997. Tectonosedimentary subdivisions in the neoproterozoic to early Cambrian cover of the Taoudenni Basin (Algeria-Mauritania-Mali). J. Afr. Earth Sci. 24 (4), 425–443. https://doi.org/10.1016/s0899-5362(97)00073-0.

Murphy, J.B., Fernández-Suárez, J., Keppie, J.D., Jeffries, T.E., 2004a. Contiguous rather than discrete Paleozoic histories for the Avalon and Meguma terranes based on detrital zircon data. Geology 32, 585–588. https://doi.org/10.1130/g20351.1.

Murphy, J.B., Fernández-Suárez, J., Keppie, J.D., Jeffries, T.E., 2004b. Lithogeochemical and Sm–Nd and U–Pb isotope data from the Silurian–lower Devonian Arisaig group clastic rocks, Avalon terrane, Nova Scotia: a record of terrane accretion during the Appalachian–Caledonide orogen. Geol. Soc. Am. Bull. 116, 1183–1201. https://doi.org/10.1130/b25423.1.

Naidoo, D.D., Bloomer, S.H., Saquaque, A., Hefferan, K., 1991. Geochemistry and significance of metavolcanic rocks from the Bou Azzer-El Graara ophiolite (Morocco). Precambrian Res. 53 (1–2), 79–97. https://doi.org/10.1016/0301-9268(91)90006-v.

Nance, R.D., Murphy, J.B., 1994. Contrasting basement isotopic signatures and the palinspastic restoration of peripheral orogens: example from the Neoproterozoic Avalonian-Cadomian belt. Geology 22 (7), 617–620. https://doi.org/10.1130/0091-7613(1994)022<0617:cbisat>2.3.co;2.

Nicoll, G., Straathof, G., Tait, J., Lo, K., Ousmane, N., El Moctar Dahmada, M., Berndt, J., Key, R., 2010. Provenance analysis and tectonic setting of the neoproterozoic sediments within the Taoudeni Basin, northern Mauritania. Geophys. Res. Abstr. 12. EGU2010-7094-2.

O'Connor, E.A., Barnes, R.P., Beddoe Stephens, B., Fletcher, T., Gillespie, M.R., Hawkins, M.P., Loughlin, S.C., Smith, M., Smith, R.A., Waters, C.N., Williams, M., 2010. Geology of the Dràa, Kerdous, and Boumalne Districts, Anti Atlas, Morocco. Nottingham British Geological Survey, Keyworth, p. 324.

Ouguir, H., Macaudière, J., Dagallier, G., 1996. Le Protérozoïque supérieur d'Imiter, Saghro oriental, Maroc : un contexte géodynamique d'arrière-arc. J. Afr. Earth Sci. 22, 173–189. https://doi.org/10.1016/0899-5362(96)00002-4.

Pearce, J.A., Cann, J.R., 1973. Tectonic setting of basic volcanic rocks determined using trace element analyses. Earth Planet Sci. Lett. 19 (2), 290–300. https://doi.org/10.1016/0012-821x(73)90129-5.

Pehrsson, S.J., Berman, R.G., Eglington, B., Rainbird, R., 2013. Two Neoarchean supercontinents revisited: the case for a Rae family of cratons. Precambrian Res. 232, 27–43. https://doi.org/10.1016/j.precamres.2013.02.005.

Pratt, J.R., Barbeau Jr., D.L., Garver, J.I., Emran, A., Izykowski, T.M., 2015. Detrital zircon geochronology of Mesozoic sediments in the Rif and middle atlas belts of Morocco: provenance constraints and refinement of the west african signature. J. Geol. 123, 177–200. https://doi.org/10.1086/681218.

Puchkov, V.N., Krasnobaev, A.A., Sergeeva, N.D., 2014. The new data on stratigraphy of the Riphean stratotype in the southern Urals, Russia. J. Geosci. Environ. Protect. 2, 108–116. https://doi.org/10.4236/gep.2014.23015.

Rainbird, R., Cawood, P.A., Gehrels, G., 2012. The great Grenvillian sedimentation episode: record of supercontinent Rodinia's assembly. In: Busby, C., Azor, A. (Eds.), Recent Advances in the Tectonics of Sedimentary Basins. Blackwell Publishing Ltd., pp. 583–601

Rainbird, R.H., McNicoll, V.J., Theraiault, R.J., Heaman, L.M., Abbott, J.G., Long, D.G.F., Thorkelson, D.J., 1997. Pan-continental river systems draining Grenville orogen recorded by U-Pb and Sm-Nd geochronology of Neoproterozoic quartz arenites and mudrock, northwestern Canada. J. Geol. 105, 1e10. https://doi.org/10.1086/606144.

Rainbird, R.H., Young, G.M., 2009. Colossal rivers, massive mountains and supercontinents. Earth 54, 52–61.

Rino, S., Kon, Y., Sato, W., Maruyama, S., Santosh, M., Zhao, D., 2008. The Grenvillian and Pan-African Orogenies: World's largest orogenies through geologic time, and their implications on the origin of the superplume. Gondwana Res. 14, 51–72. https://doi.org/10.1016/j.gr.2008.01.001.

Rocci, G., Bronner, G., Deschamps, M., 1991. Crystalline basement of the west african craton. In: Dallmeyer, R.D., Lécorché, J.P. (Eds.), The West African Orogens and Circum-Atlantic Correlatives. Springer Verlag, Berlin, pp. 31–61. https://doi.org/10.1007/978-3-642-84153-8_3.

Rooney, A.D., Selby, D., Houzay, J.-P., Renne, P.R., 2010. Re–Os geochronology of a Mesoproterozoic sedimentary succession, Taoudeni basin, Mauritania: implications for basin wide correlations and re–Os organic-rich sediments systematics. Earth Planet Sci. Lett. 289, 486–496. https://doi.org/10.1016/j.epsl.2009.11.039.

Sadowski, G.R., Bettencourt, J.S., 1996. Mesoproterozoic tectonic correlations between eastern Laurentia and the western border of the Amazon craton. Precambrian Res. 76, 213–227. https://doi.org/10.1016/0301-9268(95)00026-7.

Salminen, J., Klein, R., Veikkolainen, T., Mertanen, S., Mänttäri, I., 2017. Mesoproterozoic geomagnetic reversal asymmetry in light of new paleomagnetic and geochronological data for the Häme dyke swarm, Finland: implications for the Nuna supercontinent. Precambrian Res. 288, 1–22. https://doi.org/10.1016/j.precamres.2016.11.003.

Samson, S.D., Inglis, J.D., D'Lemos, R.S., Admou, H., Blichert-Toft, J., Hefferan, K., 2004. Geochronological, geochemical, and Nd–Hf isotopic constraints on the origin of Neoproterozoic plagiogranites in the Tasriwine ophiolite, Anti-Atlas orogen, Morocco. Precambrian Res. 135, 133–147. https://doi.org/10.1016/j.precamres.2004.08.003.

Santos, J.O.S., Hartmann, L.A., Gaudette, H.E., Groves, D.I., Mcnaughton, N.J., Fletcher, I.R., 2000. A new understanding of the provinces of the Amazon craton based on integration of field mapping and U-Pb and Sm-Nd geochronology. Gondwana Res. 3 (4), 453–488. https://doi.org/10.1016/s1342-937x(05)70755-3.

Santos, J.O.S., Rizzotto, G.J., Potter, P.E., McNaughton, N.J., Matos, R.S., Hartmann, L. A., Chemale Jr., F., Quadros, M.E.S., 2008. Age and autochthonous evolution of the Sunsás orogen in west Amazon craton based on mapping and U–Pb geochronology. Precambrian Res. 165, 120–152. https://doi.org/10.1016/j.precamres.2008.06.009.

Saquaque, A., Admou, H., Karson, J., Hefferan, K., Reuber, I., 1989. Precambrian accretionary tectonics in the bou Azzer-el Graara region, anti-atlas, Morocco. Geology 17 (12), 1107. https://doi.org/10.1130/0091-7613(1989)017<1107:patitb>2.3.co;2.

Schiavo, A., Taj-Eddine, K., Algouti, A., Benvenuti, M., Dal Piaz, G.V., Eddebbi, A., El Boukhari, A., Laftouhi, N., Massironi, M., Moratti, G., Ouanaimi, H., Pasquarè, G., Visonà, D., 2007. Carte géologique au 1/50 000, Feuille Imtir. Notes Mém. Serv. Géol. (Morroco) 518, 96.

Schofield, D.I., Horstwood, M.S.A., Pitfield, P.E.J., Crowley, Q.G., Wilkinson, A.F., Sidaty, H.C.O., 2006. Timing and kinematics of Eburnean tectonics in the central Reguibat shield, Mauritania. J. Geol. Soc. 163, 549–560. https://doi.org/10.1144/0016-764905-097.

Schulte, B., Benziane, F., Yazidi, A., Boger, S., Stockhammer, S., Lehmann, A., Saadane, A., Yazidi, M., 2016. Carte géologique du Maroc, feuille au 1/50 000 Arbaa Sahel. Notes Mém. Serv. Géol. (Morroco). Rabat n° 543bis.

Shervais, J.W., 1982. Ti–V plots and the petrogenesis of modern and ophiolitic lavas. Earth Planet Sci. Lett. 59, 101–118. https://doi.org/10.1016/0012-821x(82)90120-0.

Shields, G.A., Deynoux, M., Strauss, H., Paquet, H., Nahon, D., 2007. Barite-bearing cap dolostones of the Taoudéni Basin, northwest Africa: sedimentary and isotopic evidence for methane seepage after a Neoproterozoic glaciation. Precambrian Res. 153 (3–4), 209–235. https://doi.org/10.1016/j.precamres.2006.11.011.

Shumlyanskyy, L., Hawkesworth, C., Dhuime, B., Billström, K., Claesson, S., Storey, C., 2015. 207Pb/206Pb ages and Hf isotope composition of zircons from sedimentary rocks of the Ukrainian shield: crustal growth of the south-western part of East European craton from Archaean to Neoproterozoic. Precambrian Res. 260, 39–54. https://doi.org/10.1016/j.precamres.2015.01.007.

Sircombe, K.N., 2004. AgeDisplay: an EXCEL workbook to evaluate and display univariate geochronological data using binned frequency histograms and probability density distributions. Comput. Geosci. 30, 21–31. https://doi.org/10.1016/j.cageo.2003.09.006.

Söderlund, U., Ibanez-Mejia, M., El Bahat, A., Ernst, R.E., Ikenne, M., Soulaimani, A., Youbi, N., Cousens, B., El Janati, M., Hafid, A., 2013. Reply to comment on "U–Pb baddeleyite ages and geochemistry of dolerite dykes in the Bas Drâa inlier of the anti-atlas of Morocco: newly identified 1380 Ma event in the west african craton" by André Michard and Dominique Gasquet. Lithos 174, 101–108. https://doi.org/10.1016/j.lithos.2013.04.003.

Soulaimani, A., Ouanaimi, H., Michard, A., Montero, P., Bea, F., Corsini, M., Molina, J.F., Rjimatif, E.C., Saddiqi, O., Hefferan, K., 2019. Quartzite crests in Paleoproterozoic granites (Anti-Atlas, Morocco); a hint to pan-african deformation of the west african craton margin. J. Afr. Earth Sci. 157, 103501. https://doi.org/10.1016/j.jafrearsci.2019.05.009.

Soulaimani, A., Ouanaimi, H., Saddiqi, O., Baidder, L., Michard, A., 2018. The anti-atlas pan-african belt (Morocco): overview and pending questions. C. R. Geosci. 350, 279–288. https://doi.org/10.1016/j.crte.2018.07.002.

Soulaimani, A., Blein, O., Chèvremont, P., Ouanaimi, H., Hafid, A., Admou, H., Baudin, T., Bouabdelli, M., Razin, P.H., Abia, E.H., Beni Akhy, R., 2013. Notice explicative carte géol. Maroc (1/50 000), feuille Agadir Melloul. Notes Mém. Serv. Géol. (Morroco) n°549, MEM/BRGM.

Spencer, C.J., Kirkland, C.L., Taylor, R.J.M., 2016. Strategies towards statistically robust interpretation of in situ U-Pb zircon geochronology. Geosci. Front. 7, 581–589. https://doi.org/10.1016/j.gsf.2015.11.006.

Stacey, J.S., Kramers, J.D., 1975. Approximation of terrestrial lead isotope evolution by a two stage model. Earth Planet Sci. Lett. 26 (2), 207–221. https://doi.org/10.1016/0012.821x(75)90088-6.

Straathof, G.B., 2011. Neoproterozoic Low Latitude Glaciations: an African Perspective. Ph.D. thesis. University of Edinburgh, p. 285.

Sun, S.S., McDonough, W.F., 1989. Chemical and isotopic systematics of oceanic basalts; implications for mantle composition and processes. In: AD, Norry, M.J. (Eds.), Magmatism in the Ocean Basins. Saunders, 42. Geological Society of London, London, pp. 313–345. https://doi.org/10.1144/gsl.sp.1989.042.01.19.

Tapsoba, B., Lo, C.-H., Wenmenga, U., Iizuka, Y., Chung, S.-L., Shellnutt, G., 2018. Chemical and Sr-Nd compositions and $^{40}Ar/^{39}Ar$ ages of NW-trending dolerite dikes of Burkina Faso: evidence for a Mesoproterozoic magmatism in the west african craton. Geosci. Front. https://doi.org/10.1016/j.gsf.2017.12.015.

Tassinari, C.C.G., Macambira, M.J., 1999. Geochronological provinces of the Amazonian craton. Int. Union Geol. Sci. 22, 174–182. https://doi.org/10.18814/epiiugs/1999/v22i3/004.

Tassinari, C.C.G., Bettencourt, J.S., Geraldes, M.C., Macambira, M.J.B., Lafon, J.M., Cordani, U., Milani, E.J., Thomaz Filho, A., Campos, D.A., 2000. The Amazonian craton. In: Cordani, U.G., Milani, E.J., Thomaz Filho, A., Campos, D.A. (Eds.), Tectonic Evolution of South America: Rio de Janeiro, 31st International Geological Congress, pp. 41–95.

Tegner, C., Michelis, S.A.T., Mcdonald, I., Brown, E.L., Youbi, N., Callegaro, S., Lindström, S., Marzoli, A., 2019. Mantle dynamics of the central Atlantic magmatic province (CAMP): constraints from Platinum group, gold and lithophile elements in flood basalts of Morocco. J. Petrol. https://doi.org/10.1093/petrology/egz041.

Thiéblemont, D., 2016. An updated geological map of Africa at 1/10 000 000 scale. In: Presented at the 35th International Geological Congress: IGC 2016. https://hal-brgm.archives-ouvertes.fr/hal-01326139.

Thiéblemont, D., Goujou, J.C., Egal, E., Cocherie, A., Delor, C., Lafon, J.M., Fanning, C. M., 2004. Archean evolution of the Leo rise and its Eburnean reworking. J. Afr. Earth Sci. 39, 97–104. https://doi.org/10.1016/j.jafrearsci.2004.07.059.

Thomas, R.J., Chevakier, L.P., Gresse, P.G., Harmer, R.E., Eglington, B.M., Armstrong, R. A., De Beer, C.H., Martini, J.E.J., De Kock, G.S., Macey, P.H., Ingram, B.A., 2002. Precambrian evolution of the Sirwa Window, anti-atlas orogen, Morocco. Precambrian Res. 118, 1–57. https://doi.org/10.1016/s0301-9268(02)00075-x.

Thomas, R.J., Fekkak, A., Ennih, N., Errami, E., Loughlin, S.C., Gresse, P.G., Chevakier, L. P., Liegeois, J.P., 2004. A new lithostratigraphic framework for the Anti-Atlas Orogen, Morocco. J. Afr. Earth Sci. 39, 217–226. https://doi.org/10.1016/j.jafrearsci.2004.07.046.

Thompson, R.N., Dickin, A.P., Gibson, I.L., Morrison, M.A., 1982. Elemental fingerprints of isotopic contamination of Hebridean Palaeocene mantle-derived magmas by Archaean sial. Contrib. Mineral. Petrol. 79, 159–168. https://doi.org/10.1007/bf01132885.

Toummite, A., Liégeois, J.P., Gasquet, D., Bruguier, O., Beraaouz, E.H., Ikenne, M., 2013. Field, geochemistry and Sr-Nd isotopes of the pan-African granitoids from the Tifnoute Valley (Sirwa, anti-atlas, Morocco): a post-collisional event in a metacratonic setting. Mineral. Petrol. 107, 739–763. https://doi.org/10.1007/s00710-012-0245-3.

Triantafyllou, A., 2015. Evolution géodynamique d'un arc insulaire néoprotérozoïque de l'Anti -Atlas marocain : caractérisation des processus de croissance intra-océanique et d'accrétion. PhD thesis. Université de Nantes, Nantes, France, p. 390.

Triantafyllou, A., Berger, J., Baele, J.M., Bruguier, O., Diot, H., Ennih, N., Monnier, C., Plissart, G., Vandycke, S., Watlet, A., 2018. Intra-oceanic arc growth driven by magmatic and tectonic processes recorded in the Neoproterozoic Bougmane Arc complex (Anti-Atlas, Morocco). Precambrian Res. 304, 39–63. https://doi.org/10.1016/j.precamres.2017.10.022.

Triantafyllou, A., Berger, J., Baele, J.-M., Diot, H., Ennih, N., Plissart, G., Monnier, C., Watlet, A., Bruguier, O., Spagna, P., Vandycke, S., 2016. The Tachakoucht-Iriri-Tourtit arc complex (Moroccan Anti-Atlas): neoproterozoic records of polyphased subduction-accretion dynamics during the Pan-African orogeny. J. Geodyn. 98, 81–103. https://doi.org/10.1016/j.jog.2015.07.004.

Triantafyllou, A., Berger, J., Baele, J.-M., Mattielli, N., Ducea, M.N., Sterckx, S., Samson, S., Florent Hodel, F., Ennih, N., 2020. Episodic magmatism during the growth of a Neoproterozoic oceanic arc (Anti-Atlas, Morocco). Precambrian Res. 105610. https://doi.org/10.1016/j.precamres.2020.105610.

Triantafyllou, A., Hodel, F., Berger, J., Macouin, M., Baele, J.M., Mattielli, N., Monnier, C., Ducea Mihai, N., Poujol, M., Langlade, J., Trindade, R.I.F., 2019. The Bou Azzer and Sirwa Ophiolites (Anti-atlas, Morocco): Insight into Polyphased Subduction-Accretion Dynamics during Neoproterozoic Times. GSA Annual Meeting, Phoenix, Arizona, USA. https://doi.org/10.1130/abs/2019AM-336212.

Tuduri, J., Chauvet, A., Barbanson, L., Labriki, M., Dubois, M., Trapy, P.-H., Lahfid, A., Poujol, M., Melleton, J., Badra, L., Ennaciri, A., Maacha, L., 2018. Structural control, magmatic-hydrothermal evolution and formation of hornfels-hosted, intrusion-related gold deposits: insight from the Thaghassa deposit in Eastern Anti-Atlas, Morocco. Ore Geol. Rev. 97, 171–198. https://doi.org/10.1016/j.oregeorev.2018.04.023.

Vaasjoki, M., Tapani Rämö, O., Sakko, M., 1991. New U-Pb ages from the Wiborg rapakivi area: constraints on the temporal evolution of the rapakivi granite-anorthosite-diabase dyke association of southeastern Finland. Precambrian Res. 51 (1–4), 227–243. https://doi.org/10.1016/0301-9268(91)90102-g.

Villeneuve, M., 2005. Paleozoic basins in West Africa and the Mauritanide thrust belt. J. Afr. Earth Sci. 43 (1–3), 166–195. https://doi.org/10.1016/j.jafrearsci.2005.07.012.

Waldron, J.W.F., White, C.E., Barr, S.M., Simonetti, A., Heaman, L.M., 2009. Provenance of the Meguma terrane, Nova Scotia: rifted margin of early Paleozoic Gondwana. Can. J. Earth Sci. 46, 1–8. https://doi.org/10.1139/e09-004.

Walsh, G.J., Aleinikoff, J.N., Benziane, F., Yazidi, A., Armstrong, T.R., 2002. U-Pb zircon geochronology of the Paleoproterozic Tagragra de Tata inlier and its Neoproterozoic cover, western Anti-Atlas, Morocco. Precambrian Res. 117, 1–20. https://doi.org/10.1016/s0301-9268(02)00044-x.

Walsh, G.J., Benziane, F., Aleinikoff, J.N., Harisson, R.W., Yazidi, A., Burton, W.C., Quick, J.E., Saadane, A., 2012. Neoproterozoic tectonic evolution of the Jebel Saghro and bou Azer-el Graara inliers, eastern and central anti-atlas, Morocco. Precambrian Res. 216–219, 23–62. https://doi.org/10.1016/j.precamres.2012.06.010.

Wang, C., Zhang, J.-H., Li, M., Li, R.-S., Peng, Y., 2015. Generation of ca. 900–870Ma bimodal rifting volcanism along the southwestern margin of the Tarim Craton and its implications for the Tarim–North China connection in the early Neoproterozoic. J. Asian Earth Sci. 113, 610–625. https://doi.org/10.1016/j.jseaes.2015.08.002.

Weil, A.B., Van der Voo, R., MacNiocall, C., Meert, J.G., 1998. The Proterozoic supercontinent Rodinia: paleomagnetically derived reconstructions for 1100–800 Ma. Earth Planet Sci. Lett. 154, 13–24. https://doi.org/10.1016/s0012-821x(97)00127-1.

Williams, I.S., 1998. U-Th-Pb geochronology by ion microprobe. In: McKibben, M.A., Shanks, W.C., Riley, W.I. (Eds.), Applications of Microanalytical Techniques to Understanding Mineralising Processes. Reviews in Economic Geology, vol. 7, pp. 1–35. https://doi.org/10.5382/Rev.07.01.

Winchester, J.A., Floyd, P.A., 1977. Geochemical discrimination of different magma series and their differentiation products using immobile elements. Chem. Geol. 20, 325–343. https://doi.org/10.1016/0009-2541(77)90057-2.

Youbi, N., Söderlund, U., Ernst, R.E., Ait Malek, M., Barzouk, A., Ait Lahna, A., Palassia, M., Gong, Z., Evans, D., Wen, B., Jing, X.-Q., Boumehdi, M.A., Ikenne, M., Bensalah, M.K., Admou, H., Bajddi, A., Maacha, L., 2019. Ca. 1.65 Ga mafic sills emplaced into the quartzite of jbel Lkest from Kerdous Inlier, Anti-Atlas, West African craton, Morocco: additional evidence that the basal part of Taghdout group is nearly 1 Ga older than previously thought. In: The 7 International Science Conference Abstracts. Tomsk, p. 165.

Youbi, N., Bouougri, el H., Ait Lahna, A., Kouyaté, D., Tassinari, C.C.G., Admou, H., Mata, J., Boumehdi, M.A., Bensalah, M.K., Basei, M., AS, Sato, K., Ernst, R.E., Söderlund, U., Chaib, L., Bairouk, L., Gärtner, A., Linnemann, U., Ikenne, M., Bodinier, J.-L., 2018. A grande província ígnea de Iguerda-Taifast (ca. 885 Ma) no Anti-Atlas (Marrocos-Cratão Oeste africano): os enxames de diques máficos de Ifzwane e os vulcanitos máficos do grupo Tizi n'Taghatine. In: X Congresso National de geologia, Acçores, Portugal, Vulcânica, 2, p. 21.

Youbi, N., Ernst, R.E., Söderlund, U., Boumehdi, M.A., Ait Lahna, A., Tasssinari, C.C.G., El Moume, W., Bensalah, M.K., 2020. The Central Iapetus magmatic province: an updated review and link with the ca. 580 Ma Gaskiers glaciation. In: Adatte, Thierry, Bond, David P.G., Keller, Gerta (Eds.), Mass Extinctions, Volcanism, and Impacts: New Developments, 544. Geological Society of America Special Papers. https://doi.org/10.1130/2020.2544(02. December 31, 2019.

Youbi, N., Kouyaté, D., Söderlund, U., Ernst, R.E., Soulaimani, A., Hafid, A., Ikenne, M., El Bahat, A., Bertrand, H., Chaham, K.R., Ben Abbou, M., Mortaji, A., El Ghorfi, M., Zouhair, M., El Janati, M., 2013. The 1750 Ma magmatic event of the west african craton (Anti-Atlas, Morocco). Precambrian Res. 236, 106–123. https://doi.org/10.1016/j.precamres.2013.07.003.

Youbi, N., Martins, L.T., Munhá, J.M., Ibouh, H., Madeira, J., Ait Chayeb, H., El Boukhari, A., 2003. The late Triassic-early Jurassic volcanism of Morocco and Portugal in the framework of the central Atlantic magmatic province: an overview. In: Hames, W.E., Machone, J.G., Renne, P.R., Ruppel, C. (Eds.), The Central Atlantic Magmatic Province: Insights from Fragments of Pangea, vol. 136. American Geophysical Union Geophysical Monograph Series, pp. 179–207. https://doi.org/10.1029/136gm010.

Zhang, C.-L., Ye, X.-T., Ernst, R.E., Zhong, Y., Zhang, J., Li, H.-K., Long, X.-P., 2019. Revisiting the Precambrian evolution of the Southwestern Tarim terrane: implications for its role in Precambrian supercontinents. Precambrian Res. https://doi.org/10.1016/j.precamres.2019.01.018.